Newsletters on Stratigraphy, Vol. 52/3 (2019), 249–296 **Article**
Published online October 18, 2018; published in print June 2019

The Schandelah Scientific Drilling Project: A 25-million year record of Early Jurassic palaeo-environmental change from northern Germany

B. van de Schootbrugge[1, 2]*, S. Richoz[3], J. Pross[4], F. W. Luppold[5], S. Hunze[6], T. Wonik[7], J. Blau[1], C. Meister[8], C. M. H. van der Weijst[2], G. Suan[9], A. Fraguas[1], J. Fiebig[1], J. O. Herrle[1], J. Guex[10], C. T. S. Little[11], P. B. Wignall[11], W. Püttmann[12] and W. Oschmann[1]

With 8 figures, 10 plates and 2 tables

Abstract. With the aim to understand prolonged and repeated marine anoxia after the Triassic-Jurassic mass-extinction event, a continuously cored, 338 metre thick succession of Rhaetian to Toarcian sediments was retrieved close to the village of Schandelah near Braunschweig (Lower Saxony, northern Germany). Here, preliminary biostratigraphical, lithological, sedimentological, geochemical, and geophysical borehole data are presented and discussed. Based on the presence of ammonites, ostracods, benthic foraminifers, calcareous nannofossils, and palynomorphs, all major Late Triassic and Early Jurassic stage boundaries and many of the standard Lower Jurassic ammonite zones could be defined. The deltaic Rhaetian sand- and siltstone succession (Exter Fm) contains evidence for seismic activity probably related to large-scale geodynamic processes. The Hettangian (Lias Alpha) is represented by a thick heterolithic succession composed of shallow marine sandy and silty beds with intercalated organic-rich shale, representing deposition on a shoreface with frequent storm activity. Progressive deepening during the Sinemurian to Toarcian resulted in repeated deposition of laminated organic-rich facies. Periods of relative sea-level fall likely occurred during the Late Hettangian, the Late Sinemurian, and Early Pliensbachian, where a series of hardgrounds occur indicating erosion on the sea floor followed by sea level rise leading to omission, and increased reworking. One of the most conspicuous features of the Lower Jurassic in the Schandelah-1 core is the presence of abundant authigenic carbonates (glendonites,

Authors' addresses:
[1] Institute of Geosciences, Goethe University Frankfurt, Altenhöferallee 1, 60438 Frankfurt am Main, Germany
[2] Department of Earth Sciences, Marine Palynology & Paleoceanography, Utrecht University, Princetonlaan 8A, 3584 CB, Utrecht, The Netherlands
[3] Department of Geology, Lund University, Sölvegatan 12, 22362 Lund, Sweden
[4] Institute of Earth Sciences, University of Heidelberg, Im Neuenheimer Feld 234, 69120 Heidelberg, Germany
[5] State Authority for Mining, Energy and Geology, Stilleweg 2, 30655 Hannover, Germany
[6] WWU Münster, Physikalisches Institut, Wilhelm-Klemm-Str. 10, 48149 Münster, Germany
[7] Leibniz Institute for Applied Geophysics (LIAG), Stilleweg 2, 30655 Hannover, Germany
[8] Natural History Museum Geneva, Department of Geology and Paleontology, 1 Rte de Malagnou, CH-1211 Geneva, Switzerland
[9] Laboratory of Geology: Earth, Planets and Environment, University Claude-Bernard Lyon, Bâtiment Géode, Rue Raphael Dubois 2, 69622 Villeurbanne Cedex, France
[10] University of Lausanne, Geopolis, CH-1015 Lausanne, Switzerland
[11] School of Earth and Environment, The University of Leeds, Woodhouse Lane, Leeds LS2 9JT, United Kingdom
[12] Institute for Atmosphere and Environment, Department of Environmental Analytical Chemistry, Goethe University Frankfurt, Altenhöferallee 1, 60438 Frankfurt am Main, Germany
* Corresponding author: B.vanderSchootbrugge@uu.nl

www-borntraeger-cramer.de
DOI: 10.1127/nos/2018/0259 0078-0421/2018/0259 $ 12.00

concretions, beef-calcite) within the Upper Pliensbachian with partly very negative C-isotope values (down to –37‰ V-PDB) suggesting the anaerobic oxidation of methane. A high-resolution organic carbon isotope record based on 485 analyses shows two major negative carbon isotope excursions (CIEs) within the lowermost Hettangian and Lower Toarcian, respectively. Both excursions coincide with the onset of black shale deposition and are well-known features of these time-intervals in other regions. Despite the fact that black shale deposition also characterizes parts of the Sinemurian and Pliensbachian in similar facies, no large negative CIEs are apparent. The Schandelah-1 core thus provides an unique archive of sedimentary, biotic and geochemical records of long-term Triassic-Jurassic palaeo-environmental change in the European Epicontinental Seaway.

Key words. Early Jurassic, drill core, black shales, chemostratigraphy, sedimentology, paleontology

1. Introduction

The availability of free oxygen in the atmosphere and the existence of a biosphere both make the Earth unique within the solar system. Atmospheric oxygen levels are intimately linked to the evolution of the Earth´s biosphere: free oxygen was first introduced into the atmosphere by cyanobacterial photosynthesis ~2.3 billion years ago, and its rise until ~550 million years ago was closely tied to early biological activity (Berner et al. 2007). Over the past decade, the long-held paradigm that the evolution of multicellular life on Earth during the Phanerozoic occurred under near-constant oxygen levels (Watson et al. 1978) has increasingly been questioned (Berner 2000, 2002, Berner et al. 2007). An atmosphere with significantly higher oxygen levels than today, possibly as high as 35 %, is now widely considered to have triggered gigantism and origin of flight in insects, adaptations in marine biota with diffusion-mediated respiration and colonisation of the continents by vertebrate animals (Graham et al. 1995) during the mid- to late Paleozoic Era (~350–250 myrs ago). The extreme oxygen levels during the Mid- to Late Paleozoic era resulted from the diversification and proliferation of large, ligniferous land plants, with the burial of plant material leading to extensive coal deposits. This pattern suggests a positive correlation between oxygen availability and evolutionary processes (Berner et al. 2007).

While the Mid- to Late Paleozoic Era can be characterized as a high-oxygen world, atmospheric oxygen pressure (pO_2) appears to have dropped to an unparalleled minimum during the Early Jurassic (200 to 175 myrs ago). Coupled carbon and sulfur cycle modelling suggests that oxygen concentrations may have declined to 12 % (Berner 2006). However, controlled burning experiments and the evidence for palaeo-wildfires suggest oxygen concentrations during the Jurassic may not have decreased below 17 % (Belcher and McElwain 2010). Still, lower oxygen levels may have imposed severe limitations on the evolution of marine and terrestrial biota, potentially driving a widespread loss in biodiversity. Low pO_2 in the oceans and atmosphere is thought (Berner et al. 2007) to have significantly contributed to the mass-extinction event at the Triassic-Jurassic boundary (201.6 Ma). Paradoxically, however, the Early Jurassic marks a crucial time in biotic evolution with the onset of the "Mesozoic Marine Revolution" (Vermeij 1977, 2008) that gave rise to the so-called "Modern Fauna" (Sepkoski Jr. 1996). The "Modern Fauna" is characterized by increased mobility in marine invertebrate organisms, expressed e. g. in greater burrowing activity of bivalves and the rapid diversification of predators, such as ammonites and belemnites. The evolution of large marine reptiles testifies to a dramatically increased predation pressure in Early Jurassic oceans. On land, biodiversity surged to new heights during the Early Jurassic with the rise to dominance of theropod dinosaurs, and the radiation of modern conifers and relatives of modern angiosperms. Overall, ecological complexity and mobility in vertebrate organisms increased rapidly during the Early Jurassic, traits that presumably require high blood oxygen levels (Falkowski et al. 2005).

Low atmospheric oxygen concentrations during the Early Jurassic may have facilitated organic matter preservation and black shale formation in many basins within the European Epicontinental Seaway (EES; Jenkyns 1988), while the storage of organic matter may have increased oxygen concentrations in turn. Outside of the EES, Lower Jurassic black shales are also common in the Neuquen Basin in Argentina, and Early Jurassic anoxia has been demonstrated in the Panthalassa Ocean in Japan (Wignall et al. 2010) and in North America (Martindale et al. 2017). The global significance of these black shale deposits is, however,

yet poorly constrained and controversially discussed. While some authors have proposed a global Oceanic Anoxic Event (OAE) during the Early Jurassic Toarcian (Jenkyns 1988, Hesselbo et al. 2000), others have argued for a merely regional distribution of dysoxic to anoxic conditions in Early Jurassic seas (Röhl et al. 2001, van de Schootbrugge et al. 2005). Understanding both the spatial distribution of anoxia and the extent of anoxia within the paleo-water column is crucial in order to constrain Early Jurassic oxygen levels: in analogy to the enhanced organic carbon burial during the Carboniferous, particularly strong anoxic conditions (i. e., on a near-global to global scale) would result in increased atmospheric oxygen availability because of the removal of oxydizable carbon into the sedimentary reservoir. Indeed, there is some evidence for an increase in oxygen following the Toarcian OAE coming from charcoal abundance, which has been used as a proxy for burning of vegetation (Baker et al. 2017).

With the aim to understand the repeated occurrence of Lower Jurassic black shales in the European Epicontinental Seaway, a consortium spearheaded by the Goethe University Frankfurt, obtained a 338 metre long core from the North German Basin close to the village of Schandelah that spans from the Rhaetian to the Toarcian. Here, we present initial results, including geophysical borehole data, lithological and sedimentological descriptions, biostratigraphy based on ammonites, ostracods, nannofossils, and palynomorphs, and preliminary organic carbon isotope data that aid in correlating the succession with nearby outcrops and other cores. This overview will serve future multidisciplinary research by providing a solid framework.

2. Methods

The drilling was carried out by Daldrup und Söhne (Ascheberg, Germany), from August 5 to September 18, 2008. The exact location of the drill site is 52° 18'23" N, 10°42'66" W, elevation 84 m in the municipality of Lehre, Landkreis Helmstedt, Lower Saxony (Fig. 1). The drill rig used was a Wirth B1A/B2A, drilling a 146 mm diameter hole and producing a 100 mm diameter core using rotary drilling. In accordance with environmental regulations, the soil was protected from oil and other pollutants with plastic foil and a containment basin. Water from a regional water reservoir was used as drilling fluid. After being introduced under pressure in the core hole, the exiting

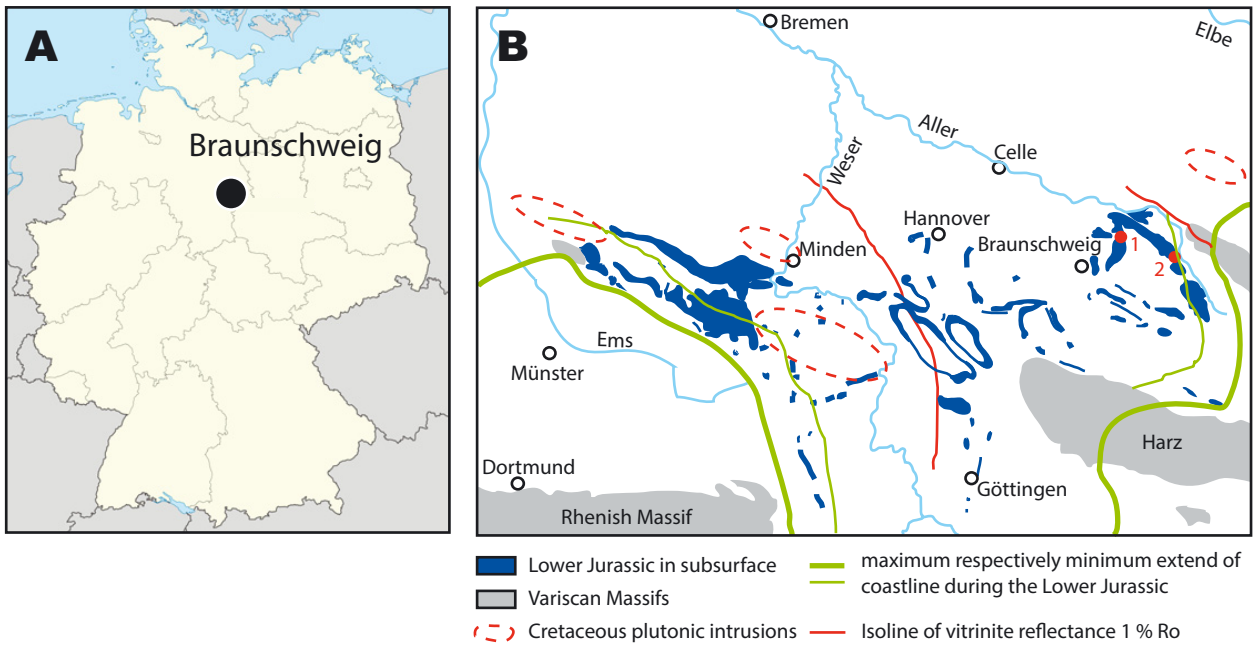

Fig. 1. Location map of drilling site. (A) Map of Germany with Braunschweig, the largest town in the vicinity of Schandelah, which is 18 km East of Braunschweig. (B) Map of Lower Saxony with the occurrences of Lower Jurassic sediments (under the quaternary cover) showing also the presence of Lower to Upper Cretaceous magmatic intrusions. The isoline of vitrinite reflectance for 1 % Ro was drawn after Koch and Arnemann (1975) and Teichmüller et al. (1984); 1 = Schandelah-1 core, 2 = Mariental-1 core.

20190916-124004
A17159/29840/83D368CB

water was collected in a settling tank and reused. Eleven water samples were taken at regular intervals (07.08.2008; 12.08.2008; 04.09.2008) during the drilling process and these are stored at the Institute of Geosciences of the Goethe University Frankfurt.

The terminal depth was 338 metres below surface (mbs; Fig. 2). The first 5.50 mbs were not recovered, due to extensive weathering and destructive drilling. Until a depth of 12.00 mbs the core quality was rather poor due to partial weathering of the strata. The interval 226.90–227.10 mbs had to be re-drilled after a core piece fell down when the core-catcher was pulled up, hence the stratigraphic succession in that interval may be compromised. During drilling, several fractures, resulting in a loss of water, were encountered (27.50–27.80 mbs; 34.05–35.25 mbs; 104.50–104.84 mbs; 116.28–116.52 mbs; 161.19–161.68 mbs; 164.18–164.89 mbs; 254.10–254.29 mbs; 299.07–299.55 mbs). After completion of the drilling operation, the drill hole was filled with concrete, in accordance with requests by *Barbara Rohstoffbetriebe GmbH* and the *Geological Survey of Lower Saxony*.

The core was transported to the Institute of Geosciences at the Goethe University Frankfurt and was cut into sample and archive halves. The entire core was logged and photographed and sampled at 10 cm intervals. Each sample was split into three aliquots. These samples are stored at the Institute of Geosciences (Goethe University Frankfurt). Subsequently the sample half of the core was split entirely in order to sample for ammonites. After logging, photographing, and sampling the archive half of the core was transported to the German core repository for scientific drilling in Berlin Spandau operated by BGR and GFZ Potsdam, where it is permanently stored and will be accessible to the scientific community for future research.

Downhole geophysical measurements were performed by the Leibniz Institute for Applied Geophysics (LIAG) from 17 mbs to 134 mbs. Furthermore,

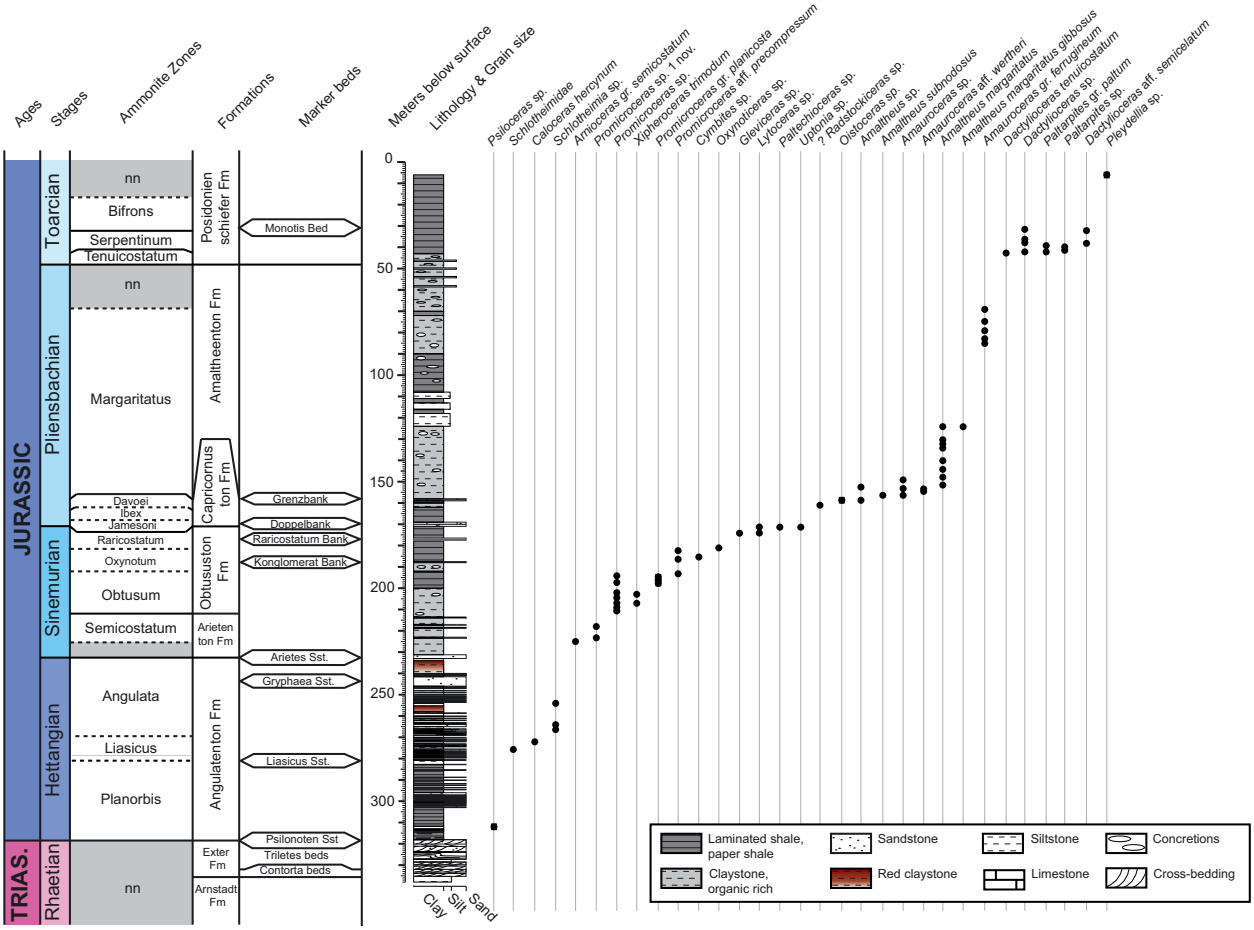

Fig. 2. Lithology and ammonite biostratigraphy of the Schandelah-1 core.

20190916-124004
A17159/29840/83D368CB

Tegtmeyer Geophysik GmbH measured gamma ray and resistivity from 130 mbs to 194 mbs. After pulling up the casings the lower part of the hole collapsed, and therefore there is no logging data from below 194 mbs. The following wireline logs were successfully recorded in the borehole: gamma ray (GR), resistivity (dual laterolog with two penetration depths: Rdeep and Rshallow), density (DENS), p-wave velocity (VP), magnetic susceptibility (SUSC), borehole diameter (CALI), and dipmeter. The dipmeter log is used to detect fracture and strata dip angles and directions. For a detailed description of the physical principles of the applied methods see e. g. Serra (1984), Fricke and Schoen (1999), Ellis (2007), and Rider and Kennedy (2011). The sampling rate was set to 5 cm except VP with 10 cm. Based on a 'smooth' CALI, with only one interval of significant washouts (40–55 mbs), the data quality and reliability is excellent for almost all tools over the entire logged section. The software GeoBase® (Antares, Germany) and WellCAD® (Advanced Logging Technology, Luxembourg) were used for data acquisition, pre-processing and processing.

The Lower Jurassic of northwest Germany has been investigated intensely for calcareous microfossils stimulated by oil- and gas exploration during the last century (Bartenstein and Brand 1937, Franke 1936, Triebel 1959, Klingler 1959, 1962, Malz 1971, Beutler et al. 1996). However, a detailed micropalaeontological zonation based on ostracods or benthic foraminifers is still lacking for northwest Germany. Due to their shorter ranges, ostracods are more useful than benthic foraminifers for establishing a Lower Jurassic zonation. For ostracods and benthic foraminifers sampling was carried out using amalgamated sample intervals to increase the microfossil yield. Bulk sediment sample weights ranged between 60 and 240 g. The dried samples were wet-sieved with a 63 µm mesh sieve. The dried residue was then sieved into fractions and picked using a binocular microscope, and the number of foraminifers and ostracod species was documented. Key taxa were photographed using a SEM. The type material is housed at the Geozentrum Hannover (BGR – Bundesanstalt für Geowissenschaften und Rohstoffe), under the type numbers BGR/LBEG Hannover 16111 to 16124.

A comprehensive calcareous nannofossil zonation scheme for Lower Jurassic low- to mid-latitude successions from NW Europe has been proposed by Bown and Cooper (1998), and it has been successfully applied in Italy and southern France (Mattioli and Erba 1999, Ferreira et al. 2016), Portugal (Veiga de Oliveira et al. 2007) and northern Spain (Perilli et al. 2010). However, a detailed nannofossil zonation is currently not available for the Lower Jurassic of northwest Germany. For calcareous nannofossil analyses, sample intervals vary between 1 to 3 m. A total of 110 samples were prepared using standard smear slides techniques (Bown and Young 1998, Herrle and Bollmann 2004). Semiquantitative analyses were performed with a ZEISS Axio Imager A2 light microscope at a magnification of 1250 × equipped with a CANON imaging system. At least 1000 fields of view were studied in random traverses of each slide.

Samples were processed for palynology using standard techniques of alternating steps with HCl and HF to remove mineral phases, followed by subsequent sieving (mesh size 10µ) and slide fabrication. Samples were only scanned for the presence of age-diagnostic pollen, spores and dinoflagellate cysts.

For organic carbon isotope analyses, a total of 484 powdered samples were decarbonized with HCl (10 %) and then washed with deionized water until neutrality. The residues were dried at 60 °C for 24 hours and subsequently ground to a homogeneous powder using an agate mortar and pestle. Carbon isotope analysis of total organic carbon was subsequently performed using a Flash Elemental Analyzer 1112 (Thermoquest), connected to the continuous flow inlet system of a MAT 253 gas source mass spectrometer (Thermoquest) at the Goethe University Frankfurt. USGS 24 standard was analyzed along with the samples in order to prove for accuracy and precision. Both samples and standards reproduced within ±0.2 %. The $\delta^{13}C$ values are reported relative to Vienna-Pee Dee belemnite standard (VPDB).

In addition, 73 samples of authigenic carbonates (concretions, glendonites) as well as bulk carbonates from the interval 74.00 to 99.00 mbs were also analysed for carbonate carbon and oxygen isotope signatures.

3. The Rhaetian

3.1. Biostratigraphy

The Rhaetian (338.00 to 318.60 mbs) in the Schandelah core did not contain any ammonites, foraminifers, or ostracods, and no biozonation based on ammonites is possible for this interval in the core (Fig. 2). In contrast, organic-walled microfossils have proven to

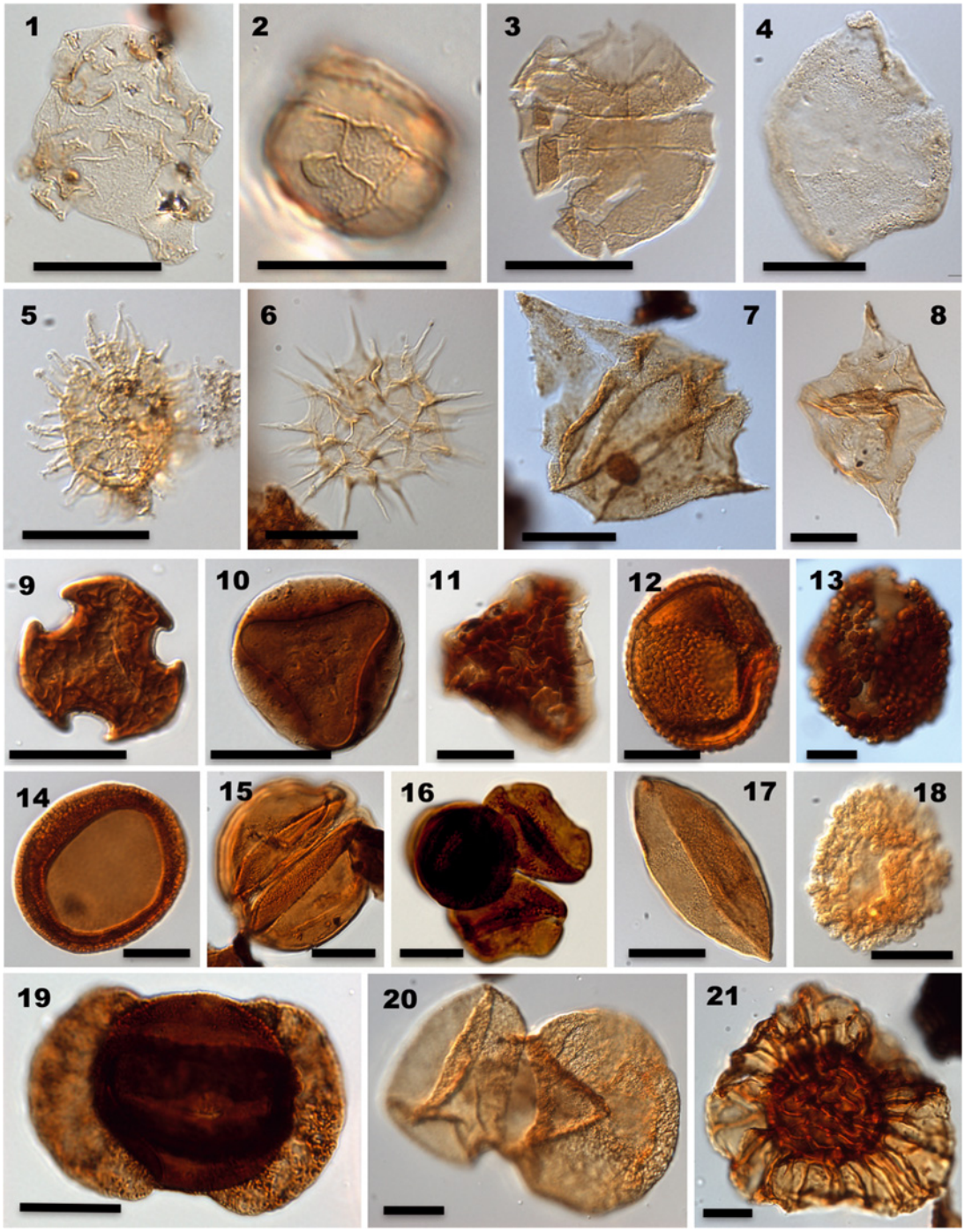

Plate 1. **1** – *Lunnomidinium scaniense Lindström 2002* (Sch 333.20 mbs). **2** – Indet dinoflagellate cyst. (Sch 333.00 mbs). **3** – *Dapcodinium priscum* Evitt 1961 emend. Below 1987 (Sch 334.60 mbs). **4** – *Nannoceratopsis senex* Van Helden 1977 (Sch 132.00 mbs). **5** – *Beaumontella langii* Below 1987 (Sch 316.70 mbs). **6** – *Luehndea spinosa* Morgenroth 1970 (Sch 42.90 mbs). **7** – *Rhaetogonyaulax rhaetica* Loeblich & Loeblich 1968 (Sch 333.20 mbs). **8** – *Liasidium variabile* Drugg 1978 (Sch 200.00 mbs). **9** – *Triancoraesporites ancorae* Rheinhardt 1962 (Sch 336.50 mbs). **10** – *Zebrasporites seebergensis* Klaus 1960 (Sch 336.00 mbs). **11** – *Perinosporites thuringiacus* Schulz 1962 (Sch 333.00 mbs). **12** – *Polypodiisporites polymicroforatus* Lund 1977 (335.30 mbs). **13** – *Ricciisporites tuberculatus* Lundblad 1954 (Sch 333.50 mbs). **14** – *Chasmatosporites apertus* Nillson 1958 (Sch 336.80). **15** – *Rhaetipollis germanicus* Schulz 1967 (Sch 334.00 mbs). **16** – *Classopollis torosus* Cornet & Traverse 1975 (316.70 mbs). **17** – *Cycadopithes* sp. (Sch 338.00 mbs). **18** – *Cerebropollenites mesozoicus* Schulz 1967 (Sch 44.00 mbs). **19** – *Lunatisporites rhaeticus* Warrington 1974 (Sch 336.00 mbs). **20** – *Brachysaccus* sp. (337.50 mbs). **21** – *Semiretisporis gothae* Rheinhardt 1962 (Sch 334.00 mbs). In all photographs scale bar 20 µm.

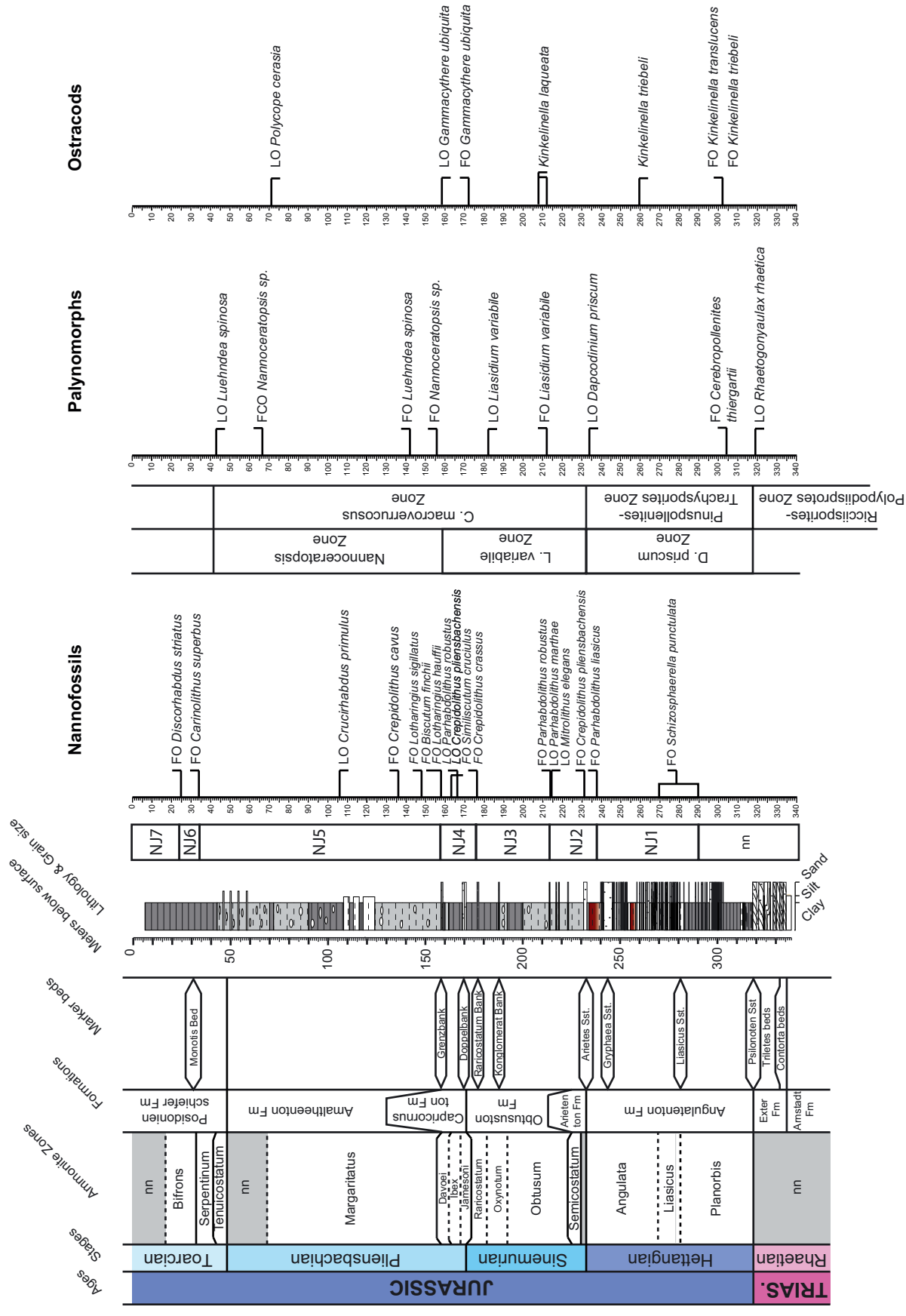

Fig. 3. Biostratigraphy of Schandelah-1 core based on microfossils (nannofossils, palynomorphs, ostracods and foraminifers).

20190916-124004
A17159/29840/83D368CB

be very reliable biostratigraphic tools for the Rhaetian and for correlating the Triassic-Jurassic boundary (Lindström et al. 2017). A first useful marker was found at 335.00 mbs in the form of the dinoflagellate cyst *Lunnomidinium scaniense* (Plate 1). In the Danish Basin this dinoflagellate cyst occurs exclusively around the middle-upper Rhaetian boundary (Lindström 2002, 2006). This is the first time *L. scaniense* has been published outside of the Danish Basin. Two other important dinocyst marker species, *Rhaetogonyaulax rhaetica* and *Dapcodinium priscum*, are present from the base of the core, but reach a distinct acme around 332.00 mbs. Whereas *D. priscum* is known to range into the Lower Jurassic (Evitt 1961), the last occurrence of *R. rhaetica* is closely associated with the end-Triassic extinction and Triassic-Jurassic (Rhaetian-Hettangian) boundary (Lindström 2006). *Rhaetogonyaulax rhaetica* has a last occurrence at 320.10 mbs (Fig. 3). The upper Rhaetian is further confirmed by the presence of a suite of marker pollen and spore species, including *Semiretisporis gothae, Classopollis torosus, Perinosporites thuringiacus*, and various morphotypes of *Triancoraesporites*.

The transition from the Rhaetian to Hettangian is characterized by several last occurrences of a suite of typical Triassic pollen species that became victims of the end-Triassic mass-extinction. The pollen species *Lunatisporites rhaeticus*, *Ovalipollis ovalis*, and *Ricciisporites tuberculatus* (Plate 1) disappear together at 319.50 mbs, providing the deepest level for the Triassic-Jurassic boundary. In the same interval the palynological assemblage is dominated by high abundances of fern spore species, particularly *Polypodiisporites polymicroforatus* (Plate 1) and various morphotypes of the species-complex *Concavisporites-Deltoidospora*. These fern spore species dominate the Rhaetian Triletes Beds from 332.50 to 318.60 mbs, marking the latest Triassic "fern spike interval" described by van de Schootbrugge et al. (2009) and references therein. In the palynostratigraphy of Lund (1976, 1977) the Triletes Beds correspond to the *Ricciisporites-Polypodiisporites* Zone.

The pollen species *Cerebropollenites thiergartii* is now considered as an accessory marker for the Triassic-Jurassic boundary, occurring close to the first occurrence of the ammonite *Psiloceras spelae* in the GSSP section of Kuhjoch in Austria (Kürschner et al. 2007). Some doubts remain about the usefulness of this species as a marker for the Rhaetian-Hettangian boundary in sections at higher latitudes, as it is generally very rare and appears stratigraphically well after the T/J boundary, within the Hettangian (e. g. Heunisch et al. 2010). In the Schandelah core, *C. thiergartii* has a first appearance at 304.00 mbs, i. e. well above the Triassic-Jurassic boundary based on other palynomorphs.

3.2. Lithology

The lowermost 3.20 metres in the core from 338.00 to 334.80 mbs belong to the uppermost part of the Arnstadt Formation (Fig. 3). This interval contains reddish-brown to brown, grey, and green claystones with siderite concretions at its base, and becomes sandier towards the top. Sedimentary features include thin sandstone beds showing intense loading and flaser bedding. Although devoid of any marine macrofossil remains, the presence of dinoflagellate cysts (e. g. *Lunnomidinium*, *Beaumontella,* and *Dapcodinium*) suggests a predominantly shallow marine environment.

The overlying units belong to the Exter Formation (334.80–318.60 mbs) and are characterized by sharp-based, medium-grained, current-rippled sandstone with thin muddy partings and abundant plant material and charcoal. A possible sequence boundary is situated at the base of this unit. The most expanded part of the Rhaetian succession at Schandelah is formed by the so-called "Triletes Beds" (332.00–318.60 mbs). The beds below the Triletes Beds and above the Arnstadt Fm are known as the Contorta Beds, named after the bivalve *Rhaetavicula contorta*. The Triletes Beds consist of fine-grained grey to dark grey sand- and siltstone. The Rhaetian is characterized by a wide variety of sedimentological features. The sandstone beds show abundant small-scale cross-stratification recording current ripples that frequently show climbing sets, testimony to high sediment influx. Mud-chip conglomerate beds occur throughout, with clasts typically highly rounded and 1 cm in diameter; they are especially numerous around 322.70 mbs. Bioturbation is absent from this part of the core except between 330.35–330.10 mbs where *Catenichnus* is common in flaser-bedded facies. Liquefaction horizons are common and include flame and ball-and-pillow structures; they are well developed at 330.90 mbs, 326.50 mbs, 324.00 mbs and 322.10 mbs. Starting from 331.30 mbs, and continuing up to 322.00 mbs, a number of sedimentary features suggest seismic activity (Plate 2). Small scale inverse faulting and irregular sediment-filled fissures, that do not resemble typical desiccation cracks, are present at many levels. The fissures penetrate downwards for as

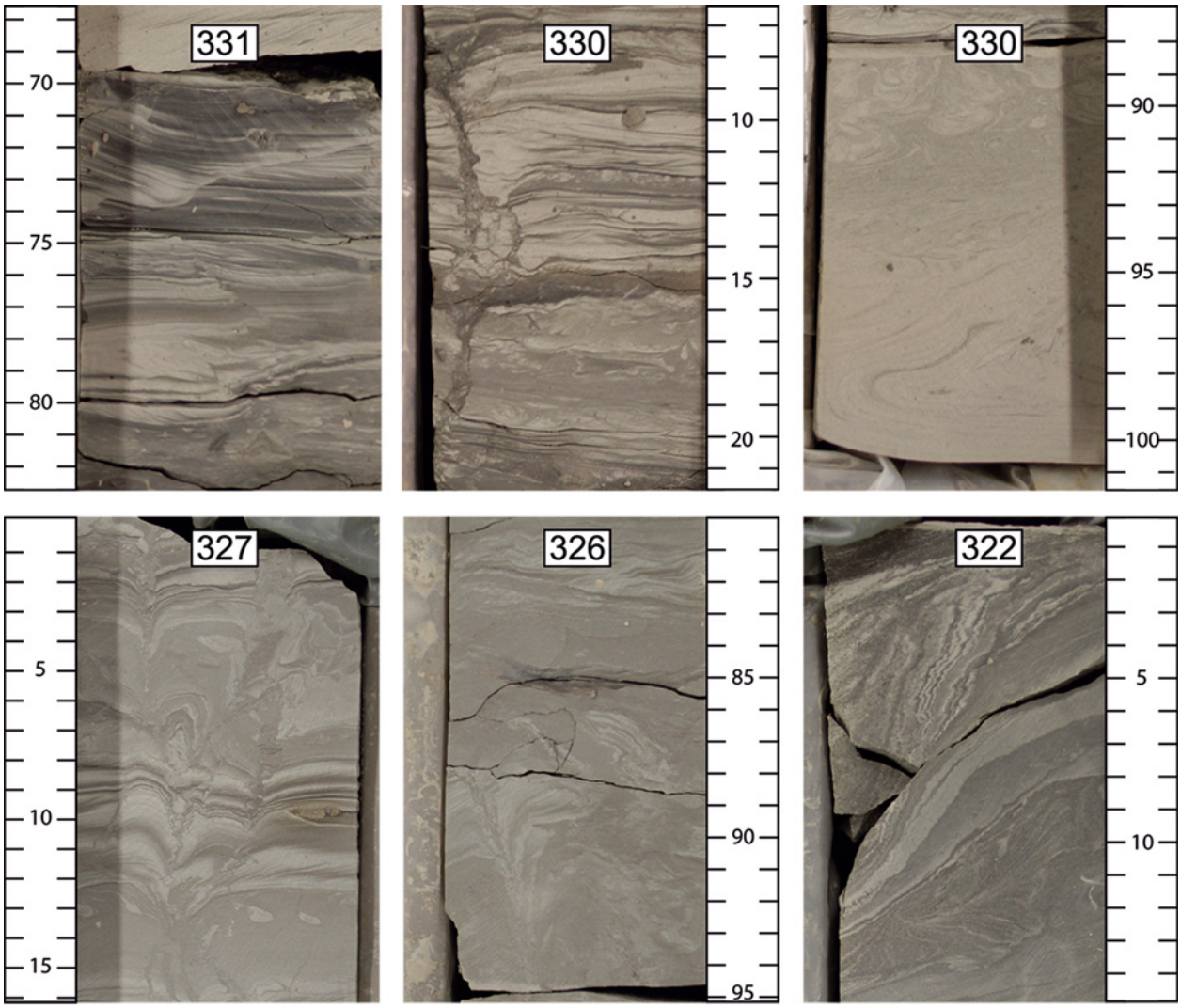

Plate 2. Examples of disturbed sediments of possible seismic origin within the Upper Rhaetian Triletes Beds. See also Lindström et al. (2015) for a comparison with similar seismites in Denmark, Sweden, and Luxembourg.

much as 10 cm and, although they generally taper downwards, they often do so in an irregular manner showing sharp changes in their width. Small mud chips, like those seen in the intraclast conglomerate, often infill the fissures and one example at 320.10 mbs also contained common bone fragments. The "Triletes Beds" are capped by a very sharp, irregular surface at 318.60 mbs that marks the transition to the distinctly different facies of the Psilonoten Sandstone (318.60–317.90 mbs). Muddy bioturbated sandstone dominate in the lower part with better laminated sandstone and shale interbed facies in the upper part of the Triletes Beds.

4. The Hettangian

4.1. Biostratigraphy

All Hettangian (318.60–233.30 mbs) ammonite zones could be assigned; however, the boundaries between these ammonite zones remain inconclusive due to the low abundance of ammonites within the Hettangian part of the core (Fig. 2). The presence of *Psiloceras* (*Neophyllites*) sp. (see also Plate 3) near the base of the Hettangian at 312.12 mbs could be correlated with the Planorbis ammonite Zone. Specimens belonging to the genus *Saxoceras* at 270.70 mbs and 264.20 mbs characterize the transition from the Lower to the Upper

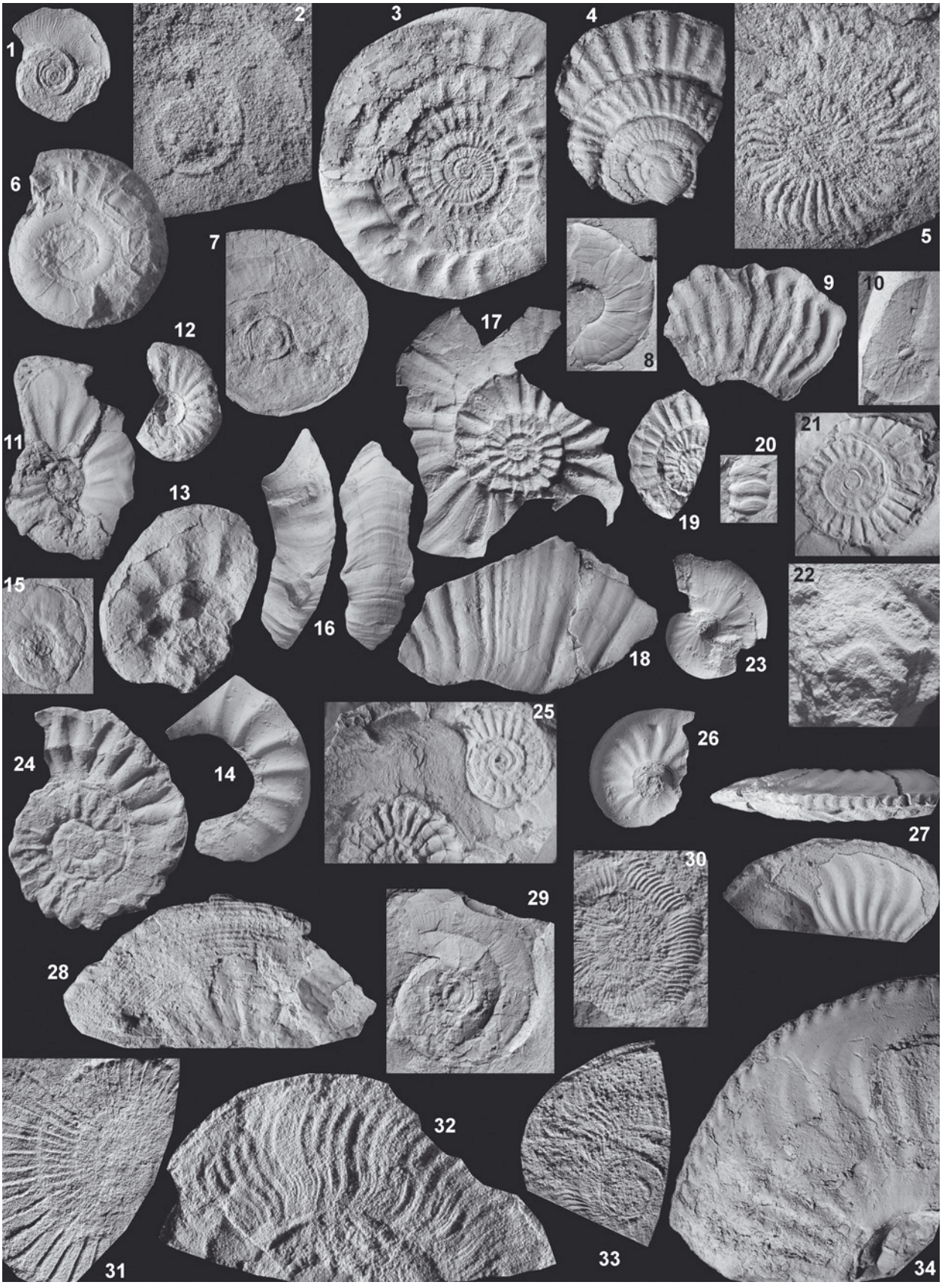

20190916-124004
A17159/29840/83D368CB

Hettangian. The Liassicus ammonite Zone was documented by the finding of a *Caloceras hercynum*. The Angulata ammonite Zone is represented by several specimens assigned to *Schlotheimia* sp.

The foraminifer *Lenticulina* and the ostracod *Kinkelinella* represent the first marine benthic microfauna occurring at 302.00 mbs (Fig. 3; Plates 4 and 5) and marking the Hettangian. However, because of a lack of index ostracods, which is probably due to the nearshore depositional setting, the Hettangian cannot be further subdivided. Biostratigraphic resolution based on foraminifers and ostracods is equally poor in comparable sequences in England, France, and Denmark.

An abrupt change in palynofacies and palynomorph assemblages occurs at 318.20 with the common appearance of typical Early Jurassic species, including *Pinuspollenites minimus, Kraeuselisporites reissingerii*, and *Trachysporites fuscus* (Plate 1). The Triassic-Jurassic boundary is thus recognized above 319.50 and below 318.20 mbs. Based on the palynology, the T/J boundary can be placed at 318.60 mbs at the base of a grey-brown sandstone bed that corresponds to the Psilonoten Sandstone (see also below). This bed is characterized by a sharp negative excursion in $\delta^{13}C_{org}$ that can be confidently correlated with a similar excursion in a nearby organic carbon isotope record obtained from the Mariental Core (van de Schootbrugge et al. 2013) (see also below). In the palynostratigraphic scheme of Lund (1976, 1977) this interval corresponds to the *Pinuspollenites-Trachysporites* Zone, spanning the entire Hettangian. Its upper boundary is marked by the appearance of *Cerebropollenites macroverrucosus.* The last common occurrence of *Dapcodinium priscum* marks the top of the *Dapcodinium priscum* Zone, which is generally understood to coincide with the Hettangian-Sinemurian boundary (Lund 1977).

Schizosphaerella punctulata (Fig. 3; Plate 6) was found at 290.00 mbs, in the lower part of the Hettangian. The FO of *S. punctulata* defines the base of the NJ1 S. punctulata calcareous nannofossil Zone. This species is extremely rare initially and becomes more common higher up in the Schandelah-1 core. The species *Parhabdolithus liasicus* first occurs at 238.00 mbs, just below the Hettangian-Sinemurian boundary (at 233.30 mbs). This main event defines the base of the NJ2 P. liasicus calcareous nannofossil Zone. At 230.00 mbs, the first appearances of *Crepidolithus pliensbachensis* and *Mitrolithus elegans* further support the position of the Hettangian-Sinemurian boundary in the Schandelah core.

In summary, the ammonite, palynomorph, and nannofossil data allow recognition of the Triassic-Jurassic boundary at 318.60 mbs. The ammonite assemblage has a low abundance, which does not permit to pinpoint the ammonite zone boundaries. There is a general congruence in the position of the Hettangian-Sinemur-

Plate 3. **1** – *Lytoceras* sp. (174.75 mbs), magnification 2x. **2** – *Psiloceras* (*Neophyllites*) sp. (312.12 mbs), magnification 2x. **3** – *Caloceras hercynum* Lange (272.14 mbs), magnification 1x. **4** – *Caloceras hercynum* Lange (272.40 mbs), magnification 2x. **5** – *Schlotheimia* sp. (264.45–50 mbs), magnification 2x. **6** – *Arnioceras* gr. *semicostatum* (Young & Bird) (225.07–12 mbs), magnification 2x. **7** – *Oxynoticeras* sp. (180.98 mbs), magnification 2x. **8** – *Oxynoticeras* sp. (180.93 mbs), magnification 2x. **9** – *Schlotheimia* sp. (267.83–88 mbs), magnification 1x. **10** – ?*Radstockiceras* sp. (161.65 mbs), magnification 2x. **11** – *Gleviceras* sp. (174.80–84 mbs), magnification 2x. **12** – *Gleviceras* sp. (174.80–84 mbs), magnification 2x. **13** – *Promicroceras* sp. 1 nov. sp. (223.05 mbs), magnification 2x. **14** – *Promicroceras* sp. 1 nov. sp. (218.63 mbs), magnification 2x. **15** – *Cymbites* sp. (185.06 mbs), magnification 2x. **16** – *Xipheroceras trimodum* Dumortier (207.71–73 mbs), magnification 2x. **17** – *Xipheroceras trimodum* Dumortier (202.85 mbs), magnification 2x. **18** – *Xipheroceras trimodum* Dumortier (202.85 mbs), magnification 2x. **19** – *Promicroceras* aff. *precompressum* Spath (182.39 mbs), magnification 2x. **20** – *Promicroceras* aff. *precompressum* Spath (193.44–46 mbs), ventral part, magnification 2x. **21** – *Promicroceras* aff. *precompressum* Spath (193.44–46 mbs), magnification 2x. **22** – *Oistoceras* sp. (158.41–51 mbs), ventral part, magnification 2x. **23** – *Amauroceras* aff. *wertheri* (Lange) (153.58 mbs), magnification 2x. **24** – *Promicroceras* gr. *planicosta* (Sowerby) (197.35 mbs), magnification 2x. **25** – *Promicroceras* gr. *planicosta* (Sowerby) (195.64–70 mbs), magnification 2x. **26** – *Amaltheus subnodosus* Howarth (156.58–60 mbs), magnification 2x. **27** – *Amaltheus margaritatus* (de Montfort) (148.92–95 mbs), magnification 1x. **28** – *Amaltheus margaritatus* (de Montfort) (151.82 mbs), magnification 2x. **29** – *Amauroceras ferrugineum* (Simpson) (79.80 mbs), magnification 2x. **30** – *Dactylioceras tenuicostatum* Young & Bird (42.83 mbs), magnification 1x. **31** – *Dactylioceras* aff. *semicelatum* (Simpson) (32.17–18 mbs), magnification 1x. **32** – *Paltarpites* gr. *paltum* Buckman (39.76–79 mbs), magnification 2x. **33** – *Paltarpites* gr. *paltum* Buckman (41.45 mbs), magnification 1x. **34** – *Amaltheus margaritatus* (de Montfort) (134.32–37 mbs), magnification 1x.

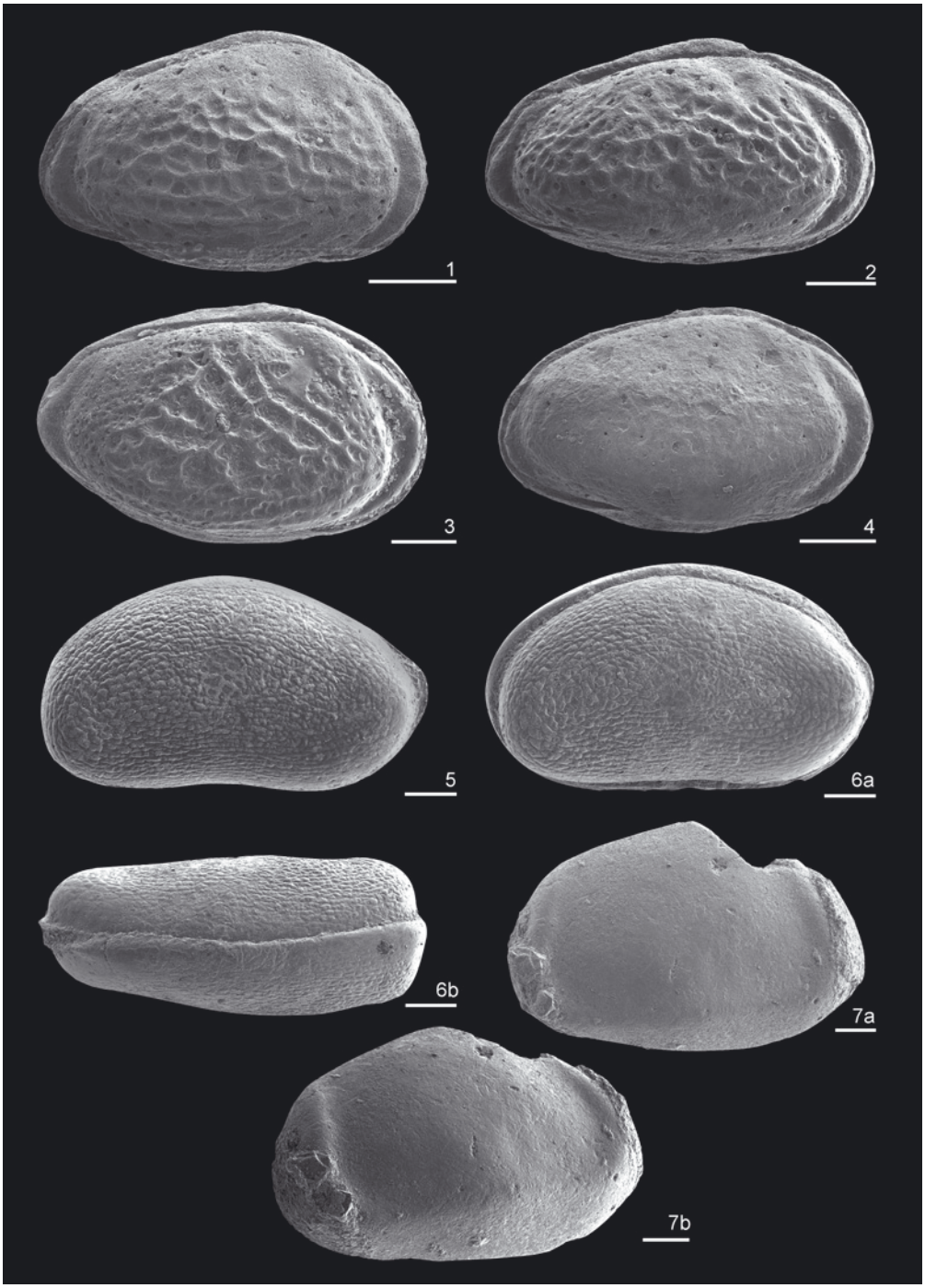

Plate 4. **1–2** – *Kinkelinella triebeli* Klingler & Neuweiler 1959, (1) lateral view of ♂ carapace, F 110354, 274.5–274.8 mbs, BGR SEM-No. 4644/1, Type-No. 16111; (2) lateral view of ♂ carapace, F 110354, 274.5–274.8 m, BGR SEM-No. 4644/2, Type-No. 16112; **3** – *Kinkelinella vulgaris Klingler & Neuweiler 1959*, lateral view of ♀ carapace, F 110460, 210.9–211.2 mbs, BGR SEM-No. 4644/4, Type-No. 16113; **4** – *Kinkelinella transluscens* Blake 1876, lateral view of ♂ carapace, F 110354, 274.5–274.8 mbs, BGR SEM-No. 4644/3, Type-No. 16114. **5–6b** – *Ogmoconchella* No. 2 Klingler 1962; (5) lateral view of left valve, length/height: 0.73/0.41 mm, F 110335, 136.2–136.7 mbs, BGR SEM-No. 4644/5, Type-No. 16115. (6 a) lateral view of carapace, RV of carapace showing different growth of valves length: 0.78 mm hight: 0.46 mm, F 110335, 136.2–136.7 mbs, BGR SEM-No. 4644/6, Type-No. 16116; (6 b) dorsal view of carapace, F 110335, 136.2–136.7 mbs, BGR SEM-No. 4644/6, Type-No. 16116; **7 a–7b** – *Ogmoconcha* cf. *ambo* Lord & Moorley 1974. (7 a) lateral view of right valve, F 110445, 58.1–58.3 mbs, BGR SEM-No. 4644/7, Type-No. 16117; (7 b) oblique view of 7 a showing the swelling of the anterior and posterior beads and the convoluted valve. Scale bar 100 µm.

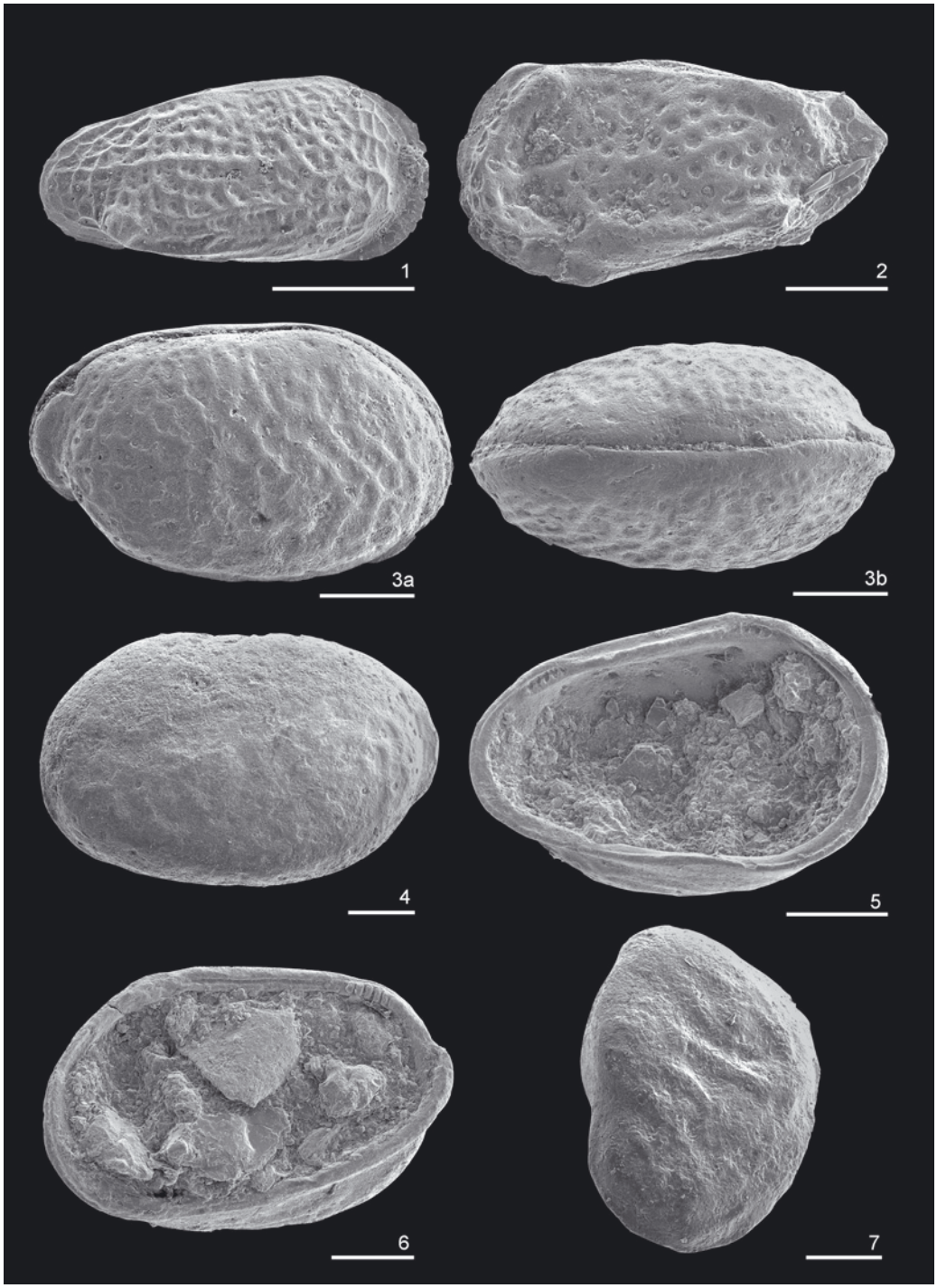

Plate 5. **1** – *Lophodentina tricostata* Michelsen 1975, lateral view of right valve; F 110328; 74.1–74.4 mbs; BGR SEM-No. 4644/8, Type-No. 16118; **2** – *Acrocythere* aff. *troesteri* Riegraf 1984, lateral view of carapace; F 110445, 58.1–58.3 mbs; BGR SEM-No. 4644/8, Type-No. 16119; **3–6** – *Domericythere brandi* gen. et spec. nov; (3 a) holotype, lateral view of carapace, length/height 0.44 mm/0.27 mm, F 110445, 58.1–58.3 mbs; BGR SEM-No. 4644/10, Type-No. 16120; (3 b) dorsal view of 3 a, BGR SEM-No. 4644/10; Type-No. 16120; (4) lateral view of left corroded valve, length/height 0.61 mm/ 0.39 mm, F 110445; 58.1–58.3 mbs, BGR SEM-No. 4644/11, Type-No. 16121; (5) inner view of left juvenile valve, length: 0.41 mm height: 0.25 mm; F 110445; 58.1–58.3 mbs; BGR SEM-No. 4644/12, Type-No. 16122; (6) lateral view of right valve, length/height 0.50 mm/0.31 mm, F 110445, 58.1–58.3 m, BGR SEM-No. 4644/13, Type-No. 16123. **7** – *Lenticulina* sp. indet., the test is covered with some oblique, smooth ridges; a possible predecessor of reticulate Lenticulines of the late Toarcian to Bajocian. F 110335, 136.2–136.7 mbs, BGR SEM-No. 4644/14, Type-No. 16124. Scale bar 100 µm.

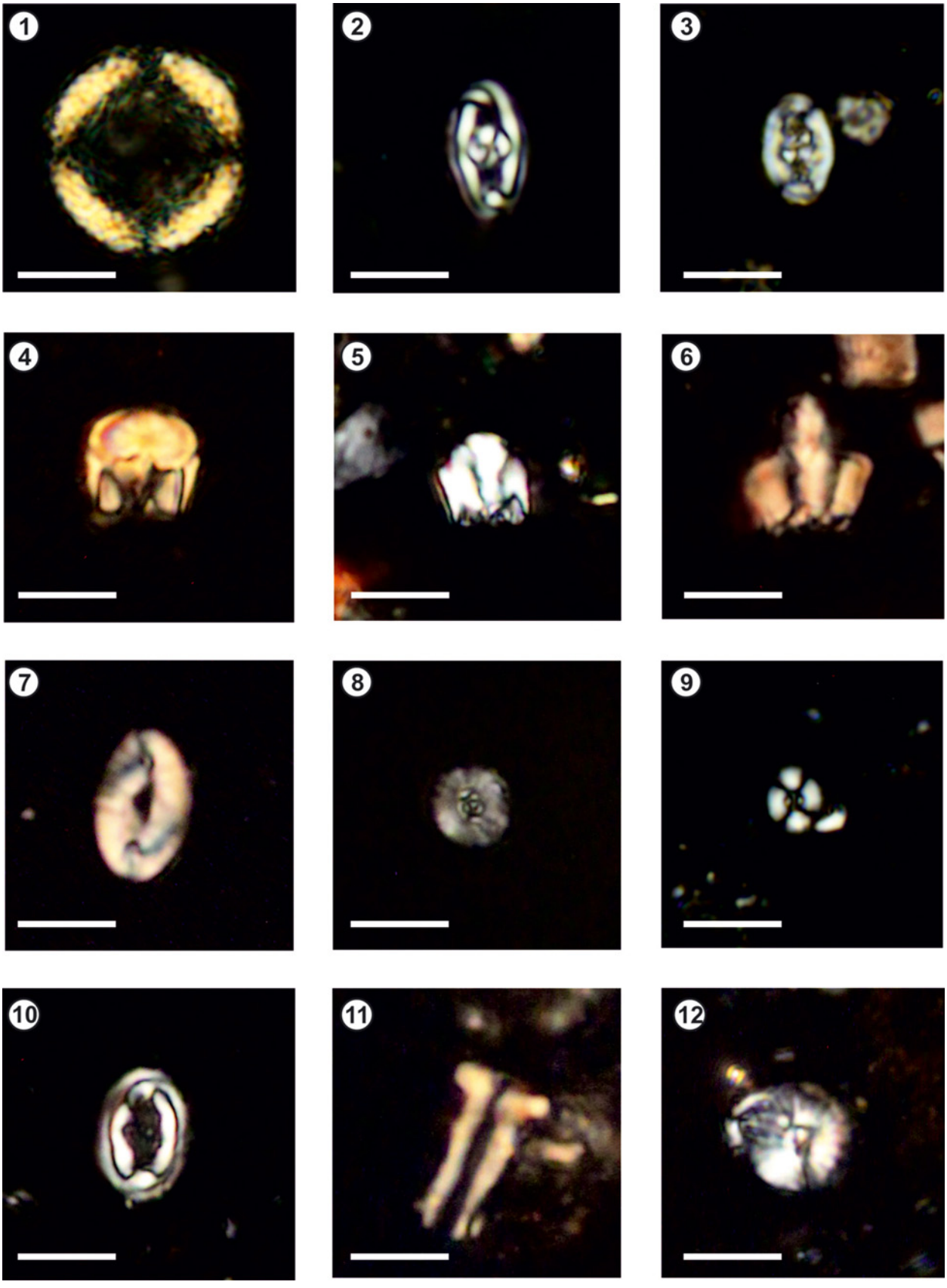

Plate 6. **1** – *Schizosphaerella punctulata* Deflandre & Dangeard 1938. Side view of single disarticulated valve. Sch 145.00 mbs. **2** – *Parhabdolithus liasicus distinctus* Deflandre 1952, Bown 1987. Distal view. Sch 175.00 mbs. **3** – *Crepidolithus pliensbachensis* Crux 1985 *emend.* Bown 1987. Distal view. Sch 176.00 mbs. **4** – *Mitrolithus elegans* Deflandre & Fert 1954. Side view. Sch 166.00 mbs. **5** – *Parhabdolithus robustus* Noël 1965. Side view. Sch 163.00 mbs. **6** – *Parhabdolithus marthae* Deflandre & Fert 1954. Side view. Sch 226.00 mbs. **7** – *Crepidolithus crassus* Deflandre & Fert 1954, Noël 1965. Distal view. Sch 39.00 mbs. **8** – *Similiscutum cruciulus* de Kaenel & Bergen 1993. Distal view. Sch 159.00 mbs. **9** – *Lotharingius hauffii* Grün et al. 1974 *emend.* Goy et al. 1979. Distal view. Sch 25.00 mbs. **10** – *Crepidolithus impontus* (Grün et al. 1974) Goy et al. 1979. Distal view. Sch 124.00 mbs. **11** – *Carinolithus superbus* Deflandre & Fert 1954, Prins in Grün et al. 1974. lateral view. Sch 33.00 mbs. **12** – *Discorhabdus striatus* Moshkovitz & Ehrlich, 1976. Distal view. Sch 18.00 mbs. In all photographs scale bar = 5 µm.

Plate 7. Examples of red lithologies within the Angulata Zone (260.00–254.00 mbs) of the Upper Hettangian. These red laminated beds are not known from other cores and outcrops in the region.

ian boundary at 233.30 mbs, between the first occurrence of the nannofossil *Parhabdolithus liasicus* and the last occurrence of the dinoflagellate cyst *Dapcodinium priscum*.

4.2. Lithology

The Hettangian (318.60–233.30) corresponds to the Angulatenton Formation. The lower part of the Hettangian from 318.60 to 298.00 mbs consists of laminated dark-grey mudstone with intervals that contain paper shales (e. g. around 314.00–312.00 mbs, and between 306.00–305.00 mbs). These paper shales are strongly reminiscent of the Posidonia Shales of Toarcian age. Whereas there are abundant well-preserved palynomorphs present, the macrofossil content is extremely low in the lower 20 metres of the Hettangian, except perhaps for trace fossils that occur throughout. The remainder of the Hettangian succession at Schandelah is for the most part characterized by alternations of silt- and sandstone lenses that are interspersed with organic-rich mudstone and shale. The sandstone layers show signs of reworking, bioturbation, and cross-bedding. Gutter casts are abundant. Fossil content is low throughout the Hettangian, but crinoid stems frequently occur at 274.50 to 274.80 mbs and 259.60 to 260.00 mbs.

A few intervals stand out from the sandstone-mudstone alternations. Starting at 254.80 to 258.65 mbs distinctly red-coloured laminated claystones occur (Plate 7). The transition into and out of these red claystones appears to be gradual, and apart from the colour, the lithology is not strikingly different from under- and overlying dark-grey laminated shales. It remains unclear whether these colour changes are primary or whether they are diagenetic in origin, possibly related to varying redox conditions. A second reddish interval occurs from 238.00 to 234.00 mbs, so just below the Arietes Sandstone. Whether there is a genetic relationship between the coarse-grained sandstone beds and potential oxidation of the shales needs further investigation.

5. The Sinemurian

5.1. Biostratigraphy

The Lower Sinemurian is only evidenced by the presence of the ammonite *Arnioceras* gr. *semicostatum* (Fig. 2), indicating the Semicostatum ammonite Zone. No ammonites from either the Bucklandi or the Turneri Zones were encountered. A hiatus likely exists at the base of the Sinemurian and the Turneri Zone likely is missing completely. Starting at 214.00 mbs, the lower part of the Upper Sinemurian (Obtusum ammonite Zone) is well represented by the presence of *Promicroceras* aff. *precompressum*, *Promicroceras* gr. *planicosta*, and *Xipheroceras trimodum* (Plate 3). The uppermost Sinemurian Raricostatum and Oxynotum ammonite zones are difficult to recognize and only indicated by the presence of *Gleviceras* sp. and *Oxynoticeras* sp. The finding of *Paltechioceras* at 172.00 mbs is indicative of the Raricostatum Zone of the Upper Sinemurian, suggesting that the Pliensbachian-Sinemurian boundary is located at the base of the so-called "Doppelbank" (see also below). The latter species may indicate the Denotatus Subzone.

The base of the Obtusum Zone is also marked by the occurrence of *Kinkelinella laqueata*, which has a very short range around 214.00 mbs (Fig. 3), *Kinkelinella*, is a genus that only evolved into a distinct suite of species during the Late Sinemurian and it is therefore a useful group to distinguish the Upper Sinemurian. The biostratigraphical boundary between the Sinemurian and Pliensbachian in the Schandelah core is characterized by the index ostracods *Gammacythere ubiquita* and *Pleurifera harpa* (175.2–161.2 mbs), which is close to the "Doppelbank".

One of the most significant palynological index species for the Sinemurian is the dinoflagellate cyst *Liasidium variabile*, which has a first occurrence (FO) around 212.00 mbs at the base of the Obtusum Zone. This species is possibly invasive into the European Epicontinental Seaway and may have migrated from the palaeo-Pacific during the opening of the Hispanic Corridor in the Late Sinemurian (van de Schootbrugge et al. 2005). *Liasidium variabile* has a range that is restricted to the Upper Sinemurian Obtusum and Oxynotum Zones (Feist-Burkhardt and Pross 2009). It has a LO in the Schandelah core at 182.00 mbs, and based on the available ammonite zonation, it would thus range from the Obtusum Zone into the Oxynotum Zone.

The FO of *Parhabdolithus robustus* at 214.00 mbs can be considered as a good indicator for defining the Lower to Upper Sinemurian boundary, in accordance with the FO of *Liasidium variabile* as well as ammonites belonging to the Obtusum Zone. The NJ2 P. liasicus calcareous nannofossil Zone is divided into two subzones, NJ2 a Parhabdolithus marthae and NJ2 b M. elegans subzones, based on the LO of *P. marthae*. In

Plate 8. Examples of typical lithological features of the Sinemurian and Hettangian. Core section 306.00–308.00 mbs**:** Example of laminated dark grey shales at the base of the Hettangian. Part of this core section was not cut in order to preserve the integrity of the core. Core section 262.00–264.00 mbs: Example of lithofacies from the base of the Angulata Zone (Hettangian) showing part of the "Angulaten Sandstein" and organic-rich beds alternating with sandy storm deposits (heterolithic facies). This facies is abundant throughout the Hettangian starting at 292.00 mbs. Core section 232.00–234.00 mbs: Lithology at the base of the Sinemurian showing the "Arieten Sandstein". This coarse-grained sandstone bed is a hardground with abundant bivalves assigned to *Gryphaea* at the top and is intensely bioturbated throughout.

contrast, Bown and Cooper (1998) identified the LO of *P. marthae* earlier within the Lower Sinemurian Semicostatum Zone in NW Europe. The most important nannofossil marker for the Sinemurian stage is *Crepidolithus crassus*, which first occurs at 176.00 mbs. This event defines the base of the NJ3 Crepidolithus crassus calcareous nannofossil Zone.

5.2. Lithology

The entire Lower Sinemurian is characterized by a facies that is strongly reminiscent of the Toarcian paper shales, with generally well laminated black to dark grey shales and claystones. The basal part is known as the Arietenton Fm, which is overlain by the Obtususton

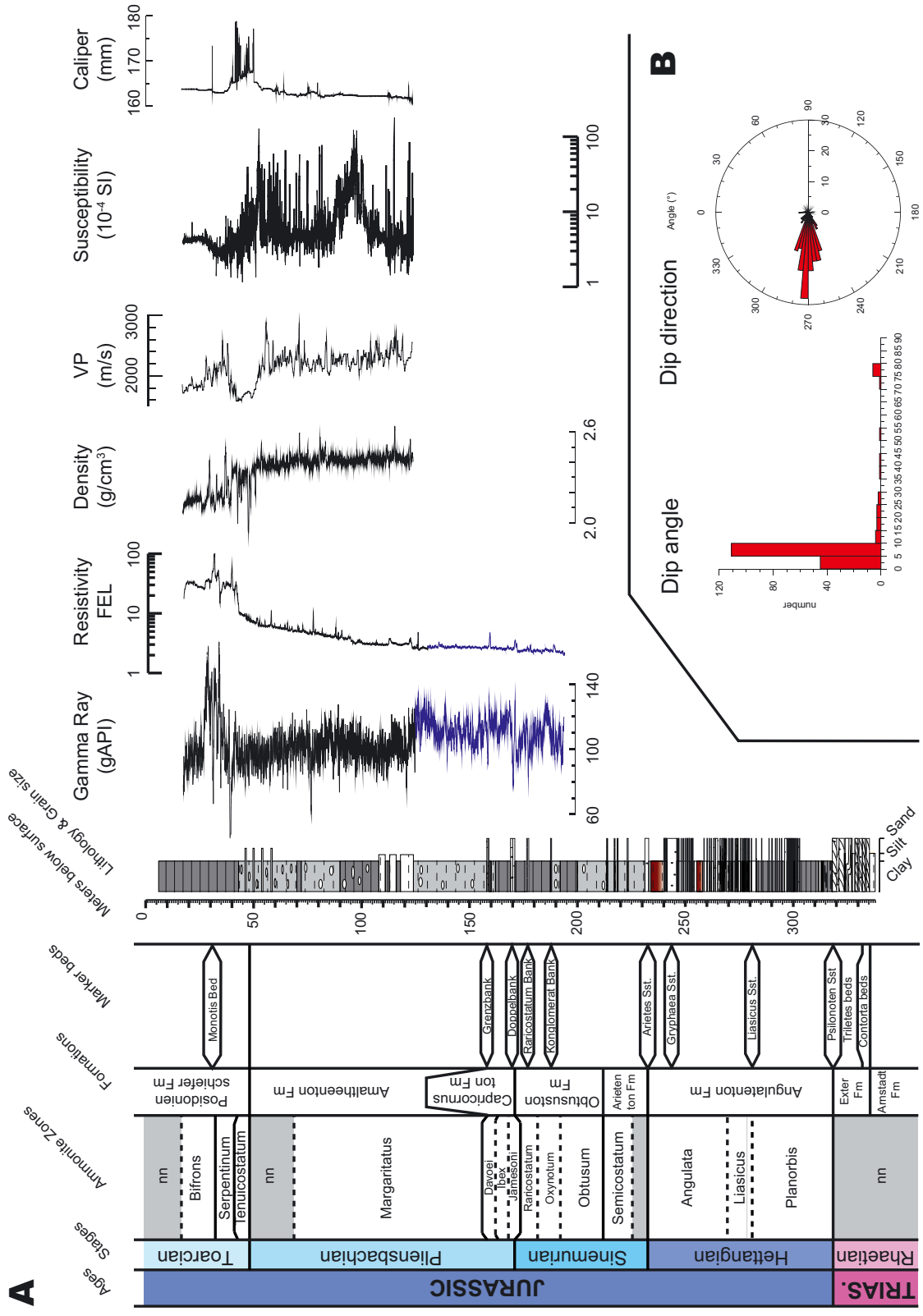

Fig. 4. (A) Geophysical downhole measurements for the interval 0–194 mbs. The following parameters are plotted (left to right): natural radioactivity (GR), resistivity (Rdeep), density (DENS), p-wave velocity (VP), magnetic susceptibility (SUSC), and borehole diameter (CALI). Data above 132 mbs were measured by LIAG, those below 132 mbs by Tegtmeyer Geophysik. (B) Interpretation of sediment layers observed in the dipmeter log (depth section 20–130 mbs). The histogram shows the dip values (5°–10°) and the rosette-diagram the main strike direction of this interval (270°–275°).

20190916-124004
A17159/29840/83D368CB

Fm. The very base of the Sinemurian (233.30 to 230.20 mbs) consists of two hardground beds that are separated by a grey claystone. Both hardgrounds consist of calcareous sandstone and are heavily bioturbated at their tops, containing abundant *Gryphaea*. This double hardground corresponds to the "Arietes Sandstone" marking the boundary between the Hettangian and Sinemurian (Plate 8).

A further regional marker bed occurs from 188.10 to 187.70 mbs (Fig. 5). Due to its conglomeratic nature it is known as the "Konglomerat Bank", which occurs within the Oxynotum Zone. From 177.27 to 176.94 mbs a conglomeratic sandy limestone occurs that appears heavily bioturbated and is indurated. The matrix of this bed consists of bioclasts (small pieces of broken bivalves), siderite nodules, pale-brown coloured bioclastic limestone clasts, some lignitic fragments, green limestone clasts, and grey sparite. This bed is identified as the "Raricostatum Bank" and serves as a regional marker bed (Fig. 2, 5). Both the Konglomerat Bank (187.7–188.1 mbs) and the Raricostatum Bank (176.9–177.3 mbs) are clearly visible in the gamma ray (GR) log (Fig. 4).

6. The Pliensbachian

6.1. Biostratigraphy

A significant marker species was identified at 170.20 mbs as belonging to the diagnostic genus *Uptonia*, marking the Jamesoni Subzone of the lowermost Pliensbachian Jamesoni Zone. The presence of ?*Radstockiceras* at 161.65 mbs could indicate the presence of the Ibex Zone although it is not a good marker. The Upper Pliensbachian starts at the base of a condensed bed (hardground) at 158.51–61 mbs containing *Oistoceras* sp., indicating the topmost Lower Pliensbachian. It corresponds to the Figulinum Subzone (upper part of Davoei Zone). The fauna of the hardground is probably mixed because sections of *Amaltheus* and *Oistoceras* could be observed. In addition, *Amauroceras ferrugineum* (Margaritatus Zone; pers. comm. 2008, Alain Morard) was found at 157.97 mbs. The Upper Pliensbachian, more specifically the Margaritatus Zone, is indicated by the presence of several Amaltheidae: *Amaltheus subnodosus*, *Amaltheus margaritatus*, *Amaltheus margaritatus gibbosus*, *Amauroceras* aff. *wertheri*, and *Amauroceras* gr. *ferrugineum*. The interval from 68.00 to 43.00 mbs does not contain any ammonites, but likely corresponds largely to the Spinatum Zone.

Within the Pliensbachian the ostracod fauna is more diverse, and smooth-shelled ostracods are very common. The genera *Ogmoconcha* and *Ogmoconchella* radiated with several species, which are often difficult to identify without using biometric analyses. Besides the smooth-shelled ostracods, reticulate ostracod species, like *Trachycythere* and the small-sized ostracod *Nanacythere,* are common in the residues of the Pliensbachian part of the core. One specimen determined as *Ogmoconcha* aff. *ambo*, which was previously only known from Southern Germany, could be isolated from a carbonate rich residue. A very rare but well-preserved species *Ogmoconchella* sp. no. 2 was encountered at 132.2–132.7 mbs. This species is also known from the Danish Basin (Michelsen 1975). A new genus and species is described (see Appendix) as *Domericythere brandi* gen. et sp. nov. from 58.00 mbs.

At the base of the Upper Pliensbachian (Margaritatus Zone) an influx of dinoflagellate species, particularly species belonging to the *Nannoceratopsis*–group, is observed. *Nannoceratopsis* is continuously present throughout the Upper Pliensbachian and part of the Toarcian. A general increase in abundance (First Common Occurrence) of *Nannoceratopsis* is observed throughout the uppermost part of the Upper Pliensbachian, starting at around 72.00 mbs, possibly coinciding with the base of the Spinatum Zone. The index species *Luehndea spinosa* first appears within the lower part of the Margaritatus Zone and disappears at the top of the lowermost Toarcian Tenuicostatum Zone (42.90 mbs) with the onset of widespread anoxia during this time interval.

The FO of *Similiscutum cruciulus* is located at 166.00 mbs, in the range of the Lower Pliensbachian Jamesoni-Ibex Zones boundary, marking the base of the NJ4 S. cruciulus calcareous nannofossil Zone. This zone is subdivided into two subzones, NJ4 a C. pliensbachensis and NJ4 b Crepidolithus granulatus, on the basis of the LO of *P. robustus*. In the Schandelah core, this event occurs at 163.00 mbs, at the boundary between the Lower Pliensbachian Ibex and Davoei Zones. The FO of the index species *Lotharingius hauffii* occurs at 158.00 mbs in the lowermost part of the Upper Pliensbachian Margaritatus Zone. This event defines the base of the NJ5 Lotharingius hauffii calcareous nannofossil Zone. In the Schandelah core, the FO of *Biscutum finchii* is also located at 158.00 mbs. The species *Lotharingius sigillatus* first

occurs at 148.00 mbs, within the Margaritatus Zone. The FO of *L. sigillatus* in the Schandelah core is earlier compared to NW Europe (Bown and Cooper 1998), Portugal (Veiga de Oliveira et al. 2007) and N Spain (Perilli et al. 2010, Fraguas 2011), where this event lies within the Spinatum Zone. The NJ5 Lotharingius hauffii calcareous nannofossil Zone is divided into two subzones, NJ5 a B. finchii and NJ5 b Crepidolithus impontus, based on the FO of *C. impontus*. In the Schandelah core, *C. impontus* appears at 136.00 mbs, within the Margaritatus Zone, whereas in NW Europe (Bown and Cooper 1998) this species first occurs within the Spinatum Zone. The LO of *Crucirhabdus primulus* is located at 106.00 mbs, below the Margaritatus-Spinatum Zones boundary. However, Bown and Cooper (1998) identified this event around the Pliensbachian-Toarcian boundary in NW Europe.

6.2. Lithology

The base of the Pliensbachian is formed by the so-called "Doppelbank" (Figs. 2, 5), which consists of a sandy limestone bed (171.00 to 169.70 mbs) rich in belemnites, bivalves and some ammonites. Based on the presence of the ammonite genus *Uptonia*, this bed can be assigned to the Sinemurian-Pliensbachian-boundary. At 170.65 mbs a lignitic fragment could be recognized. This bed is heavily bioturbated. From 169.70 to 158.85 mbs laminated black shale dominates. These shales contain common pyrite nodules, for example at 163.22 mbs. In addition, large brownish micritic, possibly sideritic, limestone concretions occur at numerous levels, for example at 158.90, 162.90 and 166.30 mbs. From 158.40 to 158.85 a massive limestone bed occurs that contains abundant ammonites in its upper half and abundant large thin-shelled bivalve remains, possibly *Pecten*, in its lower half. The two condensed beds appear to be separated by a thin marl veneer. This bed could be identified as the "Grenzbank" or "Davoei-Bank" marking the boundary between the Lower and Upper Pliensbachian (Fig. 2). Although the ammonites are clearly visible in cross-section, having accurate determinations would require extensive preparation leading to complete destruction of the main fabric of the rock. However, this bed is well-known from previous work by Hoffmann and Jordan (1982), who showed the presence of ammonites belonging to both the Davoei and Margaritatus Zones. Both the *Doppelbank* (169.70–171.00 mbs; Fig. 5) and the *Grenzbank* (158.4–158.9 mbs), marking the Sinemurian-Pliensbachian as well as the Upper–Lower Pliensbachian boundaries, respectively, are also easy to detect in the gamma ray log (GR; Fig. 4).

The Upper Pliensbachian consists from 158.40 to 48.00 mbs of more than 110 metres of monotonous grey to dark grey marly claystone with shale partings and interspersed tempestitic beds. The Upper Pliensbachian Margaritatus Zone extends from 158.40 to 68.70 mbs and is therefore the most expanded interval in the entire Lower Jurassic succession at Schandelah. From 158.40 to 122.70 mbs the lithology changes to dark grey calcareous shale containing abundant bivalve remains and dispersed pyrite. Ammonite remains consist mostly of *Amaltheus margaritatus*. From 122.70 to 105.85 mbs dark-grey shales occur that are devoid of concretions. Macrofaunal remains are generally rare and consist mostly of bivalves. From 105.85 to 100.40 mbs dark grey laminated shales occur that contain numerous large pyrite nodules (0.5 to 4 cm). From 92.00 to 68.70 mbs dark grey shales with thin limestone beds and large concretions occur. Dispersed pyrite nodules of several centimetres in diameter occur irregularly throughout this interval. It is likely that this part represents the Gibbosus Subzone, the uppermost Subzone of the Margaritatus Zone, in analogy to similar occurrences of authigenic carbonates that characterize this Subzone in other NW European basins (see for example discussion in van de Schootbrugge et al. (2010). Of particular interest in this respect is the occurrence of glendonites at several horizons within this interval. These ikaite pseudomorphs are generally small (1–2 cm) bipyramidal calcite crystals, and mostly occur within limestone concretions (Plates 9, 10). At numerous levels "calcite beef" replaces the original matrix. In the magnetic susceptibility (SUSC) data, the interval from 95.00 to 110.00 mbs is remarkable (Fig. 4), since the increased values are not linked with any obvious lithological changes. In the interval 100.40 to 105.90 mbs laminated shale occurs with numerous large pyrite nodules, but this finding does not explain the enhanced susceptibility values in the complete section. One could speculate that these elevated values reflect different sediment provenances during this time.

The interval from 68.70 to 48.00 mbs likely corresponds to the uppermost Pliensbachian Spinatum Zone, although the lower boundary for this zone could also be placed lower down, at around 72.00 mbs, where a general decrease in benthic meio- and microfauna is observed (e. g. ostracods and benthic foraminifers). The latter position would more closely match the last occurrence of amaltheid ammonites around

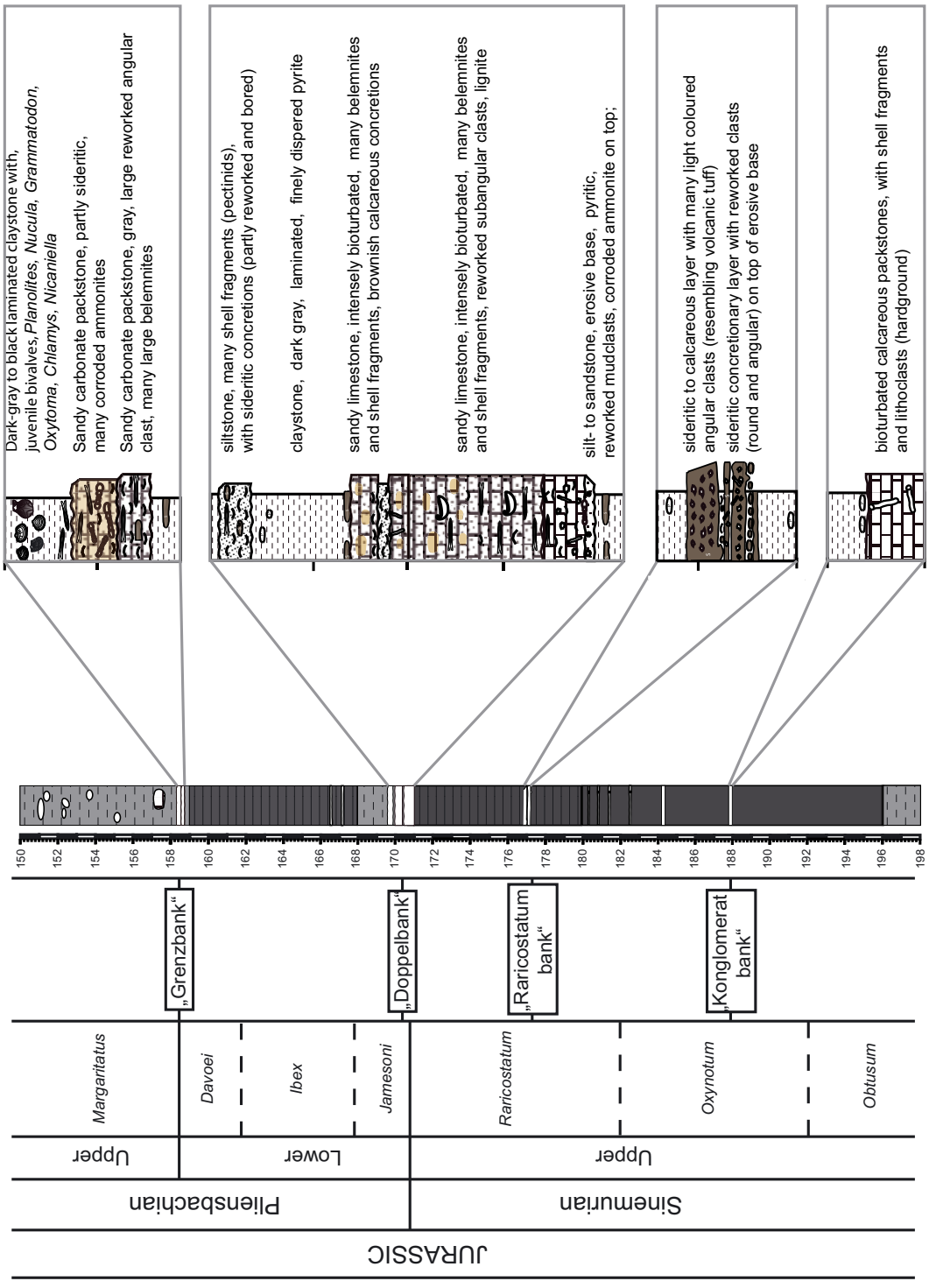

Fig. 5. Detailed log for the Sinemurian to Pliensbachian transition. The interval from 198–150 mbs contains four marker horizons. The "Konglomerat-bank" occurs in the Oxynotum Zone and is a submarine hardground with borings and calcareous lithoclasts. The "Raricostatum-bank" occurs within the Raricostatum Zone and is characterized by sideritic angular clasts, resembling an intraformational brecciated hardground. The so-called "Doppelbank" straddles the Sinemurian-Pliensbachian boundary and consists of sandy limestone with abundant fossils (bivalves, ammonites). It consists of a thicker bed and a thin bed that are separated by a laminated pyrite-rich dark grey claystone. A fourth hardground is known as the "Grenzbank", and forms the boundary between the Lower and Upper Pliensbachian. In addition to bivalves, it contains many large belemnites.

Plate 9. Examples of typical lithological features of the Toarcian, Pliensbachian and Sinemurian (from left to right). Core section 30.00–32.00 mbs: Example of laminated paper shales of Toarcian age. Within this section of the Toarcian, several calcareous beds can be recognized that have wavy laminations. The unique nature of these beds suggest that these represent the so-called "Monotis Bed" that marks the base of the Bifrons Zone. Core section 78.00–80.00 mbs: Lithofacies of the Upper Pliensbachian Margaritatus Zone. This part of the Pliensbachian is very rich in carbonate concretions with complex diagenetic histories. A zoned septarian nodule is present at 79.55 mbs, which is likely sideritic. Other more tabular concretions occur dispersed throughout this core section. Core section 186.00–188.00 mbs: Example of lithological variations in the Sinemurian. A 30 cm thick hardground bed containing lithoclasts occurs at 187.70 mbs and was identified as the Upper Sinemurian "Konglomerat-bank" (Oxynotum Zone).

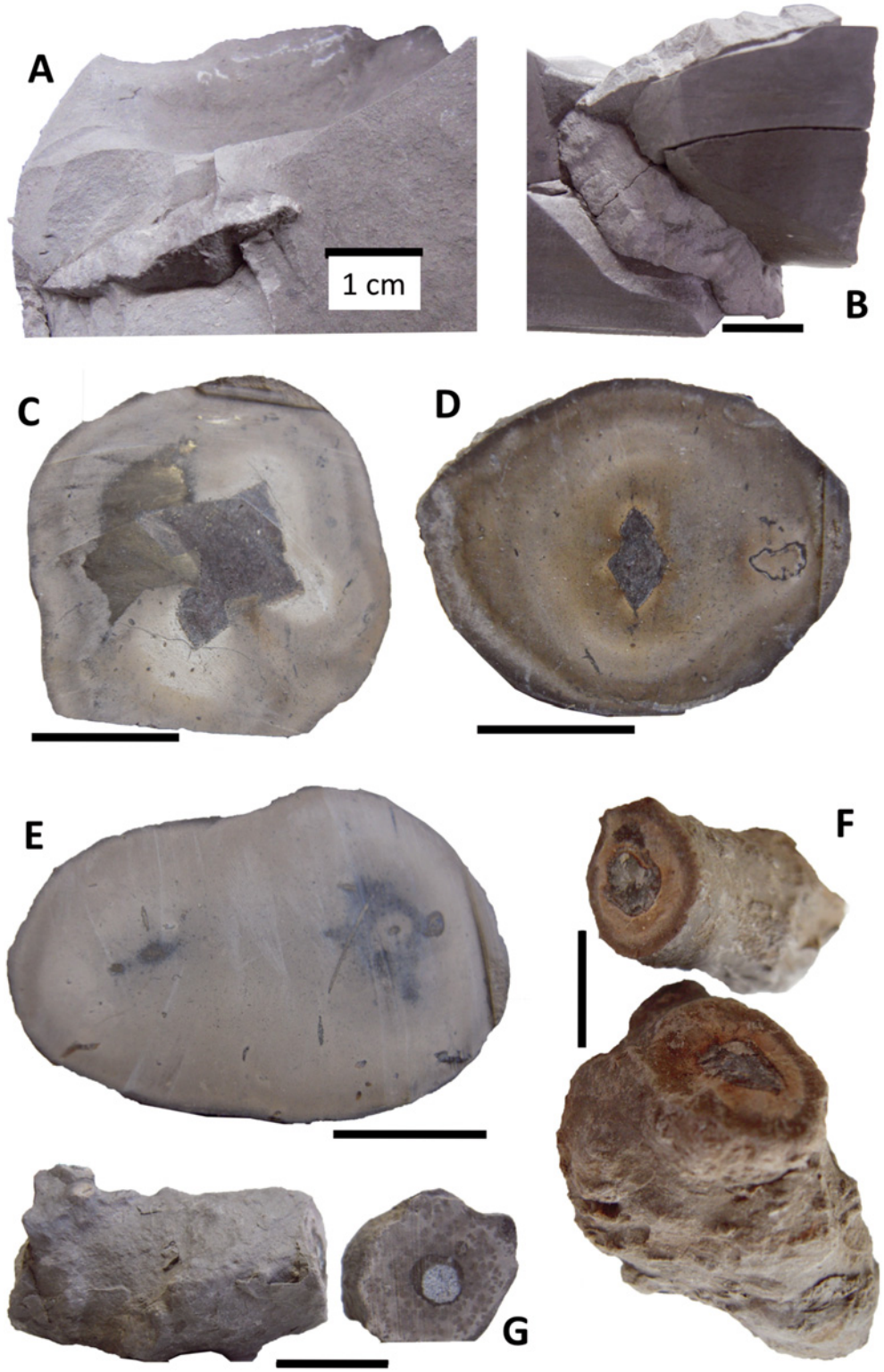

Plate 10. Examples of glendonites, glendonites within concretions, and type-I and type-II concretions. **1–2** – Individual glendonite crystals dispersed within the sediment. (1) Sample from 93.70 mbs. (2) Sample from 93.78 mbs. **3–4** – Glendonites within carbonate concretions. (3) Sample from 93.38 mbs. (4) Sample from 95.44 mbs. **5** – Type-I concretion. Sample from 91.77 mbs. **6** – Type-II concretion. Sample from 98.78 mbs. **7** – Type-II concretion, small tubular concretion possibly around burrow. Sample from 95.30 mbs.

69.00 mbs. Here, the boundary between the Spinatum and Margaritatus Zones is provisionally placed at 68.70 mbs. From 65.00 to 48.00 mbs grey shales with interspersed cm-thick sandy limestone beds dominate, which may have a tempestitic origin. Bioturbation is mainly in the form of *Planolites*. Between 65.00 and 58.00 mbs limestone concretions occur that contain septarian infillings.

7. The Toarcian

7.1. Biostratigraphy

The entire Toarcian interval is relatively rich in ammonites. Several specimens of *Dactylioceras* (*Dactylioceras* aff. *semicelatum*, *D. tenuicostatum* and *Paltarpites* gr. *paltum*) occur around 43.00 mbs and represent the Tenuicostatum Zone. *Paltarpites* gr. *paltum* is an index species of the Paltum Subzone, which is the first subzone of the Toarcian. *Dactylioceras* aff. *semicelatum* is the index species of the Semicelatum Subzone. At 5.60 mbs an ammonite was recovered belonging to the *Pseudogrammoceras* or *Pleydellia* group. In either case, this ammonite characterizes the Upper Toarcian.

Within the uppermost Pliensbachian and entire Toarcian ostracods and benthic foraminifers are absent. The Toarcian palynological assemblage is dominated by amorphous organic matter, which masks other structured palynomorphs of stratigraphic value. One key dinoflagellate cyst species, *Luehndea spinosa* has a last occurrence at 42.90 mbs at the boundary between the Tenuicostatum/Falciferum Zones. This event is synchronous across NW European basins and is related to the onset of extreme anoxia related to the Toarcian OAE (Bucefalo Palliani and Riding 1999).

A sharp decrease of the nannofossil species *Schizosphaerella punctulata* is observed slightly above the Toarcian-Pliensbachian boundary, which likely marks the "*Schizosphaerella* crisis" described in different European basins (Bucefalo Palliani and Riding 2002, Erba 2005, Mattioli et al. 2004, Tremolada et al. 2005, van de Schootbrugge et al. 2005, Mattioli et al. 2008, Suan et al. 2008, Fraguas et al. 2012). The first Toarcian biostratigraphic marker is *Carinolithus superbus*, which first occurs at 34.00 mbs, within the Serpentinum Zone. This event defines the base of the NJ6 *Carinolithus superbus* calcareous nannofossil Zone. Following Bown and Cooper (1998) the FO of *C. superbus* occurs within the boreal Falciferum Zone that roughly corresponds to the Tethyan Serpentinum Zone (Perilli et al. 2010). The FO of *Discorhabdus striatus* is located at 25.00 mbs, within the Bifrons Zone. This event marks the beginning of the NJ7 Discorhabdus striatus calcareous nannofossil Zone. This FO of *D. striatus* in the Schandelah core is slightly younger than the FO proposed by Bown and Cooper (1998) for the same species. They recognized this event at the Falciferum-Bifrons zonal boundary.

7.2. Lithology

The Toarcian extends from 48.00 to 5.50 mbs and consists primarily of laminated organic-rich shale in "Posidonienschiefer"-style facies, i. e. paper shales (Fig. 2; Plate 9). The entire Toarcian interval is extremely rich in fish remains, ranging from scales to small bones and teeth. In addition, bivalves are common, notably *Bositra, Pseudomytiloides*, and *Meleagrinella*. The Lower Toarcian, with its three ammonite zones (Tenuicostatum, Serpentinum, and Bifrons) extends from from 48.00 to 17.00 mbs. The Pliensbachian-Toarcian boundary at 48.00 mbs appears gradual, transitioning from claystone with sandstone stringers to laminated shale rich in pyritic burrows. Non-deposition and/or erosion of the uppermost Subzone of the Spinatum Zone and a major part of the Tenuicostatum Zone is widespread across the European Epicontinental Seaway (see e. g. Guex et al. 2001), but no clear evidence of any hiatus was observed in the Schandelah core. The boundary between the Tenuicostatum and Serpentinum Zones is placed at 42.90 mbs at the last occurrence of the dinoflagellate cyst *L. spinosa* and the onset of a large negative C-isotope excursion (see also below). The disappearance of the dinoflagellate cyst species *L. spinosa* at 42.90 mbs suggests that the Tenuicostatum Zone is represented by about 5 metres of sediment. These 5 metres differ clearly from the overlying Posidonienschiefer Fm. as they are strongly bioturbated and show abundant pyrite-filled burrows. The GR-, Rdeep-, DENS-, and SUSC-curves show clear changes around 42.00 mbs, which coincides with the start of black shale deposition of the Toarcian Oceanic Anoxic Event. The base of the Bifrons Zone coincides with the "Monotis Bank" (31.25–31.70 mbs), which is a regional marker bed (Schmitz 1980). This bed consists of at least two thinner intervals that are enriched in carbonate and show a peculiar wavy lamination (see also Plate 9).

A lithological change is observed at 17.00 mbs, marking the Lower-Upper Toarcian boundary. The Upper Toarcian likely extends from 17.00 to 5.50 mbs, but no further subdivision is possible based on the available data. From 17.00 to 14.50 mbs dark grey laminated shales occur that appear finer grained than the overlying shale. In this interval finely disseminated pyrite occurs and the fresh cores smelled strongly of sulphur. From 14.50 to 9.50 mbs dark grey laminated shales with minor quartz and pyrite occur. The quartz in this interval appears more fine-grained than in the previous interval. From 9.50 to 5.50 mbs the sediments consist of dark grey laminated organic-rich shale with minor amounts of quartz (lutite). At 7.70 mbs large pyrite nodules could be observed. The topmost 5.50 m of the core were destroyed due to destructive drilling and could not be recovered.

8. Carbon isotope record

The organic carbon isotope record from the Schandelah-1 core is based on 485 data points and represents a new chemostratigraphic reference curve for the Lower Jurassic in the Lower Saxony Basin (Table 1). Chemostratigraphy based on the organic and carbonate carbon isotopes uses positive and negative excursions for the correlation of sedimentary successions across basins and in between basins. In combination with biostratigraphy it is a powerful tool for precise high-resolution correlations in particular in Mesozoic successions (Jenkyns 2002). The range of organic carbon isotope values of the Schandelah-1 core is typical for Mesozoic hemipelagic marlstones (e. g. Galli et al. 2007, Hesselbo et al. 2007; Fig. 6). The $\delta^{13}C_{org}$ values vary between –34.0 and –23.0 ‰ (V-PDB). The stratigraphic reproducibility of the structure of the $\delta^{13}C_{org}$ records from coeval marine environments and terrestrial sections of the Rhaetian/Hettangian boundary and as well as the Upper Pliensbachian to Toarcian interval corroborates the view that the $\delta^{13}C_{org}$ values measured are primary in nature, and thus suitable for $\delta^{13}C_{org}$ stratigraphy.

Table 1. Schandelah Core organic carbon isotopes.

Sample	depth (m)	$\delta^{13}C_{org}$ (VPDB)
SCH	5.30	–29.57
SCH	6.00	–29.42
SCH	7.00	–29.30
SCH	11.00	–29.47
SCH	12.10	–29.56
SCH	13.00	–29.19
SCH	14.00	–29.20
SCH	15.00	–29.36
SCH	16.00	–29.17
SCH	17.00	–29.25
SCH	20.00	–29.38
SCH	20.60	–29.81
SCH	22.00	–29.40
SCH	23.00	–29.25
SCH	24.00	–29.49
SCH	25.00	–29.70
SCH	26.00	–29.47
SCH	26.00	–29.59
SCH	28.00	–28.30
SCH	28.00	–28.99
SCH	29.00	–28.66
SCH	29.70	–29.71
SCH	31.00	–28.99
SCH	32.00	–29.65
SCH	33.20	–29.27
SCH	34.00	–29.26
SCH	34.40	–28.95
SCH	35.00	–28.69
SCH	36.00	–29.28
SCH	36.30	–28.82
SCH	36.50	–28.64
SCH	36.90	–28.65
SCH	37.00	–28.67
SCH	37.40	–28.70
SCH	37.70	–28.36
SCH	38.00	–28.23
SCH	38.30	–28.44
SCH	38.70	–28.05
SCH	39.40	–27.39
SCH	39.90	–26.70
SCH	40.00	–26.16
SCH	40.10	–27.51
SCH	40.20	–27.69
SCH	40.30	–28.35
SCH	40.40	–27.87
SCH	40.50	–28.63
SCH	40.60	–28.49
SCH	40.70	–29.91
SCH	40.80	–29.84
SCH	40.90	–31.30
SCH	41.00	–31.49
SCH	41.00	–31.33
SCH	41.10	–30.83
SCH	41.20	–32.31
SCH	41.30	–31.71
SCH	41.40	–31.72
SCH	41.50	–32.74
SCH	41.60	–32.29
SCH	41.70	–32.11
SCH	41.80	–32.38

Sample	depth (m)	$\delta^{13}C_{org}$ (VPDB)
SCH	41.90	–33.03
SCH	42.00	–31.52
SCH	42.10	–33.20
SCH	42.20	–30.31
SCH	42.30	–32.82
SCH	42.40	–28.69
SCH	42.50	–29.92
SCH	42.60	–27.97
SCH	42.70	–28.98
SCH	42.80	–27.59
SCH	43.10	–25.98
SCH	43.20	–26.05
SCH	43.30	–26.63
SCH	43.40	–25.67
SCH	43.50	–26.07
SCH	43.60	–26.00
SCH	43.70	–26.00
SCH	43.80	–26.85
SCH	43.90	–25.77
SCH	44.00	–25.60
SCH	44.10	–26.19
SCH	44.20	–26.17
SCH	44.30	–25.87
SCH	44.40	–26.38
SCH	44.50	–25.97
SCH	44.60	–26.05
SCH	44.70	–25.95
SCH	44.90	–26.01
SCH	45.00	–25.98
SCH	45.10	–25.56
SCH	45.20	–26.03
SCH	45.30	–26.42
SCH	45.50	–25.78
SCH	45.60	–26.14
SCH	45.70	–26.10
SCH	45.80	–25.48
SCH	46.00	–26.26
SCH	46.10	–25.89
SCH	46.20	–26.04
SCH	46.30	–25.64
SCH	46.40	–26.13
SCH	46.50	–25.97
SCH	46.60	–26.57
SCH	46.80	–26.08
SCH	47.00	–26.16
SCH	47.00	–26.14
SCH	47.30	–26.20
SCH	47.50	–26.31
SCH	48.00	–25.82
SCH	50.00	–25.80
SCH	51.00	–26.10
SCH	53.00	–25.99
SCH	55.00	–26.23
SCH	56.00	–25.86
SCH	57.00	–26.28
SCH	61.00	–26.36
SCH	63.00	–26.27
SCH	64.00	–26.32
SCH	65.00	–26.19
SCH	66.00	–25.79
SCH	66.00	–26.27
SCH	67.00	–25.88
SCH	68.00	–25.75
SCH	69.00	–25.83
SCH	69.00	–26.03
SCH	70.00	–25.52
SCH	71.00	–25.73
SCH	72.00	–25.55
SCH	74.00	–25.21
SCH	75.00	–25.34
SCH	76.00	–25.12
SCH	77.00	–25.09
SCH	78.00	–25.76
SCH	79.00	–25.31
SCH	80.00	–25.54
SCH	81.00	–25.26
SCH	82.00	–25.95
SCH	83.00	–25.53
SCH	84.00	–25.24
SCH	85.00	–25.30
SCH	85.00	–25.25
SCH	86.00	–25.02
SCH	88.00	–25.41
SCH	89.00	–24.89
SCH	90.00	–25.15
SCH	91.00	–26.10
SCH	92.00	–25.01
SCH	93.00	–25.23
SCH	94.00	–25.57
SCH	95.00	–25.94
SCH	96.00	–25.42
SCH	97.00	–25.11
SCH	98.00	–25.05
SCH	99.00	–25.16
SCH	100.00	–24.95
SCH	101.00	–25.05
SCH	102.00	–25.11
SCH	103.00	–25.11
SCH	104.00	–25.05
SCH	105.00	–25.10
SCH	106.00	–25.18
SCH	106.00	–25.24
SCH	107.00	–25.30
SCH	108.00	–24.91
SCH	109.00	–25.30
SCH	110.00	–25.08
SCH	111.00	–25.24
SCH	112.00	–25.03
SCH	113.00	–25.07
SCH	114.00	–24.65

Sample	depth (m)	$\delta^{13}C_{org}$ (VPDB)
SCH	115.00	–24.74
SCH	115.00	–24.58
SCH	116.00	–24.50
SCH	117.00	–24.18
SCH	118.00	–24.41
SCH	119.00	–24.28
SCH	120.00	–24.37
SCH	121.00	–24.37
SCH	122.00	–24.22
SCH	123.00	–24.56
SCH	124.00	–24.56
SCH	124.00	–24.57
SCH	125.00	–25.52
SCH	126.00	–25.84
SCH	127.00	–25.52
SCH	128.00	–25.48
SCH	129.00	–26.00
SCH	130.00	–25.87
SCH	131.00	–25.58
SCH	132.00	–25.36
SCH	133.00	–25.57
SCH	134.00	–25.72
SCH	134.00	–25.70
SCH	135.00	–26.01
SCH	136.00	–26.12
SCH	137.00	–25.63
SCH	138.00	–25.65
SCH	139.00	–25.60
SCH	140.00	–25.78
SCH	141.00	–25.88
SCH	142.00	–25.92
SCH	143.00	–25.83
SCH	144.00	–25.63
SCH	145.00	–25.97
SCH	145.00	–25.98
SCH	146.00	–25.93
SCH	147.00	–25.70
SCH	148.00	–25.72
SCH	149.00	–25.78
SCH	150.00	–25.27
SCH	151.00	–25.37
SCH	152.00	–25.75
SCH	153.00	–25.27
SCH	154.00	–25.59
SCH	155.00	–25.69
SCH	155.00	–25.70
SCH	156.00	–25.73
SCH	157.00	–25.31
SCH	158.00	–25.27
SCH	159.00	–25.76
SCH	160.00	–25.76
SCH	161.00	–25.86
SCH	162.00	–26.06
SCH	163.00	–26.05
SCH	164.00	–26.08
SCH	165.00	–26.04
SCH	165.00	–26.00
SCH	166.00	–26.15
SCH	167.00	–26.10
SCH	168.00	–25.99
SCH	169.00	–25.99
SCH	170.00	–26.13
SCH	171.00	–25.50
SCH	172.00	–25.53
SCH	173.00	–25.59
SCH	174.00	–25.31
SCH	175.00	–25.53
SCH	176.00	–25.58
SCH	177.00	–25.96
SCH	178.00	–24.24
SCH	179.00	–24.23
SCH	180.00	–24.71
SCH	181.00	–24.75
SCH	182.00	–24.72
SCH	183.00	–24.48
SCH	184.00	–25.48
SCH	185.00	–27.24
SCH	186.00	–25.37
SCH	187.00	–25.32
SCH	188.00	–25.13
SCH	189.00	–25.15
SCH	190.00	–25.29
SCH	191.00	–25.15
SCH	192.00	–24.97
SCH	193.00	–25.05
SCH	194.00	–25.73
SCH	195.00	–24.95
SCH	196.00	–24.94
SCH	197.00	–24.77
SCH	198.00	–25.11
SCH	199.00	–25.06
SCH	200.00	–24.93
SCH	201.00	–25.06
SCH	202.00	–25.09
SCH	203.00	–25.24
SCH	204.00	–25.87
SCH	205.00	–24.98
SCH	205.00	–24.97
SCH	206.00	–25.50
SCH	207.00	–25.43
SCH	208.00	–24.97
SCH	210.00	–25.02
SCH	211.00	–24.99
SCH	211.00	–25.12
SCH	212.00	–25.03
SCH	212.00	–25.09
SCH	213.00	–24.94
SCH	213.00	–24.99
SCH	214.00	–24.36
SCH	216.00	–24.41

Sample	depth (m)	$\delta^{13}C_{org}$ (VPDB)
SCH	217.00	–25.36
SCH	217.00	–25.26
SCH	218.00	–25.44
SCH	219.00	–24.67
SCH	219.00	–26.21
SCH	220.00	–24.89
SCH	221.00	–24.69
SCH	221.00	–24.86
SCH	222.00	–24.77
SCH	224.00	–26.84
SCH	225.00	–26.86
SCH	226.00	–26.10
SCH	227.00	–26.21
SCH	228.00	–26.23
SCH	229.00	–26.22
SCH	230.00	–26.30
SCH	231.00	–25.18
SCH	231.00	–25.11
SCH	232.00	–26.34
SCH	232.00	–26.35
SCH	233.00	–26.27
SCH	233.00	–26.08
SCH	234.00	–25.13
SCH	235.00	–24.95
SCH	236.00	–25.04
SCH	237.00	–24.74
SCH	238.00	–26.10
SCH	238.00	–26.13
SCH	238.00	–24.91
SCH	239.50	–27.90
SCH	240.00	–25.90
SCH	243.00	–26.21
SCH	245.00	–26.49
SCH	246.00	–26.24
SCH	247.10	–26.22
SCH	248.00	–26.43
SCH	249.00	–26.16
SCH	250.00	–26.27
SCH	251.00	–25.68
SCH	252.00	–26.11
SCH	252.00	–26.09
SCH	253.00	–25.99
SCH	254.00	–24.26
SCH	255.00	–24.34
SCH	256.00	–24.60
SCH	257.00	–25.55
SCH	258.00	–24.86
SCH	259.00	–26.23
SCH	260.00	–26.21
SCH	261.00	–25.98
SCH	262.00	–26.18
SCH	263.00	–26.12
SCH	264.00	–26.13
SCH	265.00	–26.39
SCH	265.50	–26.90
SCH	266.00	–26.60
SCH	266.50	–25.80
SCH	267.00	–26.30
SCH	267.50	–26.60
SCH	268.00	–26.30
SCH	268.50	–26.90
SCH	269.00	–26.60
SCH	269.50	–26.40
SCH	270.00	–26.40
SCH	270.50	–26.50
SCH	271.00	–26.28
SCH	271.50	–26.50
SCH	272.00	–27.20
SCH	272.50	–26.60
SCH	273.00	–26.30
SCH	273.50	–26.30
SCH	274.00	–26.00
SCH	274.50	–26.50
SCH	275.00	–26.60
SCH	275.50	–26.80
SCH	276.00	–26.70
SCH	276.50	–26.90
SCH	277.00	–26.80
SCH	277.50	–26.80
SCH	278.00	–26.90
SCH	278.50	–26.80
SCH	279.00	–26.50
SCH	279.50	–26.40
SCH	280.00	–26.30
SCH	280.50	–26.40
SCH	281.00	–26.40
SCH	281.50	–26.40
SCH	282.00	–26.30
SCH	282.50	–26.40
SCH	283.10	–26.10
SCH	283.50	–26.50
SCH	284.00	–26.40
SCH	284.50	–26.50
SCH	285.00	–26.50
SCH	285.50	–26.10
SCH	286.00	–26.10
SCH	287.00	–26.90
SCH	287.50	–26.70
SCH	288.00	–26.80
SCH	288.50	–26.60
SCH	289.00	–26.80
SCH	289.50	–26.70
SCH	290.00	–26.70
SCH	291.00	–26.70
SCH	291.50	–26.40
SCH	292.00	–26.70
SCH	292.50	–26.20
SCH	293.10	–26.60
SCH	294.00	–26.70
SCH	294.50	–26.80

20190916-124004
A17159/29840/83D368CB

Sample	depth (m)	$\delta^{13}C_{org}$ (VPDB)
SCH	295.00	–26.60
SCH	295.50	–26.60
SCH	296.00	–26.70
SCH	296.50	–26.70
SCH	297.00	–26.90
SCH	297.50	–26.70
SCH	298.00	–26.10
SCH	298.50	–26.20
SCH	299.00	–25.02
SCH	300.00	–25.95
SCH	300.50	–25.96
SCH	301.00	–25.98
SCH	301.50	–25.88
SCH	302.00	–25.85
SCH	302.00	–25.90
SCH	302.50	–25.88
SCH	303.00	–26.03
SCH	303.50	–25.98
SCH	304.00	–25.98
SCH	304.50	–25.85
SCH	305.00	–25.85
SCH	305.50	–25.93
SCH	306.00	–26.43
SCH	306.50	–26.06
SCH	307.00	–25.91
SCH	307.50	–25.97
SCH	308.00	–25.93
SCH	308.50	–26.07
SCH	309.00	–26.06
SCH	309.50	–25.94
SCH	310.00	–26.07
SCH	310.50	–25.94
SCH	311.00	–26.03
SCH	311.50	–26.00
SCH	312.50	–26.53
SCH	312.80	–26.38
SCH	313.00	–27.30
SCH	313.50	–26.56
SCH	314.00	–26.62
SCH	314.50	–26.25
SCH	315.00	–27.13
SCH	315.50	–27.48
SCH	316.00	–26.29
SCH	316.00	–26.05
SCH	317.00	–26.52
SCH	317.50	–25.26
SCH	318.00	–28.69

Sample	depth (m)	$\delta^{13}C_{org}$ (VPDB)
SCH	318.00	–29.30
SCH	318.50	–29.21
SCH	319.50	–24.40
SCH	320.00	–24.24
SCH	320.50	–24.37
SCH	321.00	–24.51
SCH	321.00	–24.48
SCH	321.50	–24.28
SCH	322.00	–24.34
SCH	322.50	–24.38
SCH	323.00	–24.23
SCH	323.50	–24.14
SCH	324.00	–24.24
SCH	324.00	–24.26
SCH	324.50	–24.34
SCH	325.00	–24.28
SCH	325.50	–24.35
SCH	325.50	–24.24
SCH	326.00	–24.21
SCH	326.50	–24.18
SCH	327.00	–24.26
SCH	327.50	–24.15
SCH	327.50	–24.20
SCH	328.00	–23.89
SCH	328.00	–24.04
SCH	328.50	–24.06
SCH	329.00	–24.07
SCH	329.00	–24.36
SCH	329.50	–24.15
SCH	330.00	–24.21
SCH	330.50	–24.31
SCH	331.00	–24.20
SCH	331.50	–24.58
SCH	332.00	–24.28
SCH	332.50	–24.33
SCH	333.00	–24.71
SCH	333.50	–24.99
SCH	333.50	–25.12
SCH	334.00	–25.27
SCH	334.50	–25.02
SCH	335.00	–24.39
SCH	335.50	–24.24
SCH	336.00	–24.20
SCH	336.50	–24.35
SCH	337.00	–24.22
SCH	337.50	–24.56
SCH	338.00	–24.19

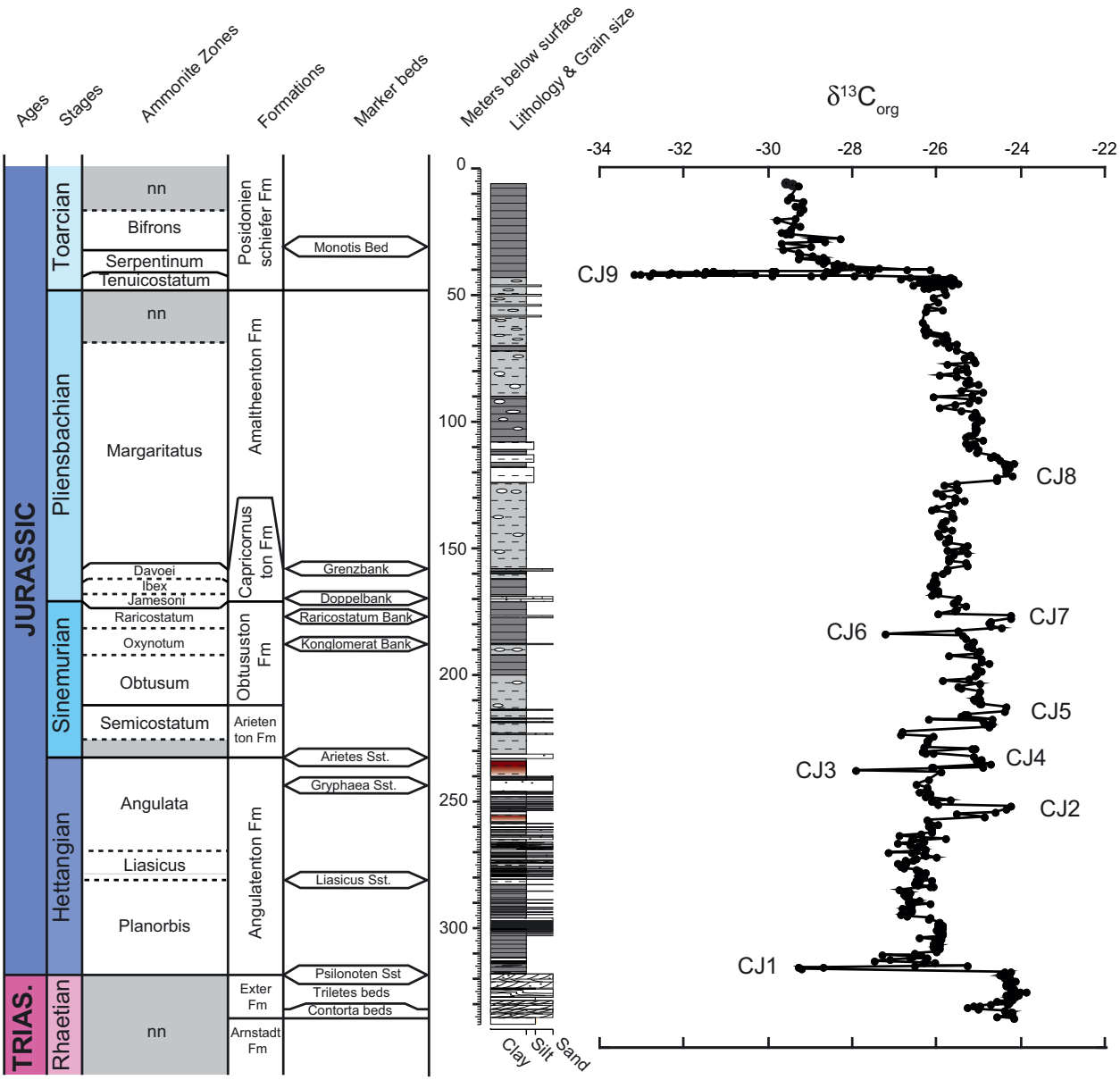

Fig. 6. Bulk organic carbon isotope record showing two large negative CIEs (CJ1, CJ9) at the Triassic-Jurassic transition and within the earliest Toarcian, respectively. Both excursions are associated with widespread euxinia. Two positive CIEs (CJ2 and CJ4) within the late Hettangian Angulata Zone are correlated to red colored laminated claystones, and might be partially lithologically controlled. A further positive excursion (CJ5) is recognized within the Lower Sinemurian Obtusum Zone and is preceded by a minor negative excursion. A positive CIE (CJ7) occurs in the Upper Sinemurian, after which values remain stable during the lower part of the Margaritatus Zone. A prominent positive CIE (CJ8) is observed within the Margaritatus Zone in association with the onset of laminated organic-rich sediments. Two negative spikes (CJ3 and CJ6) are only defined by single points and need further work.

All major negative and positive carbon isotope excursions >2 ‰ of the Schandelah core are marked by units CJ1 (Carbon Jurassic 1) to CJ9. We recognize 2 prominent negative $\delta^{13}C_{org}$ excursions just above the Rhaetian/Hettangian boundary (CJ1) and within the Lower Toarcian (CJ9). The former constitutes a shift of nearly 5‰ from Rhaetian values of around –24‰ to Hettangian values of –29‰. The major negative excursion in the Lower Toarcian is even larger and ranges from –26‰ to nearly –34‰. In addition to these major negative excursions of the Toarcian and Rhaetian/Hettangian boundary, there are

20190916-124004
A17159/29840/83D368CB

two smaller negative excursions of around 2‰ occurring in the Upper Hettangian (CJ3) and Upper Sinemurian (CJ6). In addition to the negative excursions, we identified 5 positive excursions, including positive excursions in the Upper Hettangian (CJ2, CJ4), lowermost and uppermost Sinemurian (CJ5 and CJ7), and in middle part of the Pliensbachian (CJ8).

9. Discussion

9.1. Regional correlations

The cored sediments were deposited in the Lower Saxony Basin, which witnessed progressive rifting during the Late Triassic to Late Jurassic (Betz et al. 1987, Adriasola-Muñoz et al. 2007). Contemporaneous syn-sedimentary faulting and salt diapirism resulted in large differences in Lower Jurassic sediment thicknesses. An anomalously high maturity of organic matter (Koch 1975, Teichmüller 1984) within the basin has been a matter of debate. It could have been caused by a deep-seated igneous intrusion, the so-called Bramsche Massif, of Early Cretaceous or early Late Cretaceous age (Stadler and Teichmüller 1971) or by a complex burial history (Adriasola-Muñoz et al. 2007 and references herein). However, vitrinite reflection data suggested that maturity was low enough to target the area around Schandelah as a potential drill-site. Lower Jurassic sediments around Schandelah form part of the so-called Elm-anticline. The drill site is located on the western side of the anticline, where undisturbed mostly flat-lying successions occur that span from the Permian Zechstein evaporites into the Lower Cretaceous.

The Lower Jurassic in northern Germany has not been studied in the same detail as equivalent successions in southern Germany, which have become famous for their abundant fossils, notably ammonites and ichthyosaurs, and have figured early on in reference works on Mesozoic stratigraphy (e. g. Quenstedt 1843). This general lack of coherent and concentrated information for northern Germany is in part due to an absence of well-exposed and continuous outcrops, and most studies have relied on borehole data (Littke et al. 1991). Hölder (1964) devoted only 5 pages to a summary of Lower Jurassic sedimentation in Northwest Germany in his seminal overview of Jurassic stratigraphy. What is clear is that the Lower Jurassic in northern Germany contains fewer stratigraphic gaps than equivalent strata in southern Germany (Hölder 1964) and thus holds great potential for understanding regional stratigraphy and making global correlations.

The Rhaetian-Hettangian transition in northern Germany is known in some detail from a drill core recovered at Mariental (Heunisch et al. 2010), approximately 20 km East of Schandelah. There, the Rhaetian is characterized by dark grey, cross-bedded, sandy to silty deltaic sediments with plant remains. A minimum thickness of 30 metres is estimated for the Rhaetian at Mariental, although only the Upper Rhaetian Contorta and Triletes Beds were cored. Kumm et al. (1941) describe more than 60 metres for the entire Rhaetian in northern Germany, with at least 8 metres of bonebed deposits at the base of the Rhaetian. These bone-beds have neither been encountered in Schandelah, nor in Mariental. It is therefore likely, that they occur below the maximum penetration depth in both Schandelah-1 and Mariental-1. The sedimentology of the Rhaetian in the Schandelah-1 and Mariental-1 cores is very comparable. In both locations the Upper Rhaetian consists of coarse to fine sand and siltstones with complex sedimentary structures, resulting from combined mechanical wave action and bioturbation. Similar to what is oberved in Schandelah, also Upper Rhaetian sediments in Mariental show evidence for seismic activity at several levels in the form of unusual cracks (syneresis?), flame structures, and slump folds (personal observations 2008, Richoz & van de Schootbrugge, Lindström et al. 2015).

At Mariental, Rhaetian sediments are conformable with overlying marine shales and intercalated sandstone beds of Hettangian (Lias alpha) age. The pyrite-rich layers that are present at the base of the Hettangian in Schandelah have not been observed in Mariental, however pyrite enrichment has been documented there in the lowermost Hettangian (Heunisch et al. 2010). At Mariental, the cored part of the Hettangian is around 100 metres thick (Heunisch et al. 2010). It is difficult to give an estimate of the total thickness, because the boundary with the Sinemurian was not cored, but it is likely on the order of 120 metres. The Hettangian at Schandelah is thus directly comparable with the succession encountered at Mariental, and all of the Hettangian sandstone marker beds were identified at Schandelah.

Despite an absence of ammonites in Mariental and a general lack in useful biostratigraphic marker species, lithological correlation of the Hettangian in both Schandelah and Mariental can be achieved using the three main sandstone bodies, which are recognized in both cores as the “Psilonoten-Sandstein”, “Liasicus-Sandstein”, and “Gryphaea-Sandstein”, respectively.

Some of the more massive coarse-grained sandstone marker beds can reach considerable thicknesses of up to 40 metres, but typically have thicknesses of less than 2 metres. The interspersed sediments are composed of organic-rich claystone with abundant coarser-grained storm deposits characterized by hummocky cross-stratification. Based on this comparison we can conclude that both cores represented a shallow inner-shelf environment with anoxic bottom waters that were frequently mixed by storm activity. However, the presence of reworked red claystone clasts in the Middle to Upper Hettangian of the Mariental-1 core and the absence of such reworked red claystone clasts in Schandelah seems to suggest that the environment of deposition in Mariental was shallower. Instead, in the Schandelah-1 core red claystone beds occur conformably within the Angulata Zone.

The Sinemurian (Lias beta) and Pliensbachian (Lias gamma and delta) in northern Germany are characterized by organic-rich marine claystone and marl, with intercalated ironstone within the Upper Sinemurian and lowermost Pliensbachian. The Sinemurian is well studied in an area close to Hannover based on 2 outcrops in former quarries (Fischer et al. 1986). Lowermost Pliensbachian ironstone of former economic value are well developed in a quarry in Rottorf am Klei, approximately 15 km East of Schandelah. The local occurrences of ironstone are related to Early Jurassic diapirism and synsedimentary faulting, leading to uplift and localized erosion. No complete exposures of Pliensbachian sediments exist in the region around Braunschweig, but the stratigraphy is for the most part known from scattered outcrops and several cores.

The transition from the Lower Pliensbachian into the Upper Pliensbachian is well-known from detailed work by Hoffmann and Jordan (1982). The Lower Pliensbachian is characterized by strong condensation and the development of a marker horizon known as the "Grenzbank". In the area around Schandelah this condensed bed has a thickness of 50 cm and contains ammonites belonging to the Davoei and Margaritatus Zones. The thickness of the Lower Pliensbachian in Northwest Germany is highly variable due to synsedimentary tectonics, but in an exploration drill core retrieved at Vechelde (25 km West of Schandelah), the Lower Pliensbachian had a thickness of 30 metres (Hoffmann 1982). A maximum thickness for the Upper Pliensbachian "Amaltheen-Ton" (Margaritatus and Spinatum Zones) has been estimated to range from 70 to 154 m (Kumm et al. 1941), and Schmitz (1980) takes 100 metres as an average. Temporary outcrops of the upper part of the Margaritatus and Spinatum Zones that existed as a result of construction on the A39 highway near Cremlingen (Teichert and Luppold 2013) show that sediments consist of laminated dark-grey shales and marls in the Margaritatus Zone grading into sandy shales in the uppermost Pliensbachian Spinatum Zone. The very expanded Upper Pliensbachian Margaritatus Zone at Schandelah is well known from areas outside of the North German Basin. In southern Germany the Amaltheen-Ton Formation reaches thicknesses in excess of 35 m, whereas the Upper Pliensbachian Marnes-de-Villeneuve Formation in the Grands Causses Basin in southern France is more than 50 m thick (Harazim et al. 2013).

The "Posidonienschiefer" outcropping in the area around Braunschweig counts as one of the most intensively studied Lower Jurassic formations in northern Germany (Schmitz 1968). According to Schmitz (1980) 155 cores were drilled in the area around Braunschweig with a total core length of over 16 km. Commercial exploitation of Toarcian oil shales at Hondelage, a village in the direct vicinity of Schandelah, started during World War I. Secret exploitation, mainly by prisoners of war, of the Toarcian oil shales at Schandelah began in 1943 during World War II and continued until 1945 (Schmitz 1980). Besides its importance as a resource, the oil shale at Schandelah is famous for its excellent preservation of marine fossils, including ichthyosaurs, fish, and a variety of marine invertebrates. Also terrestrial organisms are preserved, such as insects (Ansorge 2003) and pterosaurs (Wellnhofer 1986). The biostratigraphy of the Toarcian "Posidonienschiefer" is based on ammonites and has been studied in detail by a number of authors (e. g. Weitschat 1973). Thicknesses for the Lower Toarcian "Posidonienschiefer" are estimated to range between 20 to 30 metres (Hoffmann 1968).

The Toarcian succession of the Schandelah core displays the typical "Posidonienschiefer" facies known from outcrops across northwest Germany (Hoffmann 1960) and further afield in France (Schistes Cartons) and England (Jet Rock). There are, however, also clear differences between previously described, and now long-gone outcrops around Schandelah, and the occurrences of Toarcian black shales in France and England. Most previous authors report a number of concretionary levels (named after their corresponding ammonite species, e. g. Siemensi-concretions, Elegantulum-concretions) from the base of the Toarcian, but these appear to be mostly absent from the Schandelah

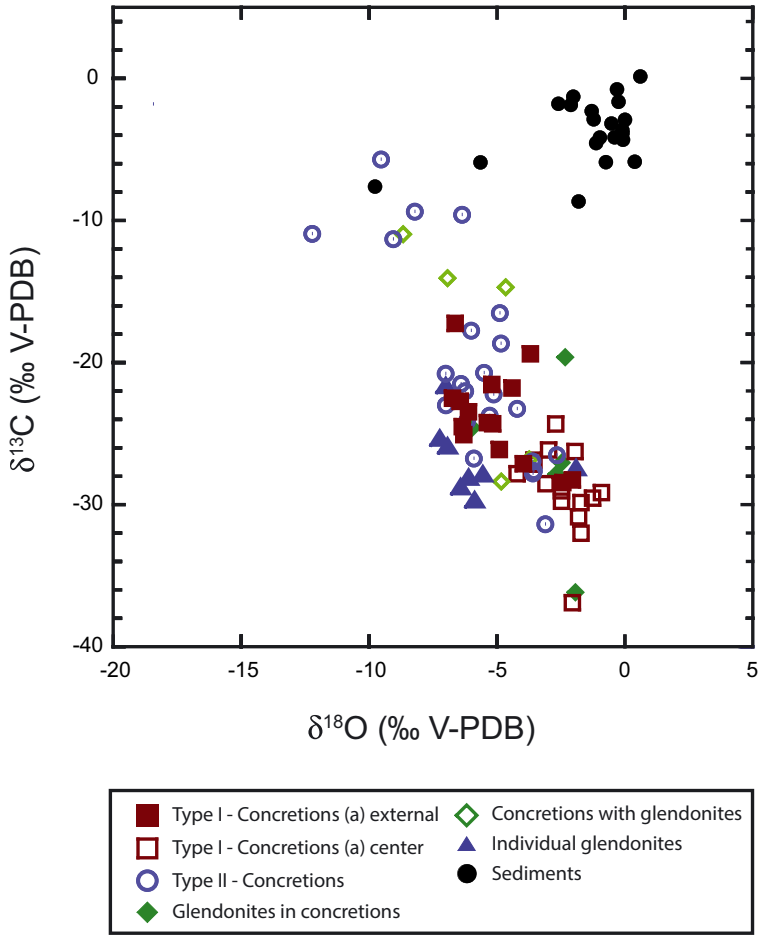

Fig. 7. Stable isotope data from bulk sediment, carbonate concretions, and glendonites. Authigenic carbonate values are clearly offset from bulk sediment values, ranging as low as –37 per mille (V-PDB). Clear differences exist between Type-I and Type-II concretions, with the latter generally having heavier carbon isotope values, and more negative oxygen isotope values.

core. One explanation could be that a large part of the Tenuicostatum Zone is missing at Schandelah due to sea level fall and erosion. According to Hoffmann (1968) the Tenuicostatum Zone has a thickness of 3 to 7 metres in the area around Braunschweig and conformably overlies the Spinatum Zone. This corresponds well to the 5 metres described here from Schandelah, and is in line with the difficult distinction between Spinatum and Tenuicostatum Zone sediments. Another reason for the absence of prominent concretionary beds in the Schandelah core could be that drilling missed possibly wider spaced concretions in the basal Toarcian. The latter explanation seems more reasonable than to assume that most of the Tenuicostatum Zone is missing.

9.2. Sea level, recurrent anoxia, and benthic diversity

Sea level and anoxia count as primary controls on the biodiversity of shallow marine benthic ecosystems, and both have been put forward as mechanisms to explain changes in biodiversity during the Early Jurassic. The recurrent development of anoxia in the European Epicontinental Seaway (EES) during the Early Jurassic (van de Schootbrugge et al. 2013) likely acted as a first order cause for changes in diversity among marine invertebrates (Hallam 1987, Little and Benton 1995, Mander et al. 2008), as well as meio- and microfauna, such as ostracods and benthic foraminifers (Boomer and Whatley 1992).

Species richness curves (Fig. 8) based on the number of species per sample show consistent patterns for macrobenthos (mainly bivalves) and microfossil groups (foraminifers, ostracods). The Rhaetian and base of the Hettangian are nearly devoid of macrofossils, except for the presence of numerous bivalves between 317 and 318 mbs. Anoxia likely was the main control on biodiversity at Schandelah in the lowermost Hettangian and the Lower Toarcian, even though during the former interval other causes, such as ocean acidification (Greene et al. 2012) and variable salinity

and temperature (van de Schootbrugge et al. 2007), related to the Triassic/Jurassic mass-extinction event also played an important role. Whereas for the Rhaetian this may be due to extremely shallow conditions and peculiar salinity conditions (Hallam 2002), the absence of marine macrofossils at the base of the Hettangian was probably a direct result of the mass-extinction event at the end of the Triassic. Intermittent colonisation of the sea floor during the earliest Hettangian has been documented both in Luxemburg (Richoz et al. 2012) and the UK (Wignall 2001, Wignall and Bond 2008), eventhough the earliest Hettangian benthic fauna is generally impoverished and dominated by few species. The absence of ostracods and benthic foraminifers in the Lower Hettangian at Schandelah is comparable to the depauperate communities of benthic foraminifers recorded in the Doniford section (UK) by Clemence et al. (2010).

The Lower Hettangian in the neighbouring Mariental core and in the Rosswinkel core from Luxemburg are known to contain biomarkers for green sulfur bacteria, indicators of photic zone euxinia (Richoz et al. 2012). Such biomarkers have also been detected at St Audrie's Bay (UK) by Jaraula et al. (2013) and in the Panthalassa Ocean by Kasprak et al., (2015). Photic zone euxinia with the presence of free H_2S in the water column would inhibit prolonged colonisation of the seafloor. It is interesting to note that nektonic organisms such as ammonites re-appeared at Schandelah (at 312.00 mbs) prior to benthic foraminifers and ostracods (at 302.00 mbs). This seems to suggest that conditions ameliorated first in surface waters and that dysoxic to euxinic conditions occurred, perhaps repeatedly, over a prolonged time interval. Ammonites fully recovered on a global scale by the end of the Hettangian, during which time the group underwent an adaptive radiation with the appearance of new lineages, including the Lytoceratidae and the Phylloceratidae (Guex et al. 2012). Such a decoupling between benthic and pelagic diversity is a hallmark for anoxic to euxinic conditions to extend into the water column, and also typifies the Toarcian (van de Schootbrugge et al. 2013).

In European sections, species richness for both benthic macro- and microfauna progressively increases during the Sinemurian and reaches a maximum within the Upper Pliensbachian Margaritatus Zone. These trends basically follow long-term sea level rise and may reflect increased niche partitioning due to habitat diversification. Several intervals within the Sinemurian and Pliensbachian show reduced diversity, notably in the Obtusum Zone, the lower part of the Margaritatus Zone, and the Spinatum Zone. It is unclear whether severe anoxia or perhaps photic zone euxinia is also to blame for these lulls in richness, since no biomarker data are available for these time slices. However, both the Obtusum and Margaritatus zones contain laminated shales that are reminiscent of Hettangian and Toarcian paper shales. Elsewhere, in the UK and Portugal the Obtusum Zone is known to contain black shales with TOC of up to 20 % (Duarte et al. 2010, Jenkyns and Weedon 2013, Duarte et al. 2014) and strong anoxia at the sea floor is suspected.

In Schandelah-1, species richness reached a nadir at the Pliensbachian-Toarcian boundary. A major extinction has been observed in this interval for ammonites, which as a group recovered during the Toarcian, i. e. during the main anoxic phase (Harries and Little 1999). These changes therefore do not appear to be connected to ocean anoxia. Instead, this interval was generally characterized by oxygenated conditions within the EES (van de Schootbrugge et al. 2013 and references therein). Across NW Europe the late Pliensbachian contains a relatively diverse and abundant cyst-producing dinoflagellate community that points to well-oxygenated bottom waters (Bucefalo Palliani and Riding 1999a, 1999b, Riding 1987, Riding and Ioannides 1996). The late Pliensbachian diversity decline may be connected to a seawater temperature decrease that is recorded in belemnite oxygen isotope records from sections in southern Germany (Bailey et al. 2003), the UK (Bailey et al. 2003), France (Harazim et al. 2013), and northern and central Spain (Rosales et al. 2004, Gomez et al. 2008). Garcia Joral et al. (2011) have linked a diversity decline in brachiopods in Spain to this late Pliensbachian cooling phase. A subsequent recovery of brachiopod faunas across the Pliensbachian-Toarcian boundary is only observed in southern Europe, presumably in places less affected by the Toarcian OAE. Colder climate conditions and sea level fall may have conspired to lead to reduced species richness in shelf environments, as has been proposed for a number of other Phanerozoic cooling events (Stanley 1988, Finnegan et al. 2012).

The Toarcian OAE counts as a minor global mass-extinction event, but it had a profound impact on the local and regional scale (Harries and Little 1999, Martindale et al. 2017). The T-OAE extinction affected mostly infaunal and epifaunal species of bivalves. Diversity of benthic macrofauna, as well as ostracods and foraminifers, did not recover in Schandelah during the Toarcian, likely as a result of prolonged anoxia in

northern Germany that lasted well beyond the Serpentinum Zone.

9.3. Carbon cycle perturbations

Anoxia and extinction during the Early Jurassic are intimately linked with perturbations in the carbon cycle as reconstructed from carbon isotope records. Numerous carbon isotope records from a multitude of sections, spanning a range of intervals within the Early Jurassic, and using various substrates (e. g. bulk carbonate and organic matter, wood particles, belemnites and other skeletal calcitic elements), have been generated over the past 20 years. Most of these studies have focused on either the Triassic-Jurassic boundary or the Toarcian OAE (e. g. Jenkyns and Clayton 1997, Hesselbo et al. 2000, van de Schootbrugge et al. 2005, 2008, Suan et al. 2008, 2010, Korte et al. 2011).

The Schandalah-1 carbon isotope record provides unprecedented insight into the Early Jurassic carbon cycle following the end-Triassic mass-extinction. Both large negative CIEs that occur in the lowermost Hettangian and Lower Toarcian are associated with widespread black shale deposition. The Hettangian negative CIE recorded in Schandelah-1 is known as the "initial" negative excursion of Hesselbo et al. (2002) described from St Audrie's Bay (UK), or "Negative-II" of Lindström et al. (2012) described from Denmark. Based on the correlation with Mariental-1 and nearby cores from Rodby and Stenlille, the negative CIE is now described as the “Spelae CIE” by Lindström et al. (2017) and overlaps with major volcanism in the CAMP large igneous province. The Spelae CIE corresponds to an interval that shows evidence for widespread photic zone euxinia (PZE) not only in Germany but also in the UK and United States (Richoz et al. 2012, Jaraula et al. 2013, Kasprak et al. 2015). Although biomarker analyses are needed to confirm the presence of PZE in Schandelah, the occurrence of abundant pyrite, amorphous organic matter, and the paper shale appearance of the Lower Hettangian sediments suggest that photic zone euxinia also dominated shallow seawater in Schandelah.

The magnitude of negative CIEs associated with the T/J boundary remain a matter of debate, as it is now well established that bulk organic C-isotope records need to be regarded with caution (see e. g. van de Schootbrugge et al. 2008, Suan et al. 2015) due to the mixing effects of different types of carbon, each with their own specific carbon isotopic signatures. The 5‰ negative CIE in Schandelah-1 is smaller than the 8‰ negative CIE recorded in compound specific isotope records from Austria (Ruhl et al. 2011), but it appears large compared to records from Nevada, where the negative CIE is barely 3‰ (Guex et al. 2004). It is likely that detailed organic matter studies, combining palynology with RockEval methods, may be able to tease out a more reliable carbon isotope signal (see Suan et al. 2015).

Beyond the T/J boundary, we have a poor understanding of the Hettangian carbon cycle. A large positive CIE documented in bulk organic matter in a Canadian section by Williford et al (2007) is neither apparent in the record from Schandelah-1, nor is it in bulk organic carbon isotope records from the Mariental-1 core (Richoz et al. 2012) and St Audrie's Bay (Ruhl et al. 2010). A smaller positive excursion of approximately 2‰ has been documented by Bachan et al. (2012) from a section in northern Italy. The large positive CIE of Williford et al (2007) was recently recalibrated to be of Late Hettangian age by Bartolini et al. (2012) and correlated with a record from New York Canyon in Nevada (United States). This only in part alleviates the problems, as none of the isotope records from NW Europe, be they from the UK (Ruhl et al. 2010), Germany (van de Schootbrugge et al. 2008), or Italy (van de Schootbrugg et al. 2008, Bachan et al. 2012), show such a large excursion in the Upper Hettangian. The record from Schandelah-1 adds more controversy, as it contains two positive excursions in the Angulata Zone. However, it is unclear what the relation is between the red intervals and the positive excursions in $\delta^{13}C_{org}$. It is possible that these excursions (CJ2 and CJ4) are artefacts of the peculiar changes in lithology and organic matter sourcing.

Carbon isotope records for the Sinemurian have generally been lacking, but a renewed interest in a possible mid-Sinemurian carbon cycle perturbation with analogies to the PETM (Riding et al. 2013), has led to some recently published data sets from sections in Canada and Portugal that can serve for comparisons (Porter et al. 2014, Duarte et al. 2014). In Schandelah, a minor positive CIE occurs in the lowermost Obtusum Zone. Akin to the record from Schandelah, relatively positive values (around –24‰ V-PDB) are recorded in the Copper Hill borehole (Riding et al. 2013) in the lowermost Sinemurian Turneri Zone. A similar isotopic signal is recorded in the "Shales-with-Beef" along the Dorset Coast (UK; Jenkyns and Weedon 2013). A low resolution organic C-isotope record from the Mochras core shows a long-term trend towards positive values reaching its highest

point in the Obtusum Zone, after which values gradually decrease and reach a low in the Lower Pliensbachian Jamesoni Zone (van de Schootbrugge et al. 2005). Outside of NW Europe, carbon isotope records from Nevada and Canada appear to support a trend towards positive values in the Leslei Zone (North-American equivalent of the Turneri Zone), followed by a gradual decline during the Carinatum Zone (= Obtusum Zone; Porter et al. 2014).

Although the Obtusum Zone in the Copper Hill core is strongly reduced in thickness when compared to Schandelah-1, Riding et al. (2013) recorded a trend towards lower carbon isotope values, similar to what we observe in Schandelah-1. A major negative CIE is recognized in the Copper Hill borehole in the Oxynotum Zone and palynological data show the proliferation of the dinoflagellate cyst *Liasidium variabile* in this interval (Riding et al. 2013). These authors attributed the Sinemurian acme of *L. variabile* to global warming due to gas-hydrate destabilization in analogy to the global spread of the dinoflagellate *Apectodinium* across the Paleocene-Eocene boundary.

One of the most prominent features of the Schandelah-1 C-isotope record is the positive CIE that occurs within the Margaritatus Zone of the late Pliensbachian (CJ8). This positive CIE is followed by a gradual decline that spans most of the upper part of the Margaritatus and Spinatum Zones. Positive CIEs in the Margaritatus Zone have also been recognized in the carbonate carbon isotope record from sections in Italy (Woodfine et al. 2008) and the UK (Jenkyns and Clayton 1986, Korte and Hesselbo 2011). It is interesting to note that the Schandelah-1 carbon isotope record shows similar trends when compared with the diversity curve, perhaps suggesting there is a link between the carbon cycle and biodiversity. If the Margaritatus Zone positive CIE was mainly driven by production instead of preservation, it could link elevated surface water productivity to increased benthic diversity.

The Toarcian negative CIE remains one of the most dramatic excursions within the Phanerozoic record. The record from Schandelah-1 further underpins the enormity of the isotope excursion seen against the backdrop of the entire Early Jurassic carbon isotope record. Whereas the magnitude of the excursion is most likely exaggerated because of the strong changes in organic matter source associated with the onset of the Toarcian OAE, this effect may only explain part of the excursion (Suan et al. 2015). The remainder can be confidently attributed to regional and/or global mechanisms. In recent years many authors have advocated as an explanation the rapid injection of light carbon into the ocean-atmosphere system, possibly via destabilizing methane hydrates on the sea floor, or via carbon released from flood basalt volcanism in the Karoo-Ferrar large igneous province.

9.4. Hydrocarbon seepage and authigenic carbonate deposition

If methane released from the sediment was one of the main driving mechanisms of the Hettangian, Sinemurian, and Toarcian carbon cycle perturbations, is there any sedimentological evidence for such a mechanism in the form of methane seepage? The Lower Jurassic successions across Europe undoubtedly count as a major source of biogenic methane, given the repeated and widespread burial of organic matter during this time interval and evidence for hydrocarbon seepage has been documented from the Sinemurian in the UK (Allison et al. 2008, Price 2008, Xu et al. 2016). One conspicuous sedimentary feature of the otherwise monotonous marly sediments that span the Sinemurian to Toarcian is the abundant presence of authigenic carbonates, such as sideritic and calcareous concretions, stratiform occurrences of "shales-with-beef", and glendonites within the Upper Pliensbachian. Glendonites, pseudomorphs of the hexahydrated calcite mineral ikaite, are widely used as a palaeoclimate proxy for near-freezing bottom water conditions and perhaps the presence of ice-caps during Mesozoic greenhouse periods (Price 1999). However, unlike for the occurrences in Schandelah-1, such glendonite records tend to stem from the high-latitudes (e. g. the Pliensbachian of Siberia; Kaplan 1978, 1979, Suan et al. 2011). Considering the palaeo-latitude of the Schandelah-1 drill site (ca. 40 °N), it is hard to imagine near-freezing conditions characterized the EES, since it was populated with mostly warm water organisms, and bordered by landmasses sustaining tropical vegetation. Indeed, belemnite oxygen isotope records from a nearby outcrop at Cremlingen suggest temperatures were around 16˚C during the Late Pliensbachian (Teichert and Luppold 2013).

An alternative mechanism for ikaite formation, with potentially important ramifications, includes the generation of methane within the sediment or its release from gas hydrates or deep seated reservoirs and its subsequent anaerobic oxidation coupled to sulfate reduction (Schubert et al. 1997, Teichert and Luppold 2013, Morales et al. 2017). From actuo-sedimentolo-

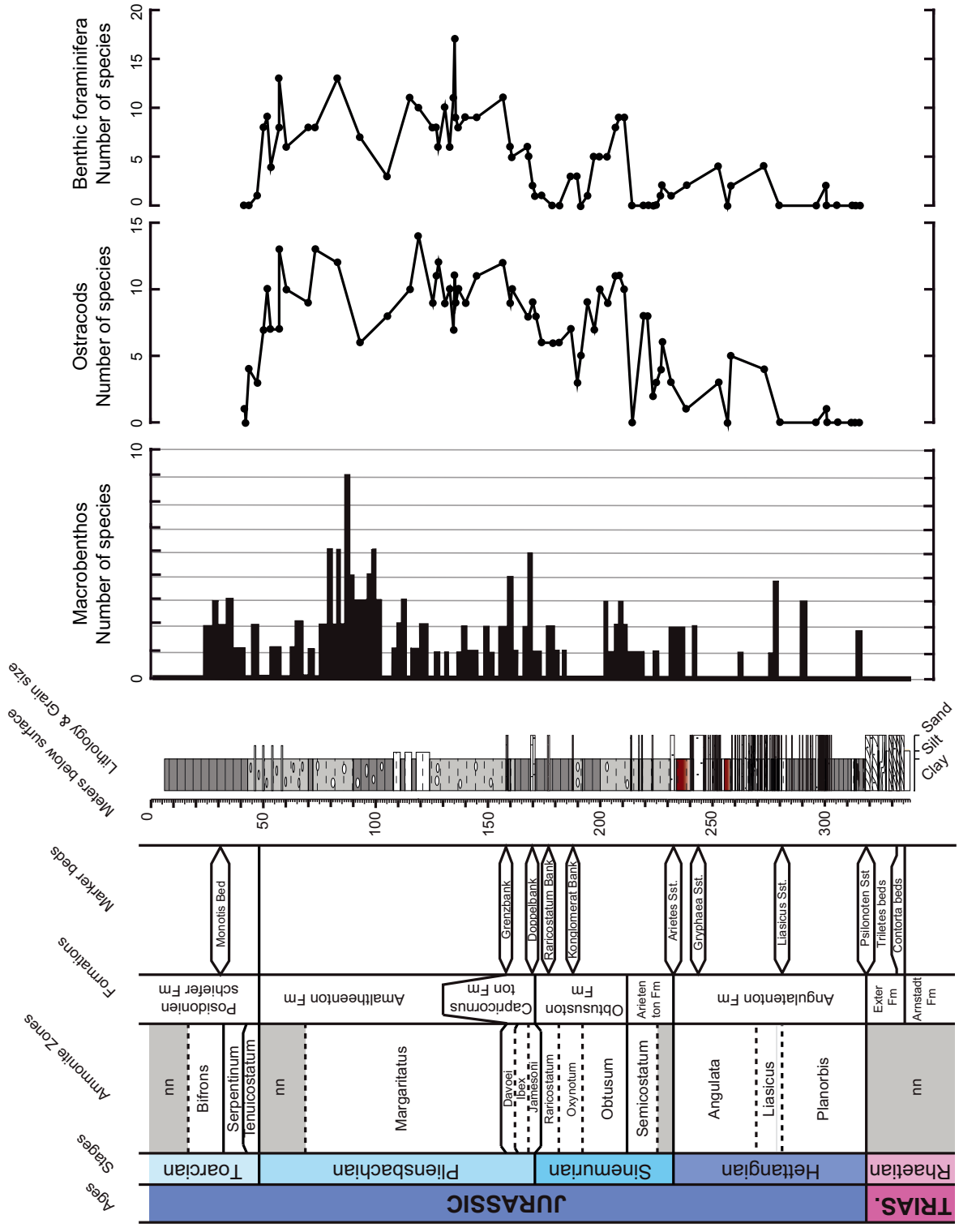

Fig. 8. Species richness plots for benthic macrofauna (mainly bivalve species), ostracods, and foraminifers. Foraminifers and ostracod species were determined from amalgamated samples. The species richness of macro fauna was determined during logging of the core.

20190916-124004
A17159/29840/83D368CB

gical studies it is becoming increasingly clear that most or all commonly occurring authigenic carbonate deposits are likely mediated by microbial activity. Especially the combined effect of sulfate reduction and anaerobic methane oxidation leads to greatly enhanced alkalinity, which is one prerequisite to trigger ikaite formation. Ikaite forms today in the Sea of Okhotsk at a site of actively seeping methane (Greinert and Derkachev 2004). Strong evidence for this mechanism is provided by stable isotope data obtained from the glendonites and associated authigenic carbonate concretions present in the Schandelah-1 core.

Two intervals (65–75 mbs and 85–100 mbs) rich in concretions, glendonites, and concretions surrounding glendonites were investigated with stable isotope methods to determine their possible link with methanogenesis and the anaerobic oxidation of methane in the sediment (Fig. 7; Table 2). We recognized two types of concretions in this interval. Type-I concretions are round to oval shaped with smooth surfaces, and have a zoned internal structure. The Type-II concretions are more irregularly shaped and some are tubular, possibly also related to burrows. These tend to have a uniform internal color and structure. All of the concretions show extremely complex, both early and late stage sediment diagenetic histories. At least some of the concretions appear to have formed during early stage diagenesis, leading to displacement of the laminated sediments around them.

Carbon isotope values of individual glendonites range from –20 to –30‰ (V-PDB). The lowest C-isotope value (–36.16‰) was measured from a glendonite encased in a carbonate concretion. Such low values are strikingly similar to those obtained from ikaite that is being formed today in the Laptev and Okhotsk Seas (Russia; Greinert and Derkachev 2004, Schubert et al. 1997). These values are also similar to those obtained by Teichert and Luppold (2013) for glendonites sampled from an outcrop at Cremlingen, although some of the glendonites in that study had values as low as –50‰. Most carbonate concretions also have low C-isotope values, however differences exist for both types. Carbonate carbon isotope value range from –24‰ to –36.88‰ for Type-I concretions, and from –5‰ to –31‰ for Type II-concretions. The two types of concretions are thus partly overlapping for their carbonate carbon isotope values, but the Type-II concretions have overall less negative values. The two types are clearly distinguishable based on their oxygen isotope values. Type-II concretions have much more negative oxygen isotope values (between –2.66‰ and –12.24‰) than Type I concretions (ranging from –4.14‰ to –0.84). Bulk sediment carbonate carbon isotope values are quite negative for carbon, but appear normal for oxygen, hinting at some diagenetic process that has added light carbon, but not affected oxygen.

The carbon and oxygen isotope data indicate that the glendonites preserved within concretions retain an original marine oxygen isotope signature that is similar to those of Type-I concretions. These glendonites and concretions also have the most negative carbon isotope values when compared to Type-II and single glendonites. In contrast, the individual glendonites have oxygen isotope values similar to those of Type-II concretions, and carbon isotope values that are less negative. This may suggest that these have been influenced by later stage diagenesis, leading to recrystallization with a different carbon source. The isotopic analyses of the glendonites and concretions are in line with a mechanism related to the anaerobic oxidation of methane, incorporating a mixture of ^{12}C-depleted carbon and background sediment carbon.

The Late Pliensbachian appears to have been a time of widespread authigenesis, and may have been a time of increased hydrocarbon seepage. Glendonites are common in the uppermost Pliensbachian of Siberia (Kaplan 1978, 1979). Contemporaneous sediments in southern France contain abundant tubular carbonate concretions that are also characterized by low C-isotope values down to –27‰ (V-PDB) (van de Schootbrugge et al. 2010). And across Northern France, the Margaritatus Zone is well known for its abundance of carbonate and ferruginous concretions. For now, the exact link between this Late Pliensbachian phase of authigenesis and the Toarcian OAE, which has been linked to widespread methane degassing (Hesselbo et al. 2000), remains unclear and warrants future scrutiny.

A number of other phenomena within the Upper Pliensbachian in Schandelah may also be used to infer methane and/or hydrocarbon diffusion. After sieving for ostracods and foraminifers, a very rich gastropod fauna was observed between 106 and 120 mbs. The gastropod shells are anomalously brown, which is here attributed to impregnation with hydrocarbons. Moreover, Schandelah contains numerous levels of "calcite beef", which are known in german literature as “Tutenmergel”, “Nagelkalk”, or “Faserkalk” (Kumm et al. 1941). Beef calcite consists of upward-fanning calcite layers (cone-in-cone) that occur predominantly in

Table 2. Carbon and oxygen isotope data from concretions and glendonites.

Depth in core	**Sample Type**				
[m]		$\delta^{13}C$	$\delta^{18}O$	$\delta^{13}C$	$\delta^{18}O$
		internal	internal	external	external
74.17	Concretion – Type I	–31.99	–1.64	–22.50	–6.73
74.43	Concretion – Type I	–29.83	–1.64	–25.05	–6.29
74.87	Concretion – Type I	–29.01	–2.40	–24.50	–6.35
76.80	Concretion – Type I	–27.81	–4.14	–22.71	–6.43
85.80	Concretion – Type I	–28.52	–3.01	–23.45	–6.11
86.78	Concretion – Type I	–26.13	–2.91	–24.21	–5.37
87.13	Concretion – Type I	–26.24	–1.87	–19.37	–3.69
88.08	Concretion – Type I	–30.83	–1.73	–26.10	–4.90
90.30	Concretion – Type I	–29.14	–0.84	–27.10	–3.97
91.01	Concretion – Type I	–29.53	–1.19	–28.24	–2.04
91.04	Concretion – Type I	–29.74	–2.40	–28.43	–2.42
91.46	Concretion – Type I	–24.31	–2.62	–21.53	–5.20
91.77	Concretion – Type I	–26.85	–3.48	–21.78	–4.41
92.41	Concretion – Type I	–27.14	–3.51	–24.29	–5.16
94.80	Concretion – Type I	–36.88	–1.97	–17.22	–6.63
74.95	Concretion – Type II	–27.60	–3.57	n/a	n/a
77.30	Concretion – Type II	–31.35	–3.12	n/a	n/a
83.50	Concretion – Type II	–22.21	–5.14	n/a	n/a
91.66	Concretion – Type II	–21.47	–6.42	n/a	n/a
91.70	Concretion – Type II	–27.78	–3.61	n/a	n/a
92.78	Concretion – Type II	–23.71	–5.30	n/a	n/a
92.99	Concretion – Type II	–23.22	–4.22	n/a	n/a
93.93	Concretion – Type II	–20.70	–5.52	n/a	n/a
94.25	Concretion – Type II	–20.77	–7.02	n/a	n/a
94.66	Concretion – Type II	–24.10	–6.19	n/a	n/a
94.70	Concretion – Type II	–22.97	–7.01	n/a	n/a
94.81	Concretion – Type II	–11.29	–9.07	n/a	n/a
95.10	Concretion – Type II	–26.72	–5.92	n/a	n/a
95.23	Concretion – Type II	–22.00	–6.26	n/a	n/a
95.30	Concretion – Type II	–17.73	–6.02	n/a	n/a
95.47	Concretion – Type II	–9.35	–8.22	n/a	n/a
95.51	Concretion – Type II	–18.63	–4.86	n/a	n/a
95.95	Concretion – Type II	–16.50	–4.90	n/a	n/a
99.26	Concretion – Type II	–5.68	–9.55	n/a	n/a
99.52	Concretion – Type II	–9.57	–6.38	n/a	n/a
99.66	Concretion – Type II	–26.93	–3.63	n/a	n/a
99.78	Concretion – Type II	–10.92	–12.24	n/a	n/a
99.83	Concretion – Type II	–26.50	–2.67	n/a	n/a
93.40	Glendonite	–21.61	–6.99	n/a	n/a
93.47	Glendonite	–25.85	–6.92	n/a	n/a
93.50	Glendonite	–29.65	–5.86	n/a	n/a
93.53	Glendonite	–25.31	–7.23	n/a	n/a
93.67	Glendonite	–27.39	–1.90	n/a	n/a
93.70	Glendonite	–27.82	–5.54	n/a	n/a
93.72	Glendonite	–28.72	–6.41	n/a	n/a
93.78	Glendonite	–28.05	–6.10	n/a	n/a
90.57	Glendonite in concretion	–36.16	–1.93	–28.37	–4.83
91.62	Glendonite in concretion	–27.85	–2.68	–26.81	–3.74
93.38	Glendonite in concretion	–19.62	–2.33	–10.96	–8.67
93.60	Glendonite in concretion	–27.04	–2.47	–14.06	–6.93
95.44	Glendonite in concretion	–24.58	–5.97	–14.70	–4.66

shale or marl facies, sometimes associated with siderite concretions or as crusts on fossils. Calcite fans are common in the Upper Pliensbachian in Schandelah (e. g. at 91.20 and 88.40 mbs) and have also been observed near Gretenberg (approx. 70 km to the East of Schandelah, near Hannover) in the Aalenian (Kumm et al. 1941). Other occurrences include those in the southern United Kingdom, such as the Shales-with-Beef Formation in the Lower Sinemurian.

Conditions leading to the deposition of "beef" within predominantly marly facies remain poorly understood. Whereas it was previously thought that the formation of calcite beef is related to late diagenetic precipitation possibly related to dewatering of the sediment (Kumm et al. 1941), more recent studies propose early diagenetic models for their formation. Greene et al. (2012) linked the occurrence of crystal fans at the Triassic-Jurassic boundary to synsedimentary palaeo-environmental changes in water column chemistry, such as a decrease in ocean water pH and an increase in sediment bicarbonate concentrations, perhaps related to CAMP volcanism. This interpretation has been challenged by Kershaw and Guo (2016) who emphasized the presence of numerous cone-in-cone occurrences also during periods characterized by no notable environmental disturbances.

Cobbold et al. (2007) and Cobbold et al. (2013) related many occurrences of beef-calcite, e. g. in the Bajocian of Argentina, to expulsion of hydrocarbons, based on fluid inclusions or as staining of calcite crystals. Unlike what is commonly thought, beef-calcites do not form during extension and faulting, but rather during compression and the upward movement of hydrocarbons. Kumm et al. (1941) stress the fact that some of the crusts in the Aalenian cover already flattened fossils from compaction and can therefore only be late diagenetic in origin. Alternatively, Heindel et al. (2015) demonstrated that Early Triassic cone-in-cone strutures formed during early diagenesis in anoxic pore waters around degrading microbial mats under the influence of sulphate reduction bacteria and methanogenesis.

Whether beef-calcite in Schandelah are genetically linked to the presence of glendonites and other authigenic carbonates, following either Cobbold et al. (2013) or Heindel et al. (2015), will require future research. Establishing such a link could be powerful evidence for hydrocarbon and/or methane generation and seepage during the Early Jurassic and could proof to be an important clue to understanding carbon cycle changes.

10. Summary and Outlook

A core was drilled at the village of Schandelah (Lower-Saxony, N Germany) with the aim to recover a complete succession of Upper Triassic (Rhaetian) to Lower Jurassic (Hettangian-Toarcian) shallow marine deposits characterized by repeated anoxia. Drilling commenced in the Upper Toarcian and reached a total depth of 338 m in the Upper Rhaetian, penetrating the Rhaetian-Hettangian boundary at 318.60 mbs, the Hettangian-Sinemurian boundary at 233.30 mbs, the Sinemurian-Pliensbachian boundary at 172.00 mbs, and the Pliensbachian-Toarcian boundary at 48.00 mbs. The biostratigraphy is based mainly on ammonites, but palynomorphs (pollen, spores and dinoflagellate cysts), calcareous nannofossils, ostracods and benthic foraminifers prove to be useful accessory markers, allowing for the establishment of a solid biostratigraphic framework. The preservation of microfossils was excellent in the case of palynomorphs, and good in the case of nannofossils, ostracods and benthic foraminifers. All stage boundaries could be recognized based on a combination of lithological and biostratigraphic markers and a subdivision on the ammonite zone level was possible for many ammonite zones, with the exception of the Marshi, Bucklandi, Turneri, and Spinatum Zones, as well as the Upper Toarcian. Correlation with nearby successions in N Germany (e. g. Mariental-1 Core) and the UK and France can be confidently achieved with the help of organic carbon isotopes. On the whole, the succession appears to be fining upwards. Coarse sandstone beds are prevalent in the Rhaetian and Hettangian, but starting in the Sinemurian and continuing in the Pliensbachian the sedimentology is dominated by a succession of laminated organic-rich shale and claystone, which is only interrupted by several massive sandstone beds in the Rhaetian and Hettangian, and a number of highly condensed sandy limestone beds showing intense reworking in the Upper Sinemurian and Lower Pliensbachian. Paper shales occur throughout the core, for example at the base of the Hettangian and in the Upper Pliensbachian, but are most prominently developed in the Toarcian (Posidonia Shales).

The Schandelah-1 core thus provides an excellent archive of Early Jurassic palaeo-environmental change and allows the development of new research questions concerning the causes and the rates of recovery after the Triassic-Jurassic mass-extinction, the underlying mechanisms for repeated organic-matter deposition in "Posidonia-style" facies, and the significance of authi-

genic carbonate deposition for understanding Mesozoic sediment biogeochemistry and global carbon cycle changes. Future work will focus on land-sea correlations using palynology, biomarker records of environmental change both prior to, during, and after anoxic events throughout the Early Jurassic. In addition, we envision the use of multi-proxy in- and organic geochemistry to disentangle local and global signals of water column redox changes.

Acknowledgements. The Goethe University Frankfurt acted as the main sponsor of this project and we thank the university for its generosity. We are extremely grateful to a large number of people, government organisations, and companies without whom this project would have been impossible to realize (listed in alphabetical order): Barbara Rohstoffbetriebe GmbH, Maria Blatt, Jonah Chietoli, Daldrup & Söhne AG, E.ON, Fides Gad, Marco Gambietz, Jessica Gogesch, Eckehard Gottwald, Gabriele Grützner, Kenji Hatsukano, Carmen Heunisch, Kei Matsuyama, Alain Morard, Tanja Rutz, Bärbel Schmincke, Volker Wilde. We thank Stephen Hesselbo and Carmen Heunisch for their thoughtful reviews that helped to substantially improve an earlier version of this manuscript. Editor Jochen Erbacher is thanked for his patience.

References

Adriasola-Muñoz, Y., Littke, R., Brix, M. R., 2007. Fluid systems and basin evolution of the western Lower Saxony Basin, Germany. Geofluids 7, 335–355.

Allison, P. A., Hesselbo, S. P., Brett, C. E., 2008. Methane seeps on an Early Jurassic dysoxic seafloor. Palaeogeography, Palaeoclimatology, Palaeoecology 270, 230–238.

Ansorge, J., 2003. Insects from the Lower Toarcian of Middle Europe and England. Acta zoologica cracoviensia 46, 291–310.

Bachan, A., van de Schootbrugge, B., Fiebig, J., McRoberts, C. A., Ciarapica, G., Payne, J. L., 2012. Carbon cycle dynamics following the end-Triassic mass extinction: Constraints from paired $\delta^{13}C_{carb}$ and $\delta^{13}C_{org}$ records. Geochemistry, Geophysics, Geosystems 13Q09008.

Bailey, T. R., Rosenthal, Y., McArthur, J. M., van de Schootbrugge, B., Thirlwall, M. F., 2003. Paleoceanographic changes of the late Pliensbachian-early Toarcian interval: a possible link to the genesis of an Oceanic Anoxic Event. Earth and Planetary Science Letters 212, 307–320.

Baker, S. J., Hesselbo, S. P., Lenton, T. M., Duarte, L. V., Belcher, C. M., 2017. Charcoal evidence that rising atmospheric oxygen terminated Early Jurassic ocean anoxia. Nature Communications 8, doi: 10.1038/ncomms15018.

Bartenstein, H., Brand, E., 1937. Mikro-paläontologische Untersuchungen zur Stratigraphie des nordwest-deutschen Lias und Doggers. Abhandlungen senckenbergische naturforschende Gesellschaft 439, 1–224.

Bartolini, A., Guex, J., Spangenberg, J. E., Schoene, B., Taylor, D. G., Schaltegger, U., Atudorei, V., 2012. Disentangling the Hettangian carbon isotope record: Implications for the aftermath of the end-Triassic mass extinction. Geochemistry, Geophysics, Geosystems 13Q01007.

Belcher, C. M., Rein, G., Haworth, M., Glasspool, I., Mander, L., Jervis, F. X., Hesselbo, S. P., McElwain, J. C., 2010. Increased fire activity at the Triassic/Jurassic boundary in Greenland due to climate-driven floral change. Nature Geoscience 3, 426–429.

Berner, R. A., 2002. Examination of hypotheses for the Permo-Triassic boundary extinction by carbon cycle modelling. Proceedings of the National Academy of Science 99, 4172–4177.

Berner, R. A., 2006. GEOCARBSULF: A combined model for Phanerozoic atmospheric O_2 and CO_2. Geochimica et Cosmochimica Acta 70, 5653–5664.

Berner, R. A., Petsch, S. T., Lake, J. A., Beerling, D. J., Popp, B. N., Lane, R. S., Laws, E. A., Westley, M. B., Cassar, N., Woodward, F. I., Quick, W. P., 2000. Isotope fractionation and atmospheric oxygen: Implications for the Phanerozoic O_2 evolution. Science 287, 1630–1633.

Berner, R. A., VandenBrooks, J. M., Ward, P. D., 2007. Oxygen and evolution. Science 316, 557–558.

Betz, D., Führer, F., Greiner, G., Plein, E., 1987. Evolution of the Lower Saxony Basin. Compressional intra-plate deformations in the Alpine Foreland. Tectonophysics 137, 127–170.

Beutler, G., Heunisch, C., Luppold, F. W., Rettig, B., Röhling, H.-G., 1996. Muschelkalk, Keuper und Lias am Mittellandkanal bei Sehnde (Niedersachsen) und die regionale Stellung des Keupers. Geologisches Jahrbuch Reihe A: 145, 67–197.

Boomer, I., Whatley, R., 1992. Ostracoda and dysaerobia in the Lower Jurassic of Wales: the reconstruction of past oxygen levels. Palaeogeography, Palaeoclimatology, Palaeoecology 99, 373–379.

Bown, P. R., Cooper, M. K. E., 1998. Jurassic. In: Bown, P. R. (Ed.), Calcareous nannofossil biostratigraphy. Kluwer Academic, London, 34–86.

Bucefalo Palliani, R., Mattioli, E., Riding, J. B., 2002. The response of marine phytoplankton and sedimentary organic matter to the early Toarcian (Lower Jurassic) oceanic anoxic event in northern England. Marine Micropaleontology 46, 223–245.

Bucefalo Palliani, R., Riding, J. B., 1999a. Early Jurassic (Pliensbachian-Toarcian) dinoflagellate migrations and cyst paleoecology in the Boreal and Tethyan realms. Micropaleontology 45, 201–214.

Bucefalo Palliani, R., Riding, James B., 1999b. Relationships between the early Toarcian anoxic event and organic-walled phytoplankton in central Italy. Marine Micropaleontology 37, 101–116.

Clemence, M.-E., Bartolini, A., Gardin, S., Paris, G., Beaumont, V., Page, K. N., 2010. Early Hettangian benthic-planktonic coupling at Doniford (SW England): Palaeoenvironmental implications for the aftermath of the

end-Triassic crisis. Palaeogeography, Palaeoclimatology, Palaeoecology 295, 102–115.

Cobbold, P. R., Rodrigues, N., 2007. Seepage forces, important factors in the formation of horizontal hydraulic fractures and bedding-parallel fibrous veins ('beef' and 'cone-in-cone'). Geofluids 7, 313–322.

Cobbold, P. R., Zanella, A., Rodrigues, N., Loseth, H., 2013. Bedding-parallel fibrous veins (beef and cone-in-cone): Worldwide occurrence and possible significance in terms of fluid overpressure, hydrocarbon generation and mineralization. Marine and Petroleum Geology 43, 1–20.

Duarte, L. V., Comas-Rengifo, M. J., Silva, R. L., Paredes, R., Goy, A., 2014. Carbon isotope stratigraphy and ammonite biochronostratigraphy across the Sinemurian-Pliensbachian boundary in the western Iberian margin. Bulletin of Geosciences 89, 719–736.

Duarte, L. V., Silva, R. L., Oliveira, L. C. V., Comas-Rengifo, M. J., Silva, F., 2010. Organic-rich facies in the Sinemurian and Pliensbachian of the Lusitanian Basin, Portugal: Total organic carbon distribution and relation to transgressive-regressive facies cycles. Geologica Acta 8, 325–340.

Erba, E., 2005. Calcareous nannofossils and Mesozoic oceanic anoxia. Marine Micropaleontology.

Evitt, W. R., 1961. *Dapcodinium priscum* n. gen. n. sp., a dinoflagellate from the Lower Lias of Denmark. Journal of Paleontology 35, 996–1002.

Falkowski, P. G., Katz, M. E., Milligan, A. J., Fennel, K., Cramer, B. S., Aubry, M. P., Berner, R. A., Novacek, M. J., Zapol, W. M., 2005. The rise of oxygen over the past 205 million years and the evolution of large placental mammals. Science 309, 2202–2204.

Feist Burkhardt, S., 2009. Palynology of the Sinemurian/Pliensbachian boundary (Lower Jurassic) in the Wutach area, SW Germany: dinoflagellate cyst systematics, biostratigraphy and heterotrophic character of *Liasidium variabile*. Neues Jahrbuch für Geologie und Palaeontologie, Abhandlungen 254, 293–313.

Ferreira, J., Mattioli, E., van de Schootbrugge, B., 2017. Palaeoenvironmental vs evolutionary control on size variation of coccoliths across the Lower-Middle Jurassic. Palaeogeography, Palaeoclimatology, Palaeoecology 465, 177–192.

Finnegan, S., Bergmann, K., Eiler, J. M., Jones, D. S., Fike, D. A., Eisenman, I., Hughes, N. C., Tripati, A. K., Fischer, W. W., 2012. The magnitude and duration of late Ordovician-early Silurian glaciation. Science 331, 903–906.

Fischer, R., Jäger, M., Konstantinopoulou, K. A., Kristan-Tollmann, E., Luppold, F. W., Ohm, H.-H., 1986. Paläontologie einer epikontinentalen Lias-Schichtfolge: Oberes Sinemurium bis Oberes Domerium von Empelde bei Hannover. Facies 15, 53–176.

Fraguas, A., Comas-Rengifo, M. J., Gómez, J.J, Goy, A., 2012. The calcareous nannofossil crisis in Northern Spain (Asturias province) linked to the early Toarcian warming-driven mass extinction. Marine Micropaleonotology 94–95, 58–71.

Fraguas, A., Young, J. R., 2011. Evolution of the coccolith genus *Lotharingius* during the late Pliensbachian–early Toarcian interval in Asturias (N Spain). Consequences of the early Toarcian environmental perturbations. Geobios 44, 361–375.

Franke, A., 1936. Die Foraminiferen des deutschen Lias. Abhandlungen der Preußischen Geologischen Landesanstalt, N. F. 169, 1–138.

Fricke, S., Schoen, J., 1999. Praktische Bohrlochgeophysik. Enke Verlag, Stuttgart.

Galli, M. T., Jadoul, F., Bernasconi, S. M., Ciriili, S., Weissert, H., 2007. Stratigraphy and palaeoenvironmental analysis of the Triassic-Jurassic transition in the western Southern Alps (Northern Italy). Palaeogeography, Palaeoclimatology, Palaeoecology 244, 52–70.

Garcia Joral, F., Gomez, J. J., Goy, A., 2011. Mass-extinction and recovery of the early Toarcian (Early Jurassic) brachiopods linked to climate change in Northern and Central Spain. Palaeogeography, Palaeoclimatology, Palaeoecology 302, 367–380.

Gomez, J. J., Goy, A., Canales, M. L., 2008. Seawater temperature and carbon isotope variations in belemnites linked to mass extinction during the Toarcian (Early Jurassic) in Central and Northern Sapin. Comparison with other European sections. Palaeogeography, Palaeoclimatology, Palaeoecology 258, 28–58.

Graham, J. B., Dudley, R., Aguilar, N. M., Gans, C., 1995. Implications of the late Paleozoic oxygen pulse for physiology and evolution. Nature 375, 117–120.

Greene, S. E., Martindale, R. C., Ritterbush, K. A., Bottjer, D. J., Corsetti, F. A., Berelson, W. M., 2012. Recognising ocean acidification in deep time: An evaluation of the evidence for acidification across the Triassic-Jurassic boundary. Earth Science Reviews 113, 72–93.

Greinert, J., Derkachev, A., 2004. Glendonites and methane-derived Mg-calcites in the Sea of Okhotsk, Eastern Siberia: implications of a venting-related ikaite/glendonite formation. Marine Geology 204, 129–144.

Guex, J., Bartolini, A., Atudorei, V., Taylor, D., 2004. High-resolution ammonite and carbon isotope stratigraphy across the Triassic-Jurassic boundary at New York Canyon (Nevada). Earth and Planetary Science Letters 225, 29–41.

Guex, J., Morard, A., Bartolini, A., Morettini, E., 2001. Decouverte d´une importante lacune stratigraphique a la limite Domerien-Toarcien: implications paleo-oceanographiques. Bull. Soc. Vaud. Sc. Nat. 87, 277–284.

Guex, J., Schoene, B., Bartolini, A., Spangenberg, J., Schaltegger, U., O'Dogherty, L., Taylor, D., Bucher, H., Atudorei, V., 2012. Geochronological constraints on post-extinction recovery of the ammonoids and carbon cycle perturbations during the Early Jurassic. Palaeogeography, Palaeoclimatology, Palaeoecology 346–347, 1–11.

Hallam, A., 1987. Radiations and extinctions in relation to environmental change in the marine Lower Jurassic of northwest Europe. Paleobiology 13, 152–168.

Hallam, A., 2002. How catastrophic was the end-Triassic mass-extinction. Lethaia 35, 147–157.

Harazim, D., van de Schootbrugge, B., Sorichter, K., Fiebig, J., Weug, A., Suan, G., Oschmann, W., 2013. Spatial variability of watermass conditions within the European Epicontinental Seaway during the Early Jurassic (Pliensbachian-Toarcian). Sedimentology 60, 359–390.

Harries, P. J., Little, C. T. S., 1999. The early Toarcian (Early Jurassic) and the Cenomanian-Turonian (late Cretaceous) mass extinctions: similarities and contrasts. Palaeogeography, Palaeoclimatology, Palaeoecology 154, 39–66.

Heindel, K., Richoz, S., Birgel, D., Brandner, R., Klügel, A., Krystyn, L., Baud, A., Horacek, M., Mohtat, T., Peckmann, J., 2015. Biogeochemical formation of calyx-shaped carbonate crystal fans in the subsurface of the Early Triassic seafloor. Gondwana Research 27, 840–861.

Hesselbo, S. P., Grocke, D. R., Jenkyns, H. C., Bjerrum, C. J., Farrimond, P., Morgans Bell, H. S., Green, O. R., 2000. Massive dissociation of gas hydrate during a Jurassic oceanic anoxic event. Nature 406, 392–395.

Hesselbo, S. P., Robinson, S. A., Surlyk, F., Piasecki, S., 2002. Terrestrial and marine extinction at the Triassic-Jurassic boundary synchronized with major carbon cycle perturbation: A link to initiation of massive volcanism. Geology 30, 251–254.

Hesselbo, S. P., Jenkyns, H. C., Duarte, L. V., Oliveira, L. C. V., 2007. Carbon isotope record of the Early Jurassic (Toarcian) Oceanic Anoxic Event from fossil wood and marine carbonate (Lusitanian Basin, Portugal). Earth and Planetary Science Letters 253, 455–470.

Heunisch, C., Luppold, F. W., Reinhardt, L., Röhling, H.-G., 2010. Palynofazies, Bio-, und Lithostratigraphie im Grenzbereich Trias/Jura in der Bohrung Mariental I (Lappwaldmulde, Ostniedersachsen). Zeitschrift der Deutschen Gesellschaft für Geowissenschaften 161, 51–98.

Hoffmann, K., 1968. Die Stratigraphie und Paläogeographie des bituminösen Fazies des Nordwestdeutschen Oberlias (Toarcium). Beihefte Geologisches Jahrbuch 58, 443–498.

Hoffmann, K., Jordan, R., 1982. Die Stratigraphie, Paläogeographie und Ammonitenführung des Unter-Pliensbachium (Carixium, Lias gamma) in Nordwest-Deutschland. Geologisches Jahrbuch A55, 3–349.

Hoffmann, K., Martin, P. R., 1960. Die Zone des *Dactylioceras tenuicostatum* (Toarcien, Lias) in NW- und SW-Deutschland. Paläontologische Zeitschrift 34, 103–149.

Hölder, H., 1964. Jura. Ferdninand Enke-Verlag, Stuttgart.

Jaraula, C. M. B., Grice, K., Twitchett, R. J., Böttcher, M. E., LeMetayer, P., Dastidar, A. G., Opazo, L. F., 2013. Elevated pCO_2 leading to late Triassic extinction, persistent photic zone euxinia, and rising sea levels. Geology 41, 955–958.

Jenkyns, H. C., 1988. The early Toarcian (Jurassic) anoxic event: stratigraphic, sedimentary, and geochemical evidence. American Journal of Science 288, 101–151.

Jenkyns, H. C., Clayton, C. J., 1986. Black shales and carbon isotope in pelagic sediments from the Tethyan Lower Jurassic. Sedimentology 33, 87–106.

Jenkyns, H. C., Clayton, C. J., 1997. Lower Jurassic epicontinental carbonates and mudstones from England and Wales: chemostratigraphic signals and the early Toarcian anoxic event. Sedimentology 44, 687–706.

Jenkyns, H. C., Jones, C. E., Gröcke, D. E., Hesselbo, S. P., Parkinson, D. N., 2002. Chemostratigraphy of the Jurassic System: applications, limitations and implications for palaeoceanography. Journal of the Geological Society, London 159, 351–378.

Jenkyns, H. C., Weedon, G. P., 2013. Chemostratigraphy ($CaCO_3$, TOC, $\delta^{13}C_{org}$) of Sinemurian (Lower Jurassic) black shales from the Wessex Basin, Dorset and palaeoenvironmental implications. Newsletters on Stratigraphy 46, 1–21.

Kaplan, M. E., 1978. Calcite pseudomorphs in Jurassic and Lower Cretaceous deposits of the Northern Area of Eastern Siberia. Geologiya i Geofizika 19, 62–70.

Kaplan, M. E., 1979. Calcite pseudomorphs (pseudogaylussite, jarrowite, thinolite, glendonite, gennoishi, White Sea hornlets) in sedimentary rocks. Origins of the pseudomorphs. Lithologiya i Poleznye Iskopaemye 5, 125–141.

Kasprak, A. H., Sepulveda, J., Price-Waldman, R., Williford, K. H., Schoepfer, S. D., Haggart, J. W., Ward, P. D., Summons, R. E., Whiteside, J. H., 2015. Episodic photic zone euxinia in the northeastern Panthalassic Ocean during the end-Triassic extinction. Geology 43, 307–310.

Kershaw, S., Guo, L., 2016. Beef and cone-in-cone calcite fibrous cements associated with the end-Permian and end-Triassic mass extinctions: reassessment of processes of formation. Journal of Palaeogeography 5, 28–42.

Klingler, W., 1962. Leitfossilen der Mikropaläontologie; B3 Lias Deutschland. In: A. D. (Ed.), Mikropaläontologen. Gebrüder Borntraeger, 73–122.

Klingler, W., Neuweiler, F., 1959. Leitende Ostrakoden aus dem deutschen Lias ß. Geologisches Jahrbuch 76, 373–410.

Koch, J., Arnemann, H., 1975. Die Inkohlung in Gesteinen des Rhaets und Lias im Südlichen Nordwestdeutschland. Geologisches Jahrbuch A29, 33–43.

Korte, C., Hesselbo, S. P., 2011. Shallow marine carbon and oxygen isotope and elemental records indicate icehouse-greenhouse cycles during the Early Jurassic. Paleoceanography 26, doi: 10.1029/2011PA002160.

Kumm, A., Riedel, L., Schott, W., 1941. Das Mesozoikum in Niedersachsen (Trias, Jura, Kreide). I. Abteilung: Trias und Lias. Gerhard Stalling AG, Oldenburg.

Kürschner, W., Bonis, N., Krystyn, L., 2007. Carbon isotope stratigraphy and palynostratigraphy of the Triassic-Jurassic transition in the Tiefengraben section – Northern Calcareous Alps (Austria). Palaeogeography, Palaeoclimatology, Palaeoecology 244, 257–280.

Lindström, S., 2002. *Lunnomidinium scaniense* Lindström, gen. et sp. nov., a new suessiacean dinoflagellate cyst from the Rhaetian of Scania, southern Sweden. Review of Palaeobotany and Palynology 120, 247–261.

Lindström, S., Erlström, M., 2006. The late Rhaetian transgression in southern Sweden: Regional (and global) recognition and relation to the Triassic-Jurassic boundary. Palaeogeography, Palaeoclimatology, Palaeoecology 241, 339–372.

Lindström, S., van de Schootbrugge, B., Dybkjaer, K., Pedersen, G. K., Fiebig, J., Nielsen, L. H., Richoz, S., 2012. No causal link between terrestrial ecosystem change and methane release during the end-Triassic mass-extinction. Geology 40, 531–534.

Lindström, S., Krarup Pedersen, G., van de Schootbrugge, B., Hovedskov-Hansen, K., Kuhlmann, N., Thein, J., Johansson, L., Ingermann Petersen, H., Awlmark, C., Dybkjaer, K., Weibel, R., Erlström, M., Nielsen, L. H., Oschmann, W., Tegner, C., 2015. Intense and widespread seimicity during the end-Triassic mass extinction due to emplacement of a large igneous province. Geology 43, 387–390.

Lindström, S., van de Schootbrugge, B., Hansen, K. H., Pedersen, G. K., Alsen, P., 2017. A new correlation of Triassic–Jurassic boundary successions in NW Europe, Nevada and Peru, and the Central Atlantic Magmatic Province: A time-line for the end-Triassic mass extinction. Palaeogeography, Palaeoclimatology, Palaeoecology 478, 80–102.

Littke, R., Baker, D. R., Leythauser, D., Rullkötter, J., 1991. Keys to the depositional history of the Posidonia Shale (Toarcian) in the Hills Syncline, northern Germany. Geological Society of London, London 58, 311–333.

Little, C. T. S., Benton, M. J., 1995. Early Jurassic mass extinction: A global long-term event. Geology 23, 495–498.

Lund, J. J., 1976. Palynostratigraphie des Oberen Keuper und Unteren Lias von NW Deutschland und seinen Nachbargebieten – Ergänzungsband Erdöl und Kohle. Compendium 75/76. 3. DGMK-Fachgruppentagung, Hannover, 140–148.

Lund, J. J., 1977. Rhaetic to lower Jurassic palynology of the onshore southeastern North Sea Basin. Danmarks Geologiske Undersogelse II Raekke 109, 1–129.

Malz, H., 1971. Zur Taxonomie "glattschaliger" Lias-Ostracoden. Senckenbergiana lethaea 52, 433–455.

Mander, L., Twitchett, R. J., Benton, M. J., 2008. Palaeoecology of the late Triassic extinction event in the SW UK. Journal of the Geological Society of London 165, 319–332.

Martindale, R. C., Them, T. R., Gill, B. C., Marroquin, S. M., Knoll, A. H., 2017. A new Early Jurassic (ca. 183 Ma) fossil Lagerstätte from Ya Ha Tinda, Alberta, Canada. Geology 45, 255–258.

Mattioli, E., Erba, E., 1999. Synthesis of calcareous nannofossil events in Tethyan Lower and Middle Jurassic successions. Rivista Italiana di Paleontologia e Stratigrafia 105, 343–376.

Mattioli, E., Pittet, B., Bucefalo Palliani, R., Röhl, H.-J., Schmid-Röhl, A., Morettini, E., 2004. Phytoplankton evidence for the timing and correlation of palaeoceanographical changes during the early Toarcian oceanic anoxic event (Early Jurassic). Journal of the Geological Society of London 161, 685–693.

Mattioli, E., Pittet, B., Suan, G., Mailliot, S., 2008. Calcareous nannoplankton changes across the early Toarcian oceanic anoxic event in the western Tethys. Paleoceanography 23, doi: 10.1029/2007PA001435.

Michelsen, O., 1975. Lower Jurassic biostratigraphy and ostracods of the Danish Embayment. Geological Survey of Denmark II 104, 1–287.

Morales, C. M., Rogov, M., Wierzbowski, H., Ershova, V., Suan, G., Adatte, T., Follmi, K. B., Tegelaar, E., de Lange, G., Middelburg, J. J., van de Schootbrugge, B., 2017. Glendonites track methane seepage in Mesozoic polar seas. Geology 45, 503–506.

Perilli, N., Fraguas, A., Comas-Rengifo, M. J., 2010. Reproducibility and reliability of the Pliensbachian calcareous nannofossil biohorizons from the Basque-Cantabrian Basin (Northern Spain). Geobios 48, 183–210.

Porter, S. J., Smith, P. L., Caruthers, A. H., Pengfui, H., Gröcke, D. R., Selby, D., 2014. New high resolution geochemistry of Lower Jurassic marine sections in western North America: A global positive carbon isotope excursion in the Sinemurian? Earth and Planetary Science Letters 397, 19–31.

Price, G. D., 1999. The evidence and implications of polar ice during the Mesozoic. Earth-Science Reviews 48, 183–210.

Price, G. D., Vowles-Sheridan, N., Anderson, M. W., 2008. Lower Jurassic mud volcanoes and methane, Kilve, Somerset, UK. Proceedings of the Geologists Association 119, 193–201.

Quenstedt, F. A., 1843. Das Flözgebirge Würtembergs. Mit besonderer Rücksicht auf den Jura. H. Laupp, Tübingen.

Rachold, V., Brumsack, H.-J., 2001. Inorganic geochemistry of Albian sediments from the Lower Saxony Basin NW Germany: paleoenvironmental constraints and orbital cycles. Palaeogeography, Palaeoclimatology, Palaeoecology 174, 121–143.

Richoz, S., van de Schootbrugge, B., Pross, J., Püttmann, W., Quan, T. M., Lindström, S., Heunisch, C., Fiebig, J., Maquil, R., Hauzenberger, C., Schouten, S., Wignall, P. B., 2012. Hydrogen sulphide poisoning of shallow seas due to end-Triassic global warming. Nature Geoscience 5, 662–667.

Rider, M. H., Kennedy, M., 2011. The geological interpretation of well logs. Whittles Publishing, London.

Riding, J. B., 1987. Dinoflagellate cyst stratigraphy of the Nettleton Bottom Borehole (Jurassic: Hettangian to Kimmeridgian), Lincolnshire, England. Proceeding of the Yorkshire Geological Society 46, 231–266.

Riding, J. B., Ioannides, N. S., 1996. A review of Jurassic dinoflagellate cyst biostratigraphy and global provincialism. Bulletin de la Societe geologique de France 167, 3–14.

Riding, J. B., Leng, M. J., Kender, S., Hesselbo, S. P., Feist-Burkhardt, S., 2013. Isotopic and palynological evidence for a new Early Jurassic environmental perturbation. Palaeogeography, Palaeoclimatology, Palaeoecology 374, 16–27.

Röhl, H., Schmid-Röhl, A., Oschmann, W., Frimmel, A., Schwark, L., 2001. The Posidonia Shale (lower Toarcian)

of SW-Germany; an oxygen-depleted ecosystem controlled by sea level and palaeoclimate. Palaeogeography, Palaeoclimatology, Palaeoecology 165, 27–52.

Rosales, I., Quesada, S., Robles, S., 2004. Paleotemperature variations of Early Jurassic seawater recorded in geochemical trends of belemnites from the Basque-Cantabrian basin, northern Spain. Palaeogeography, Palaeoclimatology, Palaeoecology 203, 253–275.

Ruhl, M., Bonis, N. R., Reichart, G.-J., Sinninghe-Damste, J. S., Kürschner, W., 2011. Atmospheric carbon injection linked to end-Triassic mass-extinction. Science 333, 430–434.

Ruhl, M., Deenen, M. H. L., Abels, H. A., Bonis, N. R., Krijgsman, W., Kürschner, W., 2010. Astronomical constraints on the duration of the Early Jurassic Hettangian stage and recovery rates following the end-Triassic mass-extinction (St Audrie´s Bay/East Quantoxhead, UK). Earth and Planetary Science Letters 295, 262–276.

Schmitz, H.-H., 1968. Untersuchungen am nordwestdeutschen Posidonienschiefer und seiner organischen Substanz. Beihefte Geologisches Jahrbuch 58, 1–219.

Schmitz, H.-H., 1980. Ölschiefer in Niedersachsen. Berichte der Naturhistorischen Gesellschaft Hannover 123, 7–43.

Schubert, C. J., Nürnberg, D., Scheele, N., Pauer, F., Kriews, M., 1997. ^{13}C isotope depletion in ikaite crystals: evidence for methane release from the Siberian shelves. GeoMarine Letters 17, 169–174.

Sepkoski Jr, J. J., 1996. Patterns of Phanerozoic extinction: A perspective from global data bases. In: Walliser, O. H. (Ed.), Global events and event stratigraphy in the Phanerozoic. Springer, Berlin, 35–51.

Serra, O., 1984. Fundamentals of well-log interpretation. Vol. 1. The acquisition of logging data. Elsevier, Amsterdam.

Stadler, G., Teichmüller, R., 1971. Zusammenfassender Überblick über die Entwicklung des Bramscher Massivs und des Niedersächsischen Tektogens. Fortschritte in der Geologie von Rheinland und Westfalen 18, 547–564.

Suan, G., Mattioli, E., Pittet, B., Lecuyer, C., Suchéras-Marx, B., Duarte, L. V., Philippe, M., Reggiani, L., Martineau, F., 2010. Secular environmental precursors to early Toarcian (Jurassic) extreme climate changes. Earth and Planetary Science Letters 290, 448–458.

Suan, G., Mattioli, E., Pittet, B., Mailliot, S., Lecuyer, C., 2008. Evidence for major environmental perturbation prior to and during the Toarcian (Early Jurassic) oceanic anoxic event from the Lusitanian Basin, Portugal. Paleoceanography 23PA1202, doi: 1210.1029/2007PA001459.

Suan, G., Nikitenko, B. L., Rogov, M. A., Baudin, F., Spangenberg, J. E., Knyazev, V. G., Glinskikh, L. A., Goryacheva, A. A., Adatte, T., Riding, J. B., Föllmi, K. B., Pittet, B., Mattioli, E., Lecuyer, C., 2011. Polar record of Early Jurassic massive carbon injection. Earth and Planetary Science Letters 312, 102–113.

Teichert, B. M., Luppold, F. W., 2013. Glendonites from an Early Jurassic methane seep – Climate or methane indicators? Palaeogeography, Palaeoclimatology, Palaeoecology 390, 81–93.

Teichmüller, M., Teichmüller, R., 1984. Inkohlung und Erdgas – Eine neue Inkohlungskarte der Karbon-Oberfläche in Nordwest-Deutschland. Fortschritte in der Geologie von Rheinland und Westfalen 32, 11–34.

Tremolada, F., van de Schootbrugge, B., Erba, E., 2005. Early Jurassic schizosphaerellid crisis in Cantabria, Spain: Implications for calcification rates and phytoplankton evolution across the Toarcian oceanic anoxic event. Paleoceanography 20, doi: 10.1029/2004PA001120.

Triebel, E., Klingler, W., 1959. Neue Ostracoden-Gattungen aus dem deutschen Lias. Geologisches Jahrbuch 76, 335–372.

van de Schootbrugge, B., Bachan, A., Suan, G., Richoz, S., Payne, J. L., 2013. Microbes, mud and methane: cause and consequence of recurrent Early Jurassic anoxia following the End-Triassic mass extinction. Palaeontology 56, 685–709.

van de Schootbrugge, B., Bailey, T., Rosenthal, Y., Katz, M., Wright, J. D., Feist-Burkhardt, S., Miller, K. G., Falkowski, P. G., 2005. Early Jurassic climate change and the radiation of organic-walled phytoplankton in the Tethys Ocean. Paleobiology 31, 73–97.

van de Schootbrugge, B., Harazim, D., Sorichter, K., Oschmann, W., Fiebig, J., Püttmann, W., Peinl, M., Zanella, F., Teichert, B. M. A., Hoffmann, J., Stadnitskaia, A., Rosenthal, Y., 2010. The enigmatic ichnofossil Tisoa siphonalis and widespread authigenic seep carbonate formation during the late Pliensbachian in southern France. Biogeosciences 7, 3123–3138.

van de Schootbrugge, B., MacArthur, J. M., Baily, T. R., Rosenthal, Y., Wright, J. D., Miller, K. G., 2005. Toarcian oceanic anoxic event: Assessment of global causes using belemnite C-isotope records. Paleoceanography 20.

van de Schootbrugge, B., Payne, J. L., Tomasovych, A., Pross, J., Fiebig, J., Benbrahim, M., Föllmi, K. B., Quan, T. M., 2008. Carbon cycle perturbation and stabilization in the wake of the Triassic-Jurassic boundary mass-extinction event. Geochemistry, Geophysics, Geosystems 9Q04028, doi: 04010.01029/02007GC001914.

van de Schootbrugge, B., Quan, T., Lindström, S., Püttmann, W., Heunisch, C., Pross, J., Fiebig, J., Petschick, R., Röhling, H.-G., Richoz, S., Rosenthal, Y., Falkowski, P. G., 2009. Floral changes across the Triassic-Jurassic boundary linked to flood basalt volcanism. Nature Geoscience 2, 489–594.

van de Schootbrugge, B., Tremolada, F., Bailey, T. R., Rosenthal, Y., Feist-Burkhardt, S., Brinkhuis, H., Pross, J., Kent, D. V., Falkowski, P. G., 2007. End-Triassic calcification crisis and blooms of organic-walled disaster species. Palaeogeography, Palaeoclimatology, Palaeoecology 244, 126–141.

Veiga de Oliveira, L. C., Duarte, L. V., Lemos, V. B., Comas-Rengifo, M. J., Perilli, N., 2007. Calcareous nannofossil biostratigraphy and correlation with ammonite zones of the Pliensbachian-lowermost Toarcian (Lower Jurassic) of Peniche (Lusitanian Basin, Portugal). In: Carvalho, D. S. (Ed.), Paleontologia: Cenarios de Vida. Editora Interciencia, Rio de Janeiro, 411–420.

Vermeij, G. J., 1977. The Mesozoic marine revolution: evidence from snails, predators and grazers. Paleobiology 3, 245–258.

Vermeij, G. J., 2008. Escalation and its role in Jurassic biotic history. Palaeogeography, Palaeoclimatology, Palaeoecology 263, 3–8.

Watson, A., Lovelock, J. E., Margulis, L., 1978. Methanogenesis, fires and the regulation of atmospheric oxygen. Biosystems 10, 293–298.

Weedon, G. P., Coe, A. L., Gallois, R. W., 2004. Cyclostratigraphy, orbital tuning and inferred productivity for the type Kimmeridge Clay (late Jurassic), Southern England. Journal of the Geological Society, London 161, 655–666.

Weitschat, W., 1973. Stratigraphie und Ammoniten des höheren Untertoarcium (oberer Lias epsilon) von NW-Deutschland. Geologisches Jahrbuch A 8, 3–81.

Wellnhofer, P., Vahldiek, B.-W., 1986. Ein Flugsaurier-Rest aus dem Posidonienschiefer (Unter-Toarcium) von Schandelah bei Braunschweig. Paläontologische Zeitschrift 60, 329–340.

Wignall, P. B., 2001. Sedimentology of the Triassic-Jurassic boundary beds in Pinhay Bay (Devon, SW England). Proceedings of the Geologists Association 112, 349–360.

Wignall, P. B., Bond, D. P. G., 2008. The end-Triassic and Early Jurassic mass extinction records in the British Isles. Proceedings of the Geologist's Association 119, 73–84.

Wignall, P. B., Bond, D. P. G., Kuwahara, K., Kakuwa, Y., Newton, R. J., Poulton, S. W., 2010. An 80 million year oceanic redox history from the Permian to Jurassic pelagic sediments of the Mino-Tamba terrane, SW Japan, and the origin of four mass extinctions. Global and Planetary Change 71, 109–123.

Williford, K. H., Ward, P. D., Garrison, G. H., Buick, R., 2007. An extended organic carbon-isotope record across the Triassic-Jurassic boundary in the Queen Charlotte Islands, British Columbia, Canada. Palaeogeography, Palaeoclimatology, Palaeoecology 244, 290–296.

Woodfine, R. G., Jenkyns, H. C., Sarti, M., Baroncini, F., Violante, C., 2008. The response of two Tethyan carbonate platforms to the early Toarcian (Jurassic) oceanic anoxic event: environmental change and differential subsidence. Sedimentology 55, 1011–1028.

Xu, W., Ruhl, M., Hesselbo, S. P., Riding, J. B., Jenkyns, H. C., 2016. Orbital pacing of the Early Jurassic carbon cycle, black-shale formation and seabed methane seepage. Sedimentology 64, 127–149.

Manuscript received: November 27, 2017
Revisions required: March 06, 2018
Revised version received: July 20, 2018
Manuscript accepted: August 03, 2018

Appendix

F. W. Luppold – Systematic palaeontology of ostracods

Family Healdiidae Harlton 1933
Genus *Ogmoconchella* Gründel 1964
Ogmoconchella No. 2 (Klingler 1962)
Plate 4, Fig. 5–6
1962 Ostracod Nr. 2 – Klingler: 103, Pl. 14, Fig. 41?
1975 *Ogmoconchella* No. 2 – Michelsen: 254, Pl. 37, Fig. 528–530.

The description of Klingler (1962) is followed, and the allocation to the genus *Ogmoconchella* of Michelsen (1975). An accentuated surface, covered with a network of short elongate scars, make the most optical difference between other species of this genus. The carapace shows more or less parallel margins, and rounded anterior and posterior ends. The end of the RV has an external lamella, larger as the left one.

Remarks: It seems that the material of Michelsen (1975) does not indicate the ornamentation surface (p. 254), because Michelsen does not mention this feature in the text. So it is not certain whether the figured specimens of Michelsen (1975) are comparable to Ostracod No. 2 of Klingler. Whereas the comparison with the material of Klingler is outstanding, the whereabouts of Klingler's material is unknown (pers. comm. H. Malz).

Dimensions: LV: length: 0.73 mm; height: 0.41 mm; Carapace: length: 0.78 mm; height: 0.46 mm.

Genus *Ogmoconcha* Triebel 1941
Ogmoconcha aff. *ambo* Lord & Moorley in Sylvester-Bradley 1974
Plate 4, Fig. 7 a–b

Remarks: Only one valve makes it possible, that this specimen belongs to the vallate ostracod *Ogmoconcha ambo*. The specimen figured at Pl. 4, Fig. 7 a–b as lateral and oblique views, show approximately the characteristic bulges at anterior and posterior ends, partly covered by calcareous cement. The ventral rim is not so distinct. The inner valve is covered with a coarse carbonate matrix. *Ogmoconcha ambo* is only known from the Upper Pliensbachian, upper part of the Spinatum Zone of southern Germany.

Family Cytheridae Baird, 1850
Genus *Domericythere* gen. nov.

Derivatio nominis: after the old lithostratigraphical unit Domerian, which corresponds with the Upper Pliensbachian substage.

Diagnosis: A genus of the Cytheridae with subrectangular oval outline and a smooth spaced reticulation. Anterior margin broad rounded, posterior end more narrow. Posterior margin more distinct than anterior. Overhanging ventro-posterior margin. Ventral surface covered with longitudinal ridges. Hinge hemi-merodont. Inner margin coincides with line of concrescence. Other features like muscle scars and pores are not visible.

Domericythere brandi spec. nov.
Plate 5.3 a–6

Derivatio nominis: After Erich Brand, a pioneer of German micropaleontology.

Holotype: Plate 5.3 a–b, BGR type-no. 16120.

Stratotype: Late Pliensbachian.

Type locality: Schandelah-1 core near Schandelah, east of Braunschweig (North Germany), depth: 58.10–58.30 mbs.

Diagnosis: A medium sized sub-rectangular to oval shaped species of the new genus *Domericythere* with smooth reticulation of the carapace.

Description: the oval-shaped carapace has its greatest length and height through the midpoint of the carapace. Dimorphism cannot be determined on this material. LV slightly larger than the right one. Anterior cardinal angle broadly, posterior more narrowly. Dorsal margin of the LV slightly concave, in the RV convex. The unornamented dorsal margin is straight to slightly convex. Hinge hemi-merodont with 6–7 teeth anteriorly and posteriorly of the RV, and complimentary elliptical sockets of the LV. Above the median bar of LV a narrow accommodation groove is present. The median bar of the LV has its opposite in the RV. Any other internal features like marginal pore canals, muscle scars cannot be observed.

Remarks: This species is at present the only species assigned to the genus. This genus is different from other genera like *Kinkelinella*, because of a more slender and triangular outline of the carapace. *Southcavea*, a genus prominent in the lower Middle Jurassic is also different. *Wicherella*, a characteristic genus from the Middle Pliensbachian of England and the western Paris basin is more comparable because of more symmetrical outline than the latter.

Dimensions in mm: (specimens figured at Plate 5): length 0.44, height 0.27; length 0.61, height 0.39; length 0.41, height 0.25; length 0.50, height 0.31;

Material: 29 valves, 2 carapaces.

Genus *Acrocythere* Neale 1960
Acrocythere aff. *troesteri* Riegraf 1984
Plate 5, Fig. 8

Remarks: Characteristic features are the smooth reticulation which is comparable with the specimen of Riegraf (1984), Plate 5, Fig. 8. The obliquely striking middle ridge is not really developed. The species is known from Lower Toarcian of Southern Germany, and from the Upper Pliensbachian (hawskerense-Subzone) in Southern France. In Schandelah-1 it is proved at 58.10–58.30 mbs.